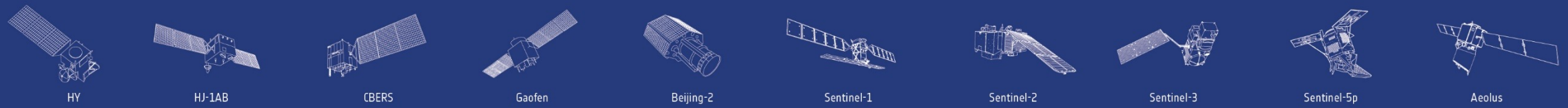

2023 DRAGON 5 SYMPOSIUM

3rd YEAR RESULTS REPORTING

11-15 SEPTEMBER 2023

PROJECT ID. 59316

PROTOTYPE REAL-TIME REMOTE SENSING LAND DATA ASSIMILATION ALONG THE SILK ROAD ENDORHEIC RIVER BASINS AND EUROCORDEX-DOMAIN

THURSDAY, 14/SEPTEMBER/2023

ID. 59316

PROJECT TITLE: PROTOTYPE REAL-TIME REMOTE SENSING LAND DATA ASSIMILATION ALONG THE SILK ROAD ENDORHEIC RIVER BASINS AND EUROCORDEX-DOMAIN

PRINCIPAL INVESTIGATORS: XIN LI, HARRY VEREECKEN

CO-AUTHORS: DONGHAI ZHENG, HARRIE-JAN HENDRICKS FRANSSEN, MIN FENG, CARSTEN MONTZKA, YINGYING CHEN, FENG LIU, CHUNFENG MA, LING ZHANG, YUSHAN ZHOU, KUN ZHANG, HAOJIN ZHAO, MIKAEL KAANDORP

PRESENTED BY: DONGHAI ZHENG

Outline

- Overview of the project
- In-situ data measurements and field data collection campaigns
- Current progress of the project
- Plan of the project for the following year

1. Overview of the project

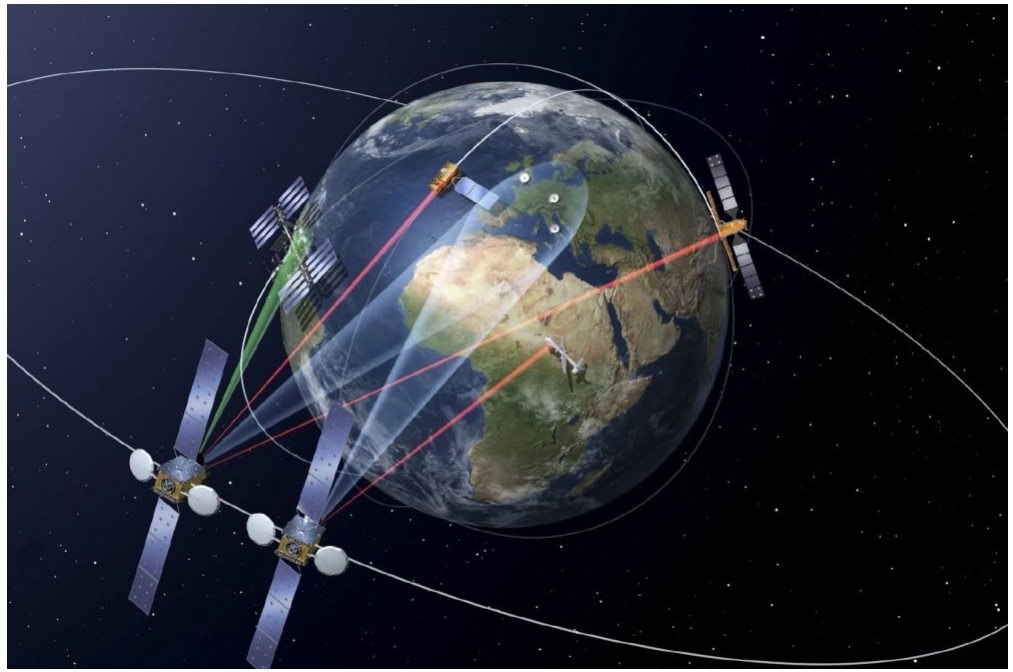

Objectives

Main objective: Develop prototypes of real-time RS land data assimilation systems for monitoring the water cycle in the silk road endorheic river basins and EUROCORDEX-domain

Sub-objectives:

- Retrieval of key water cycle variables from multi-source RS data (WP1)
- Development of real time RS LDAS (WP2)
- Calibration/validation and parameter estimations of terrestrial system models based on the RS retrievals and LDAS (WP3)
- Closing water cycle at the watershed/regional scale based on the LDAS (WP4)

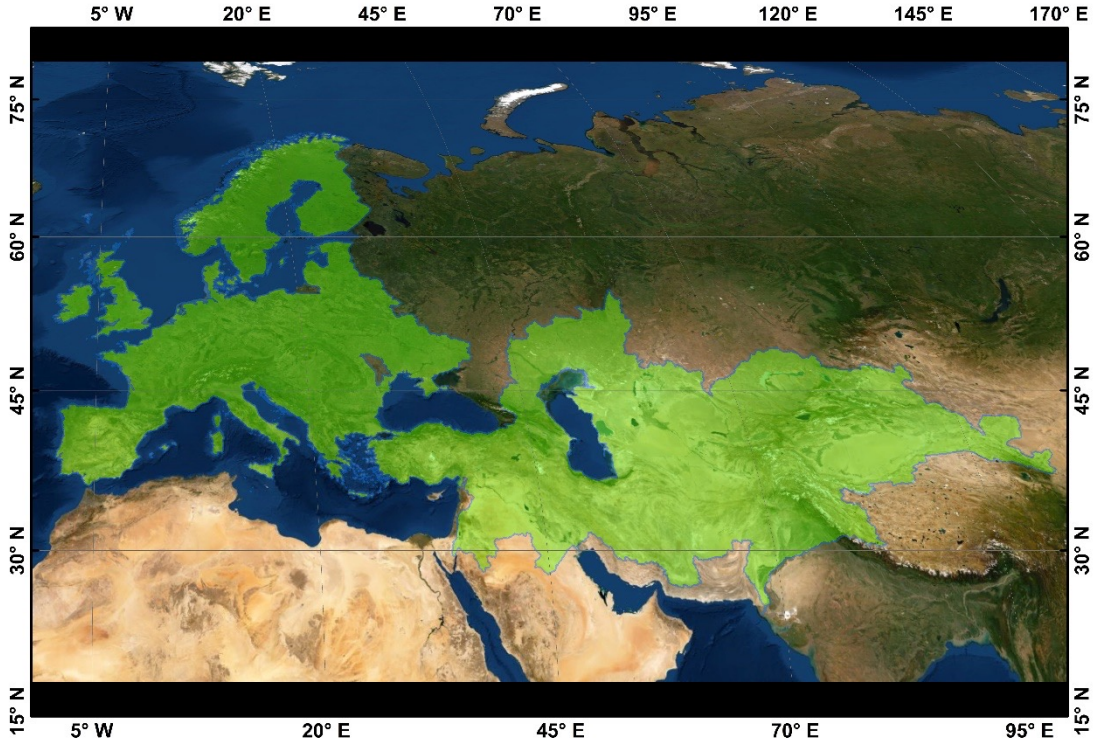

Team composition

Chinese Investigators

- Xin Li (ITP)
- Donghai Zheng (ITP)
- Min Feng (ITP)
- Yingying Chen (ITP)
- Youhua Ran (NIEER)
- Chufeng Ma (NIEER)

European Investigators

- Harry Vereecken (IBG-3)
- Harrie-Jan Hendricks Franssen (IBG-3)
- Carsten Montzka (IBG-3)

The Chinese team focus on developing LDAS for silk road endorheic river basins (LDAS_silk), and the European team focus on the EUROCORDEX-domain (LDAS_EU)

Team composition

Young Scientists

Chinese Team

- Ling Zhang (NIEER)
- Feng Liu (NIEER)
- Xu Zhou (ITP)
- Kun Zhang (ITP)
- Yushan Zhou (ITP)
- Bin Cao (ITP)

European Team

- Zhenlei Yang (IBG-3)
- Ching-Pui Hung (IBG-3)
- Bibi Naz (IBG-3)
- Haojin Zhao (IBG-3)
- Fang Li (IBG-3)

Different young scientists, graduate and undergraduate students, were involved in the project

2. In-situ data measurements and field data collection campaigns

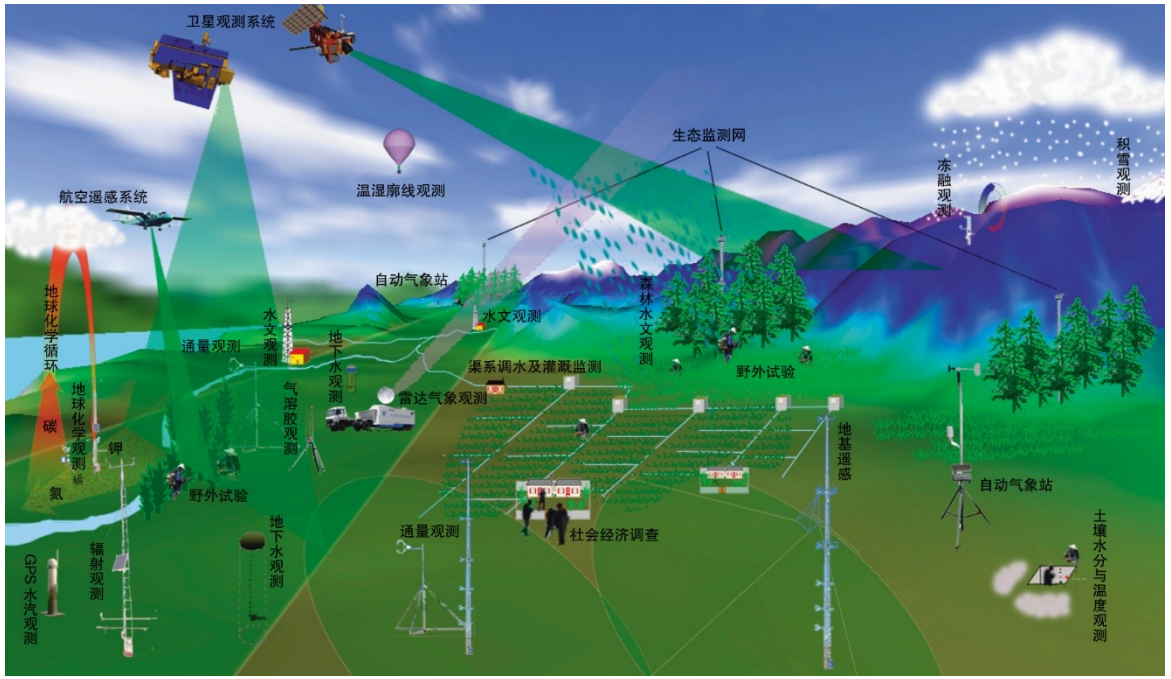

- Observation system in the Qilian Mountains
- Precipitation observation over the Tibetan Plateau
- P-band SAR flight campaign over the Bayi glacier
- International observation alliance of the Third Pole
- Observation system in Germany

2.1 Observation system in the Qilian Mountains

A unified observation network is established according to the same observation standard through reconstruction and new construction. By integrating with medium and high resolution remote sensing monitoring, a satellite-airborne-ground monitoring system has been established in the Qilian Mountains region.

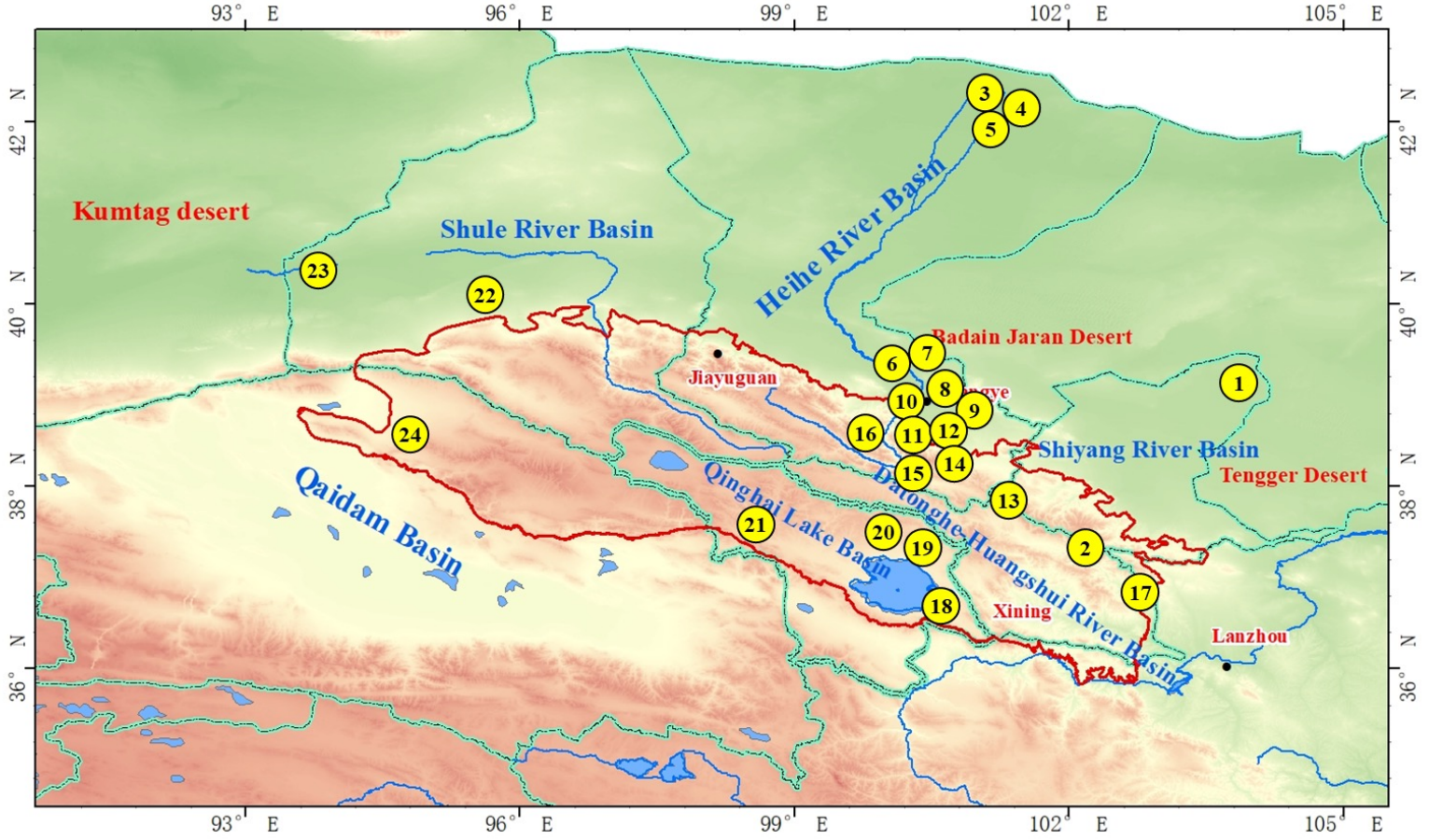

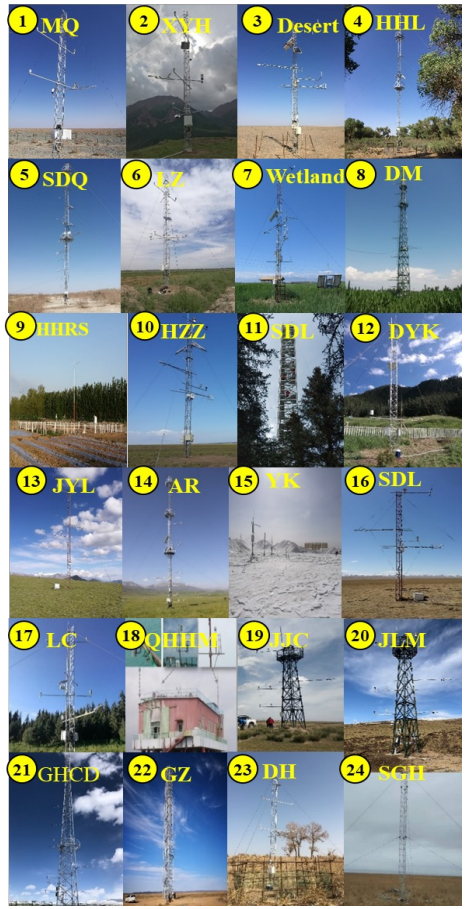

Ground observation network in Qilian Mountains (24 stations)

2.1 Observation system in the Qilian Mountains

A dense soil moisture and temperature monitoring network was constructed within the Qinghai Lake Basin on the Tibetan Plateau, which covers the footprint of SMAP, SMOS and AMSR-2 (36 km × 40 km), with total of 82 sites: 60 sites in the large network have started working since September 2019, 22 sites in the two enhanced networks (1 km × 1 km) have started working since September 2020.

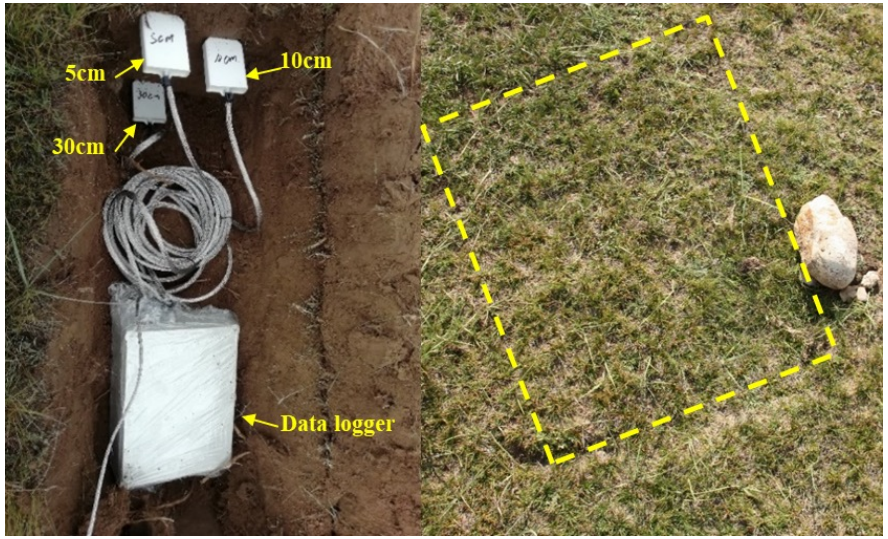

The installation of the Campbell CS655 sensors at three different depths (5 cm, 10 cm and 30 cm)

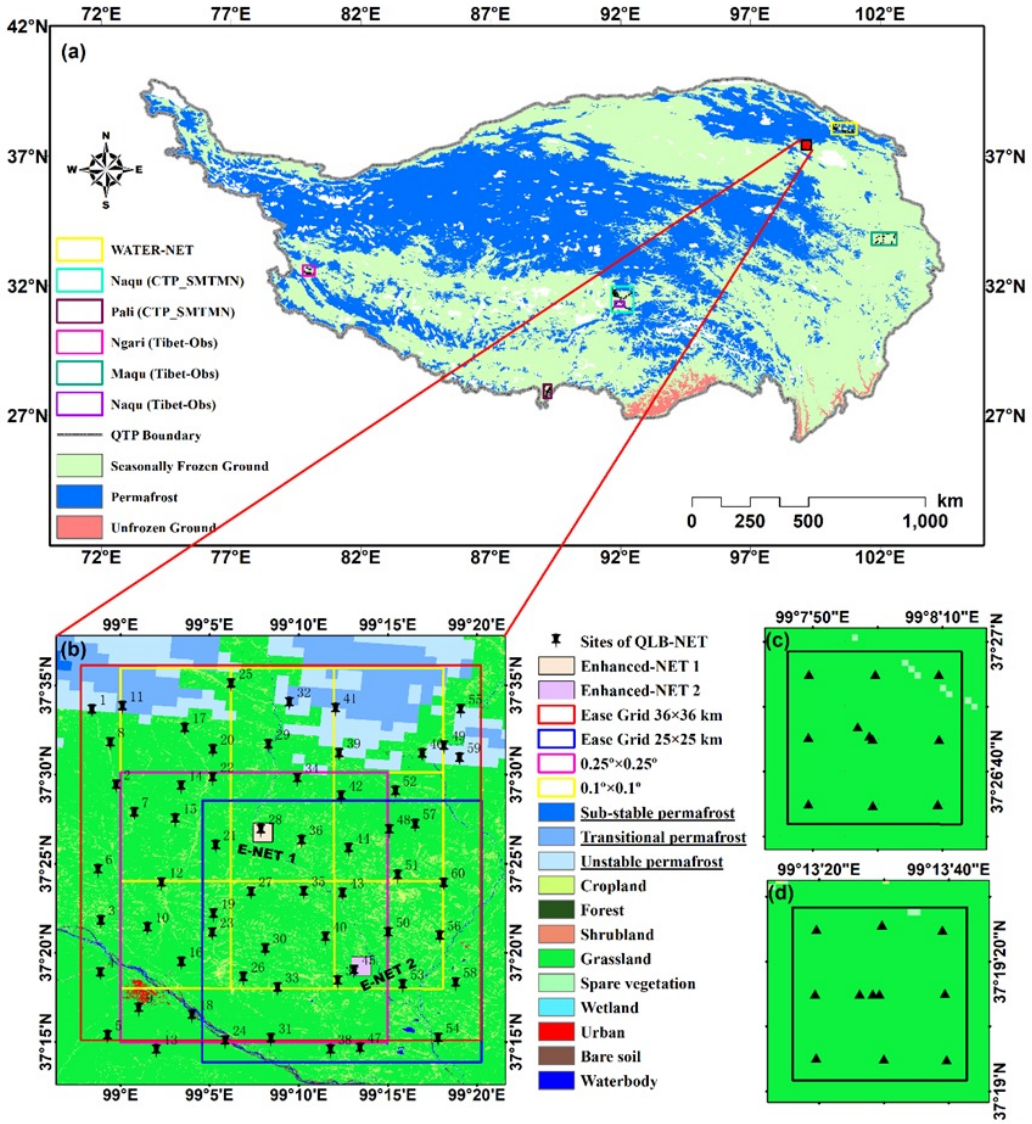

- Observation system in the Qilian Mountains
- Precipitation observation over the Tibetan Plateau
- P-band SAR flight campaign over the Bayi glacier
- International observation alliance of the Third Pole
- Observation system in Germany

2.2 Precipitation observation over the Tibetan Plateau

Cross-sectional rainfall observation network on the central-western TP

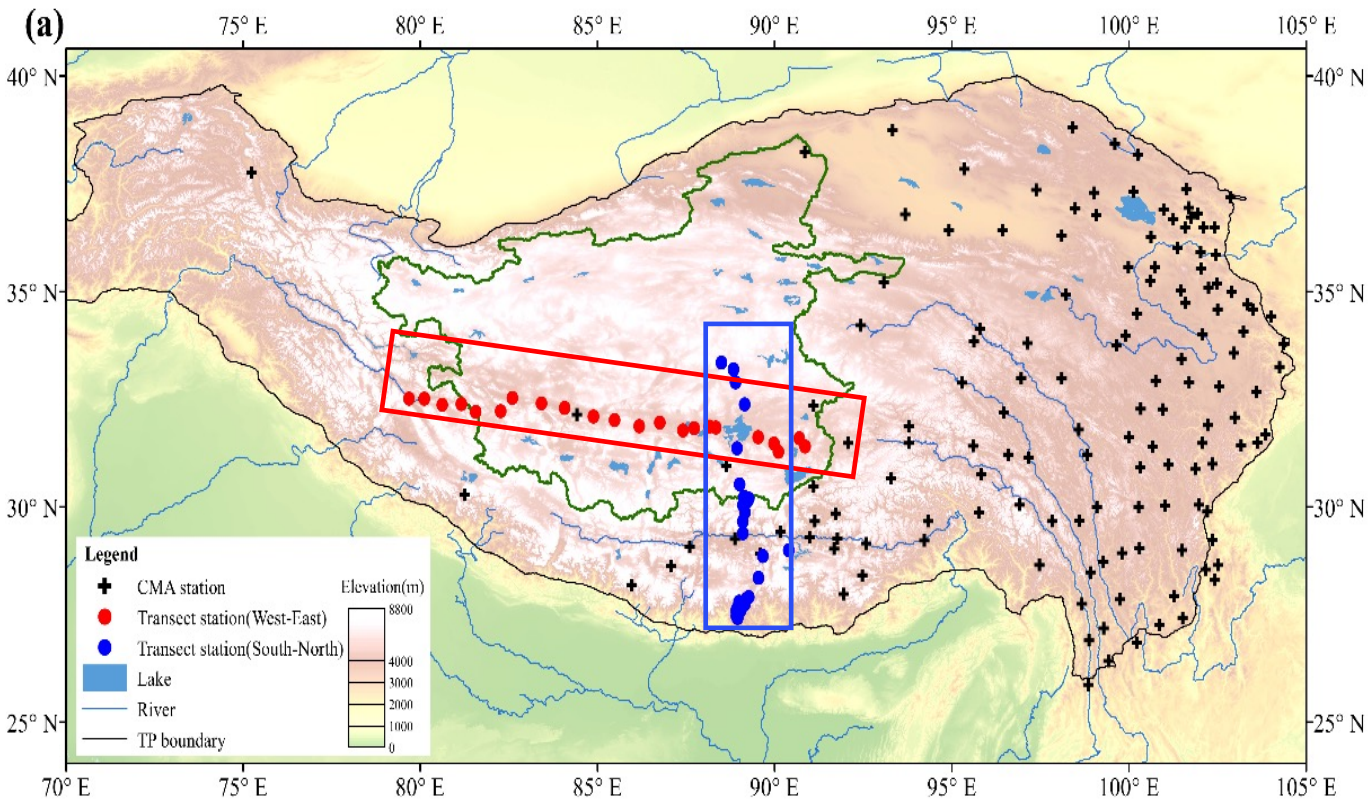

Two rainfall observation sections, 56 rainfall gauges

- **The east-west section on the Qiangtang Plateau**
  - ✓ 24 rain gauges from Naqu to Ali
  - ✓ East-west precipitation characteristics
  - ✓ making up for the lack of observation
- **The south-north section**
  - ✓ 32 rain gauges from Yadong to Shuanghu
  - ✓ crossing the Himalaya and the Gangetic, two large terrains with big elevation gradient changes.

2.2 Precipitation observation over the Tibetan Plateau

Multi-scale precipitation observation platform in the Namco basin

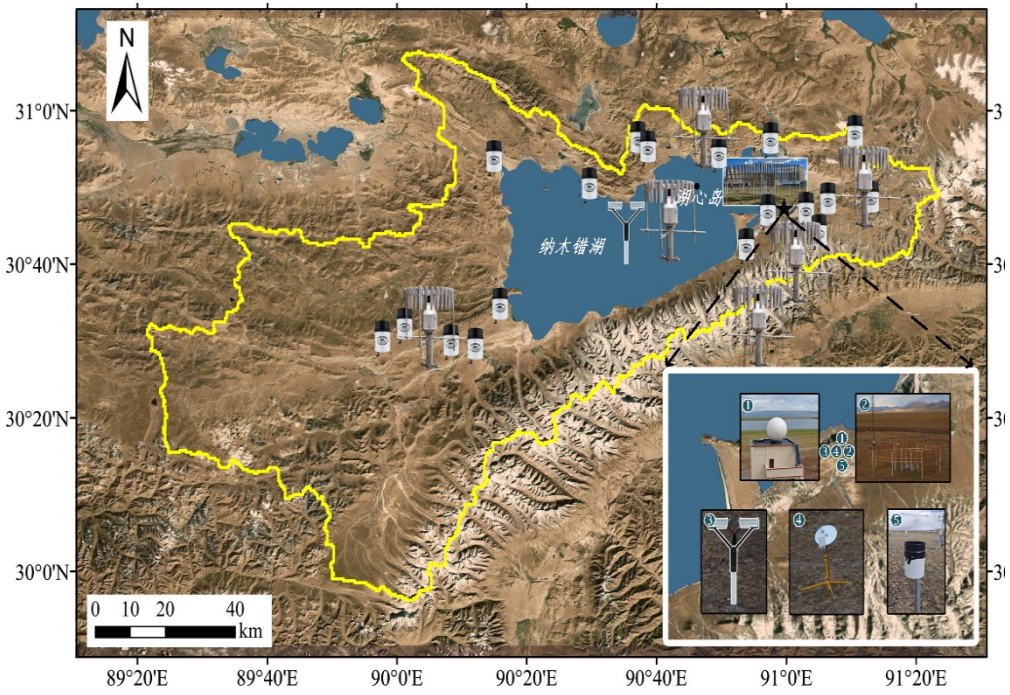

X-band radar

T200B gauge

DFIR

Microrain radar

raindrop spectrometer

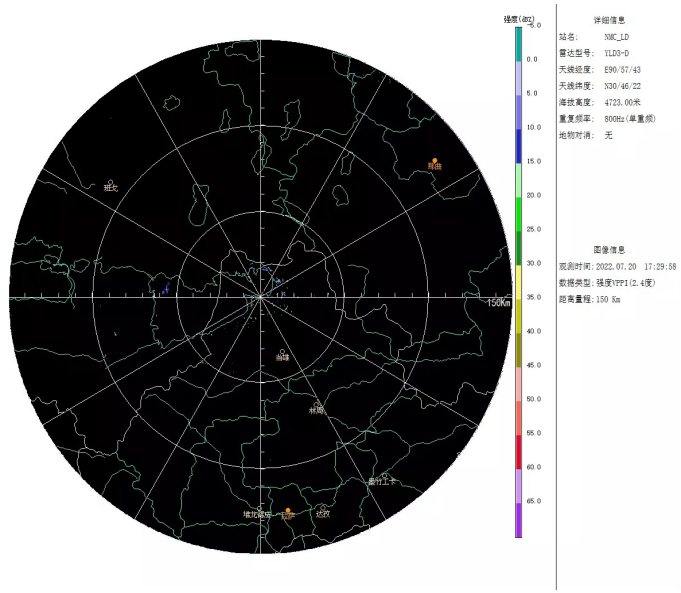

rainfall event on 20 July 2022

- ✓ Consisting of an X-band dual-polarisation radar, a micro-rain radar, a dual-fence system, two raindrop spectrometers and 24 rain gauges around the lake
- ✓ Ability to accurately observe basin-scale precipitation and wind fields

- Observation system in the Qilian Mountains
- Precipitation observation over the Tibetan Plateau
- P-band SAR flight campaign over the Bayi glacier
- International observation alliance of the Third Pole
- Observation system in Germany

2.3 P-band SAR flight campaign over the Bayi glacier

- **Objective**: Tackle the challenge in monitoring the glacier thickness using RS, and support the validation of China P-band SAR satellite mission
- **Content**: The Bayi Glacier located in the upper reaches of Heihe River, was selected to carry out joint P-band SAR-based airborne and ground experiment, to validate the performance of domestic P-band SAR system and the accuracy of SAR tomograph (TomoSAR) algorithm to retrieve glacier thickness

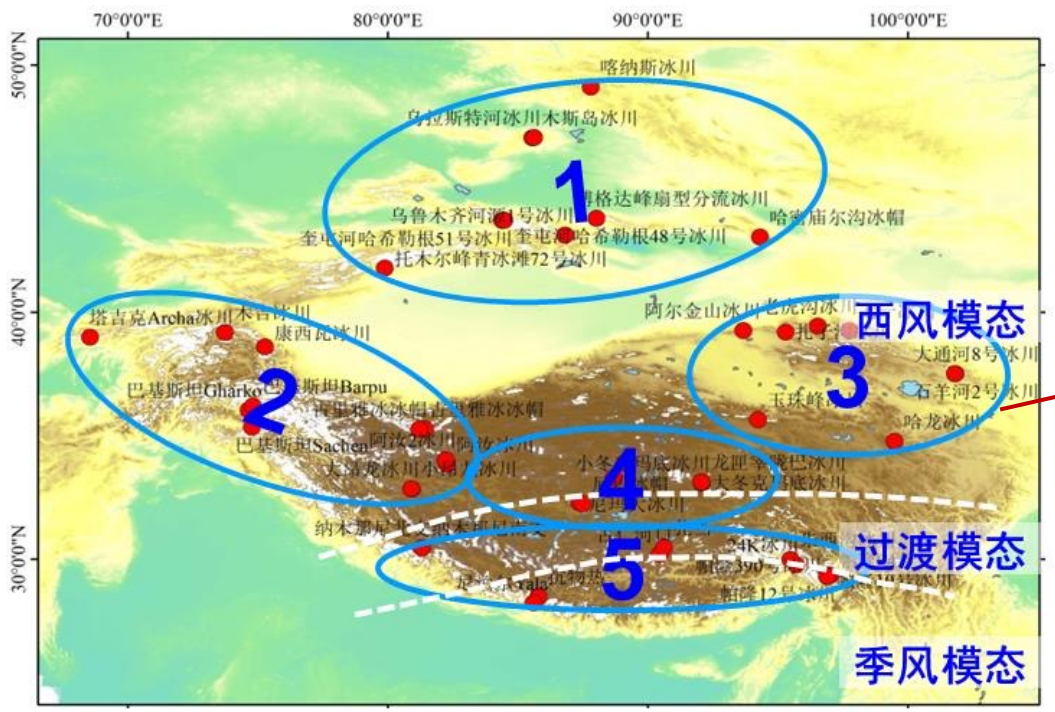

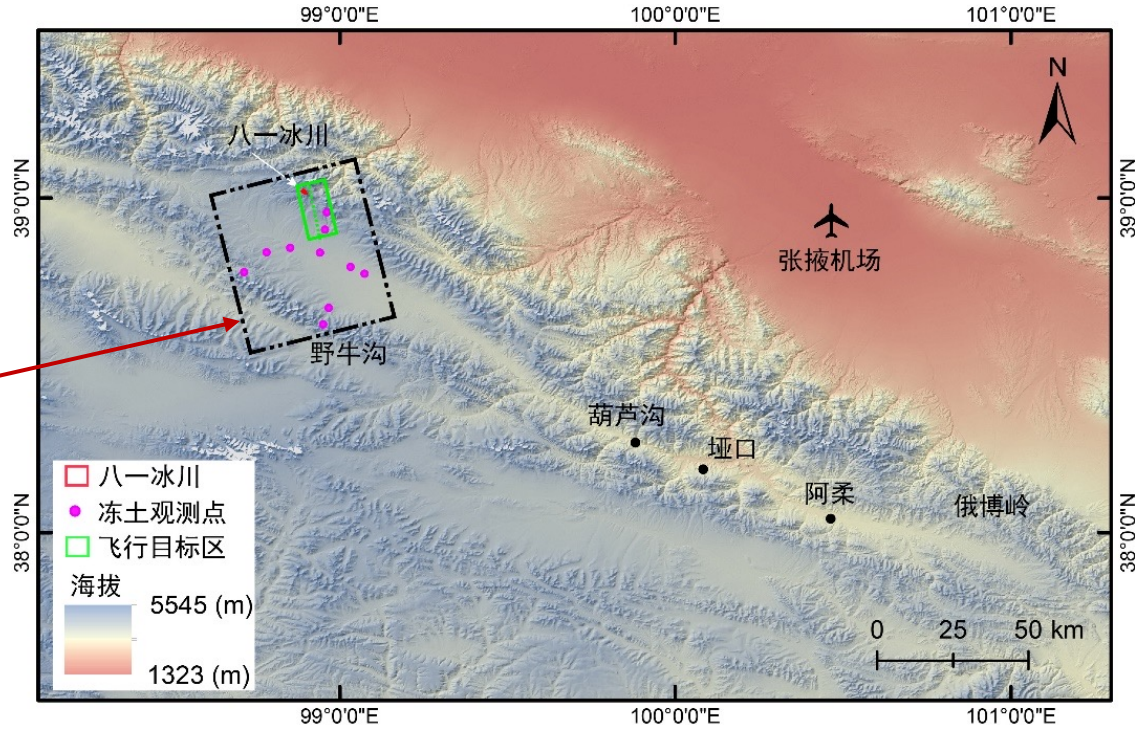

2.3 P-band SAR flight campaign over the Bayi glacier

Flight Platform

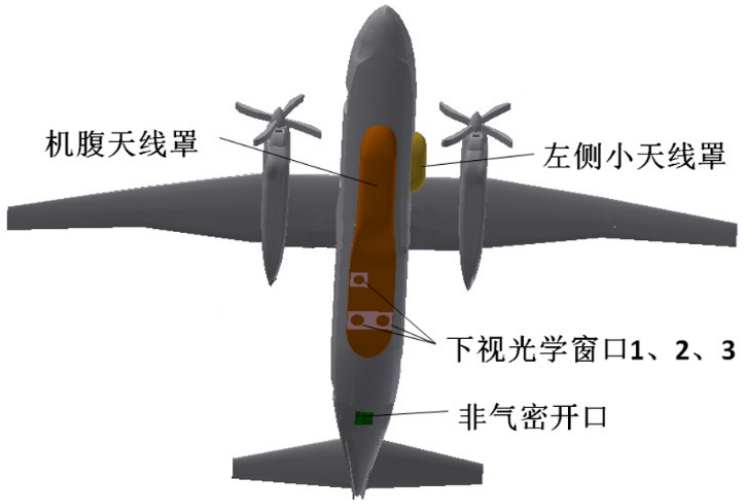

Xinzhou 60 Remote Sensing Aircraft
B configuration

Instruments

- P-band SAR: linear FM pulse signal, 0.58GHz, HH polarization
- L-band SAR: FM continuous wave signal, 1.5GHz, Full polarization
- LiDAR: ALS70, 1064nm
- Optical Camera: high resolution digital Camera ADS80

2.3 P-band SAR flight campaign over the Bayi glacier

Two observation modes are implemented to test the accuracy of TomoSAR algorithm:

- P+L-band SAR tomograph mode
- Synchronous observation with multiple instruments: LiDAR, P+L-band SAR

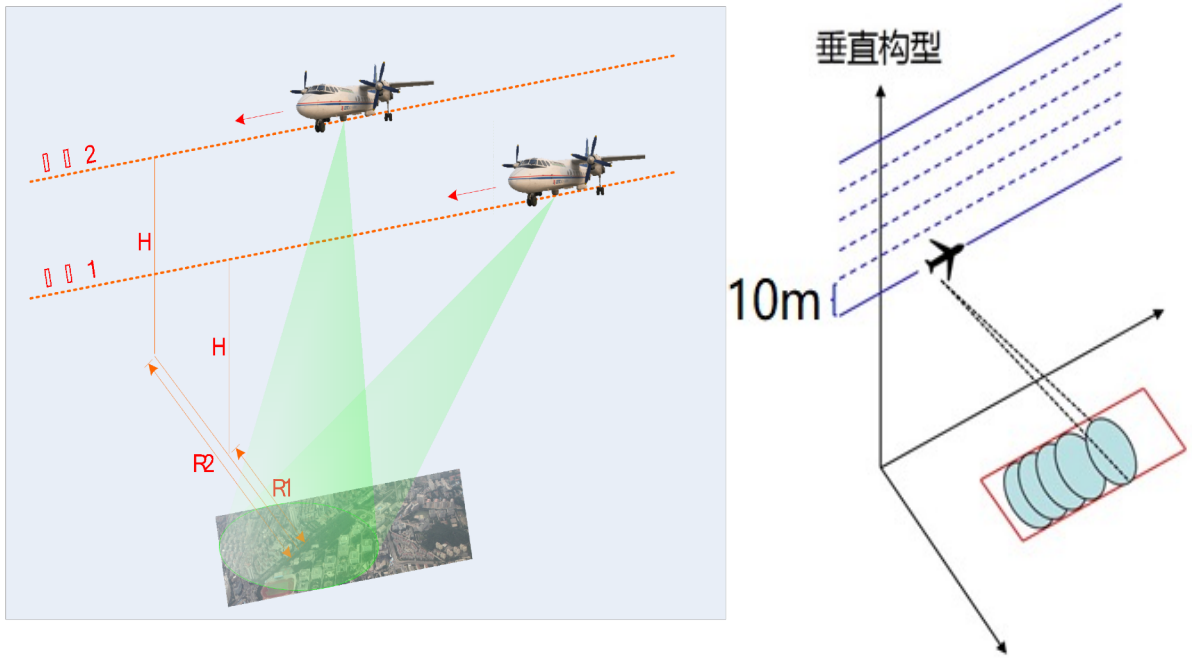

P+L-band SAR tomograph mode

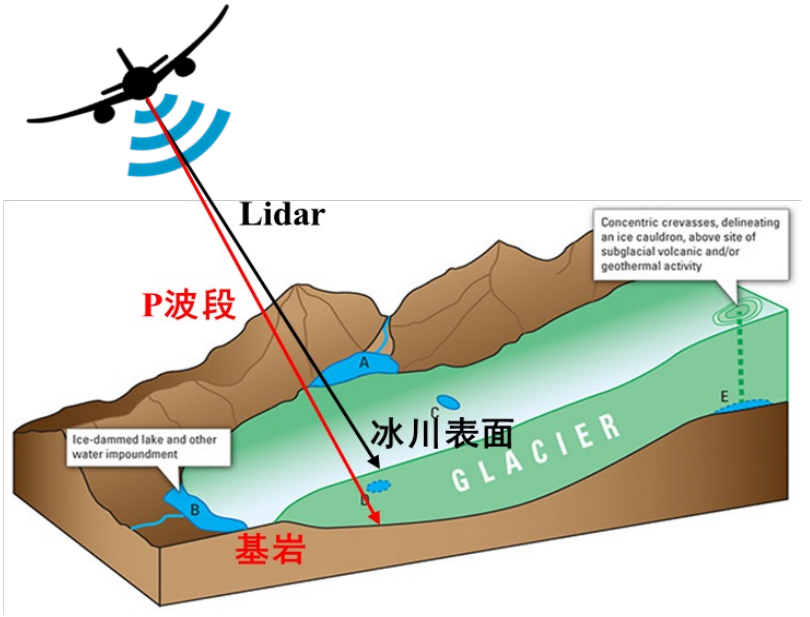

LiDAR and P+L-band SAR

2.3 P-band SAR flight campaign over the Bayi glacier

- Flight altitude: 6335-6500 m; Relative altitude: 1500-1665 m; Incidence angle: 35°
- Synchronous observation with multiple instruments: 4 flight routes
- SAR tomograph observation: 12 flight altitudes; Vertical baseline length: 15 m; Total baseline length: 165 m; Repeat flight 3-4 times
- P-band SAR tomography resolution is 2.5-3.7m, and the maximum unambiguous height is 27.5-40.2m

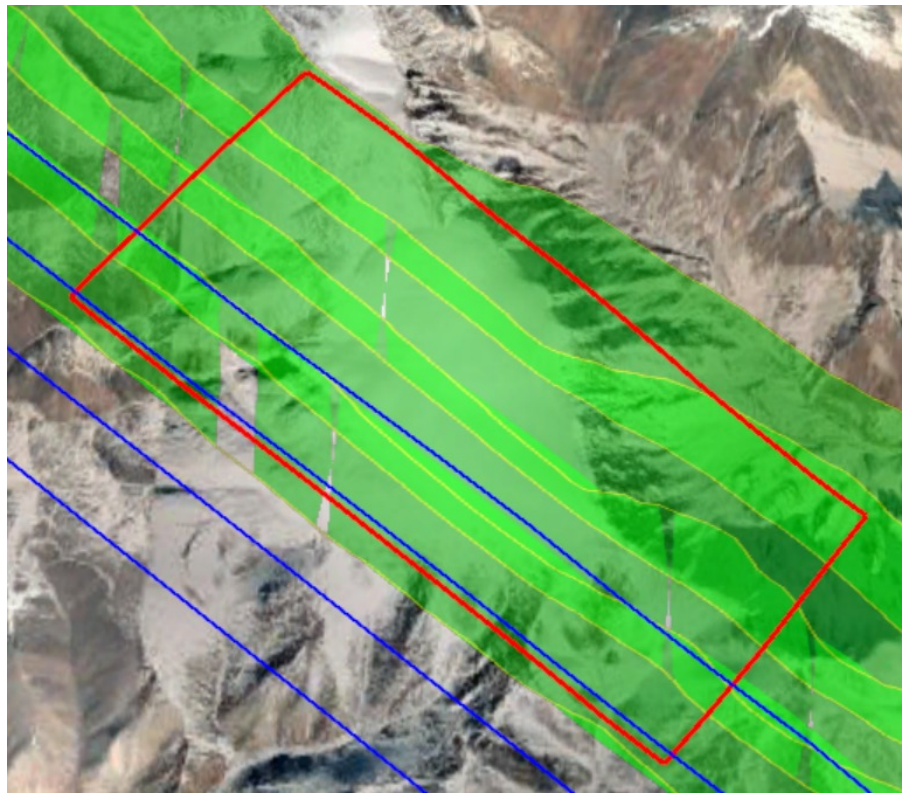

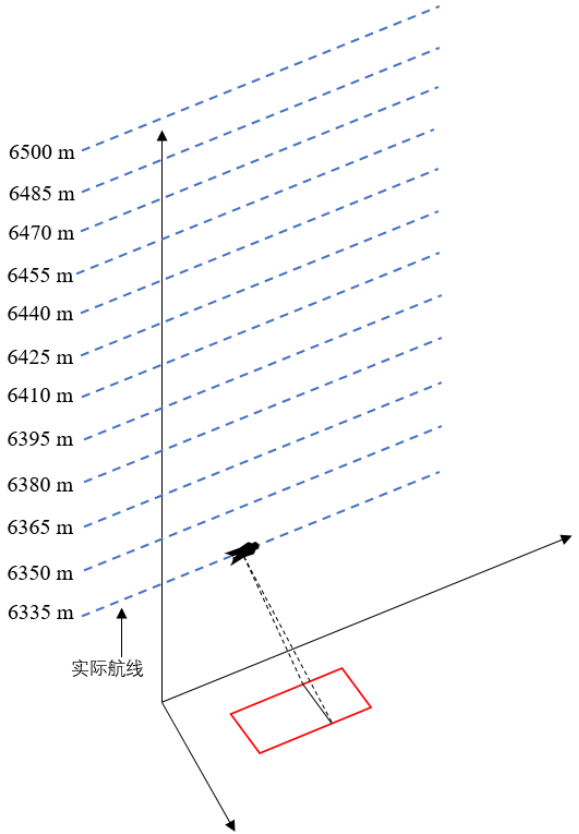

2.3 P-band SAR flight campaign over the Bayi glacier

Ground calibration of airborne instrument

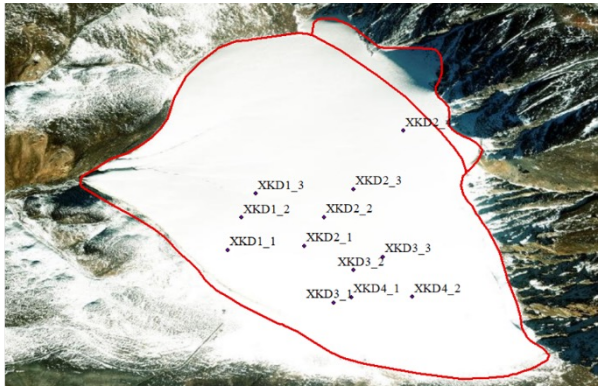

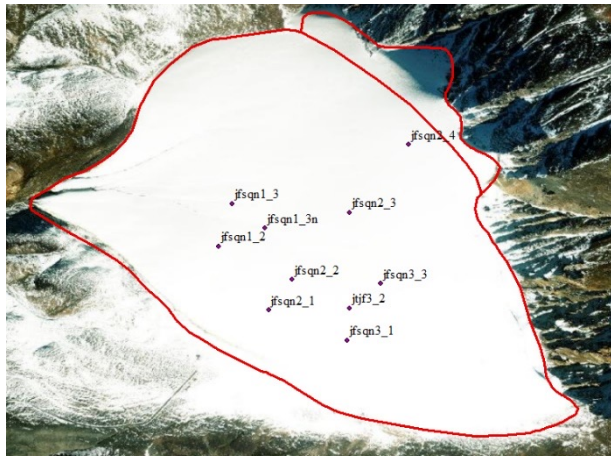

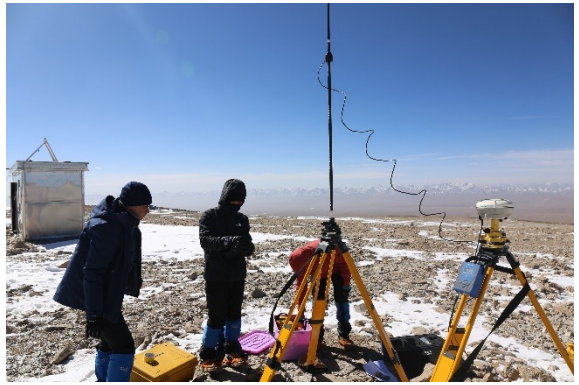

Layout of optical image control points

SAR corner reflector deployment

RTK positioning measurement

2.3 P-band SAR flight campaign over the Bayi glacier

GPR observation of glacier thickness

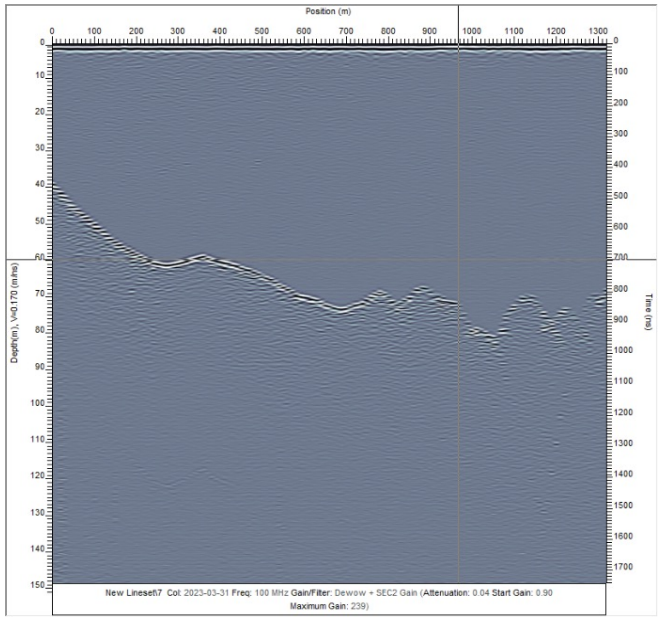

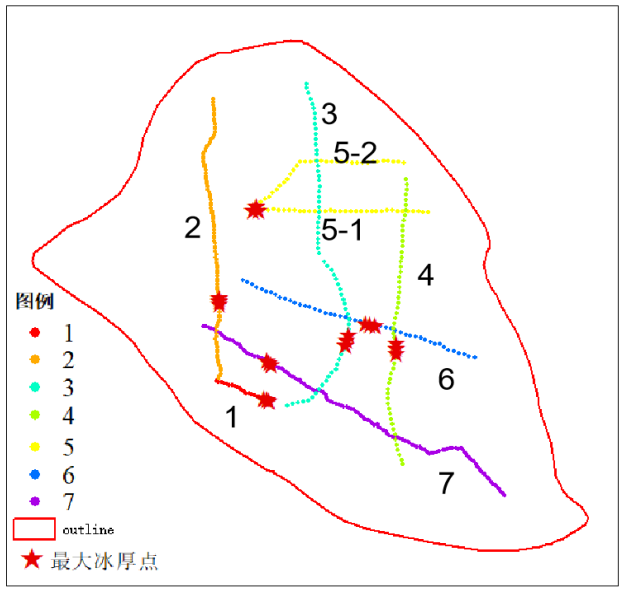

测线序号	经度	纬度	冰厚(m)
1	98.890619	39.014446	55.06
	98.890516	39.01449	54.28
	98.890408	39.014529	53.9
2	98.888439	39.017891	99.83
	98.888442	39.01799	101.58
	98.888409	39.018086	97.89
3	98.893981	39.016425	101.59
	98.894035	39.016603	102.77
	98.894118	39.016784	103.55
4	98.896201	39.01649	99.81
	98.896217	39.016318	101.19
	98.896201	39.016125	101.39
5-1	98.890144	39.021198	71.29
	98.88991	39.021188	72.08
5-2	98.889919	39.021189	74.42
	98.890063	39.021347	75.8
6	98.89531	39.017119	95.13
	98.895071	39.017145	95.53
	98.894854	39.017204	94.94
7	98.890718	39.015743	79.37
	98.890615	39.015802	80.15
	98.890534	39.015871	79.96

- Observation system in the Qilian Mountains
- Precipitation observation over the Tibetan Plateau
- P-band SAR flight campaign over the Bayi glacier
- International observation alliance of the Third Pole
- Observation system in Germany

2.4 International observation alliance of the Third Pole

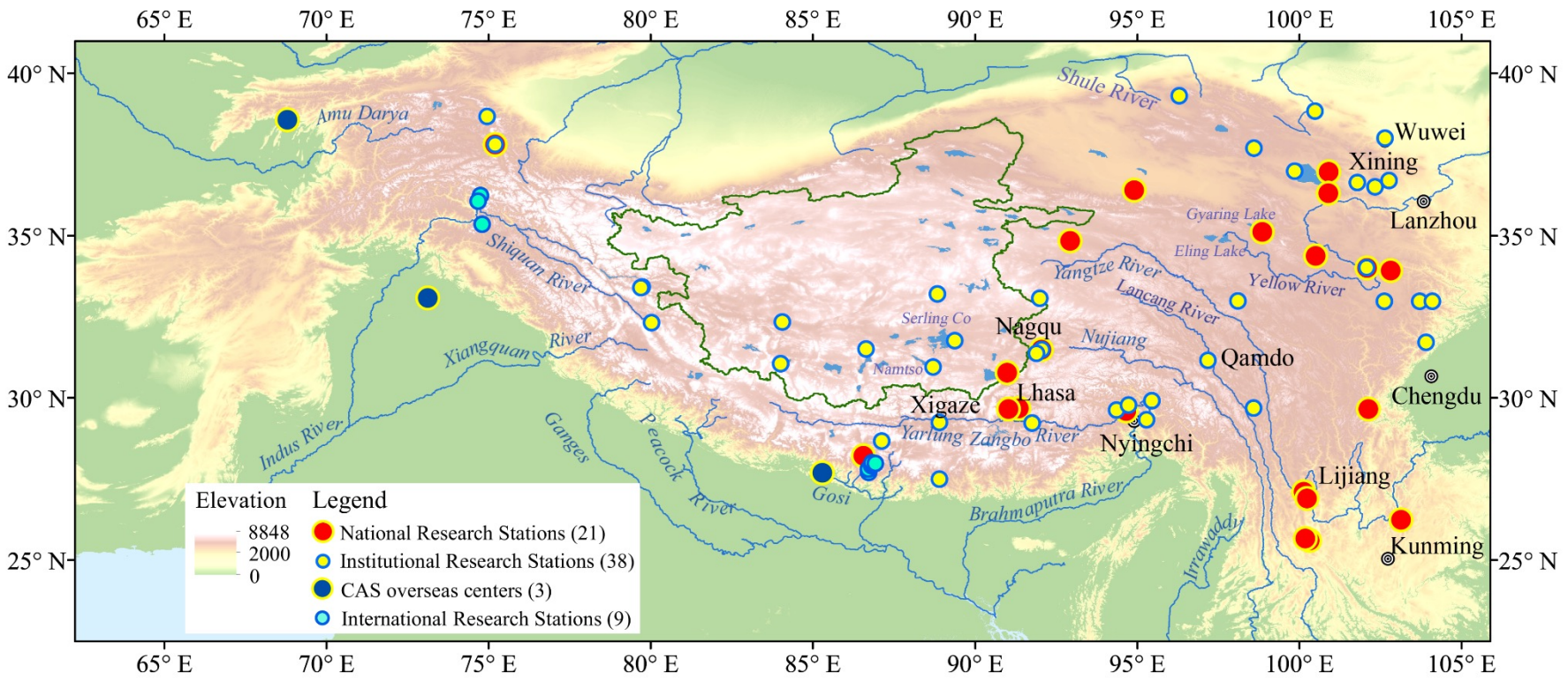


NAMORS(Nam co)


QOMS(Qomolangma)


NaPlaCE(Nagqu)


SETORS(Southeast TP)


NASDE(Ngari)


SHORS(Shuanghu)


MAWORS(Muztagh)


Medog Observation & Research Center for Earth Landscape and Earth System

- 59 domestic comprehensive stations on TP
  - 21 national stations, 38 institutional stations
- 12 international field stations
  - 3 CAS oversea centers, 3 ITPCAS oversea stations, 6 stations of Pyramid International Laboratory

8 stations operated by ITPCAS, including 3 national stations

2.4 International observation alliance of the Third Pole

Scientific observation experiments

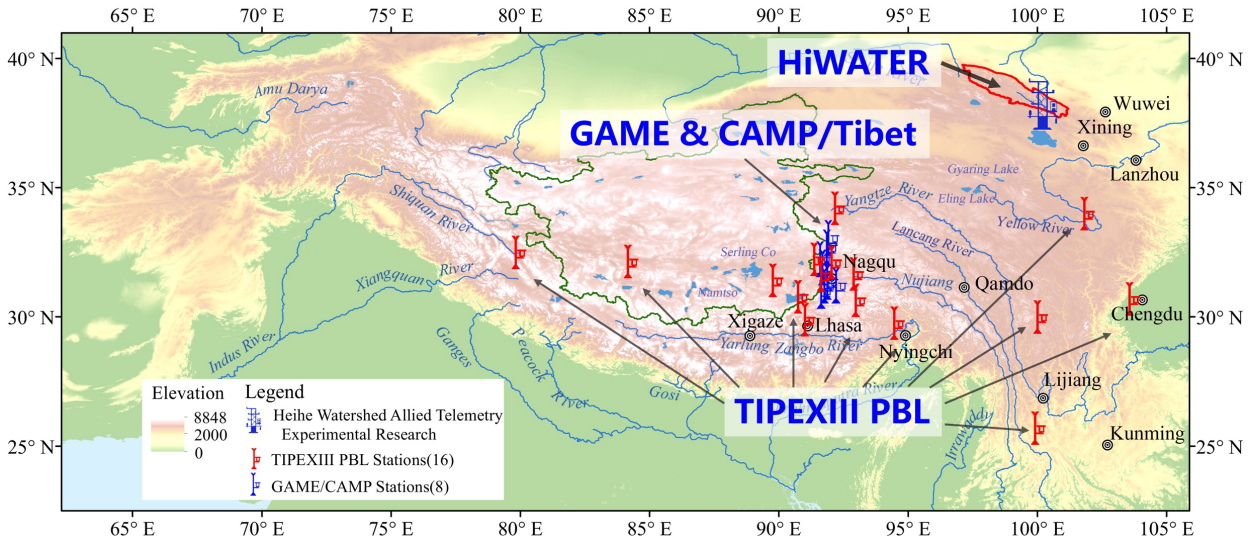

Thematic observations

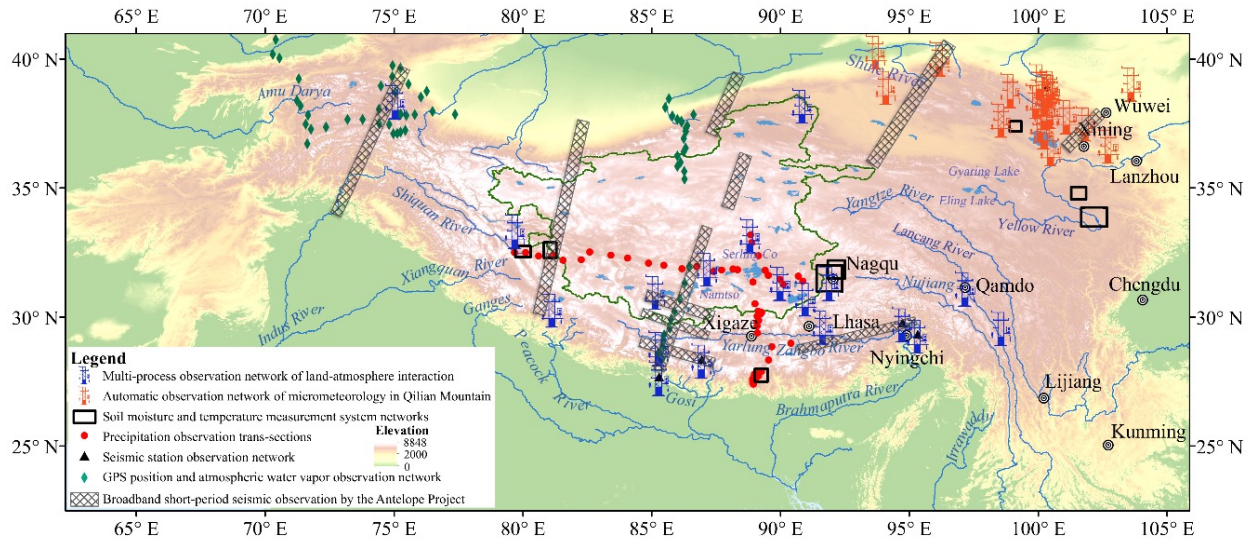

2.4 International observation alliance of the Third Pole

Objective: Build a space-airborne-ground integrated IoT observation system, consisting of a field observation system and a remote sensing observation system

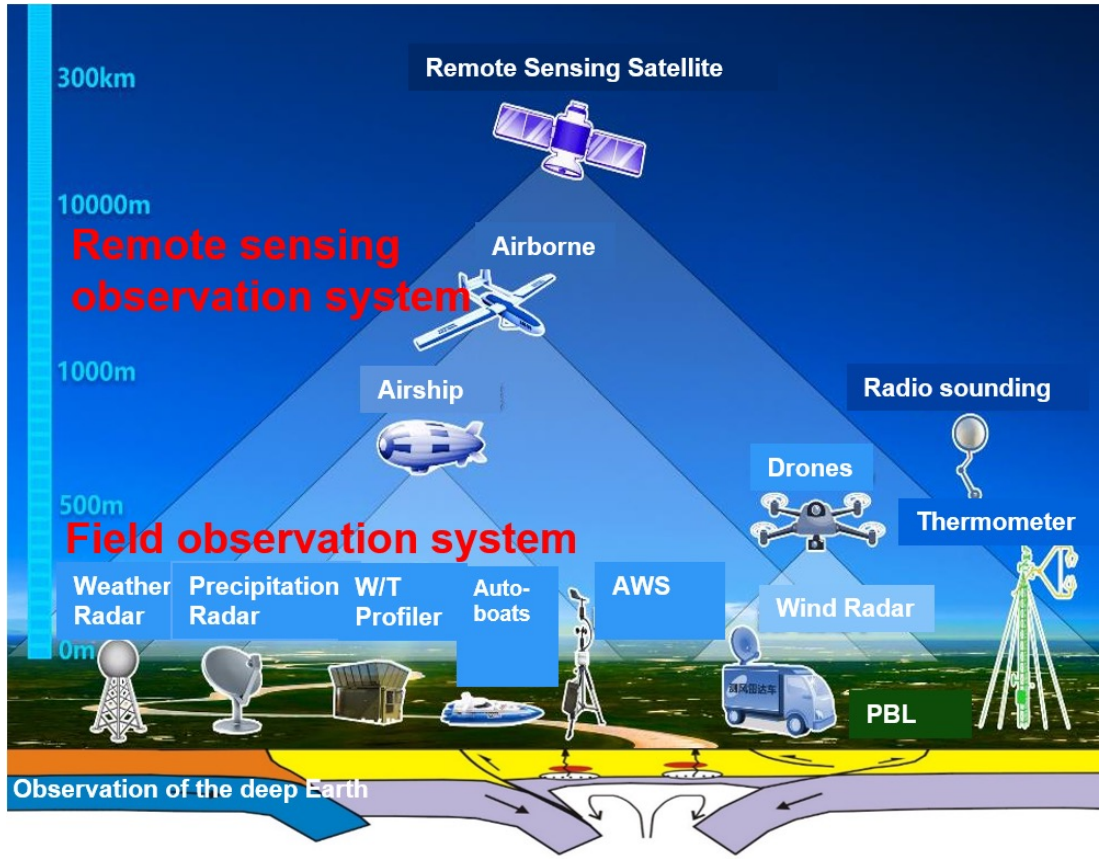

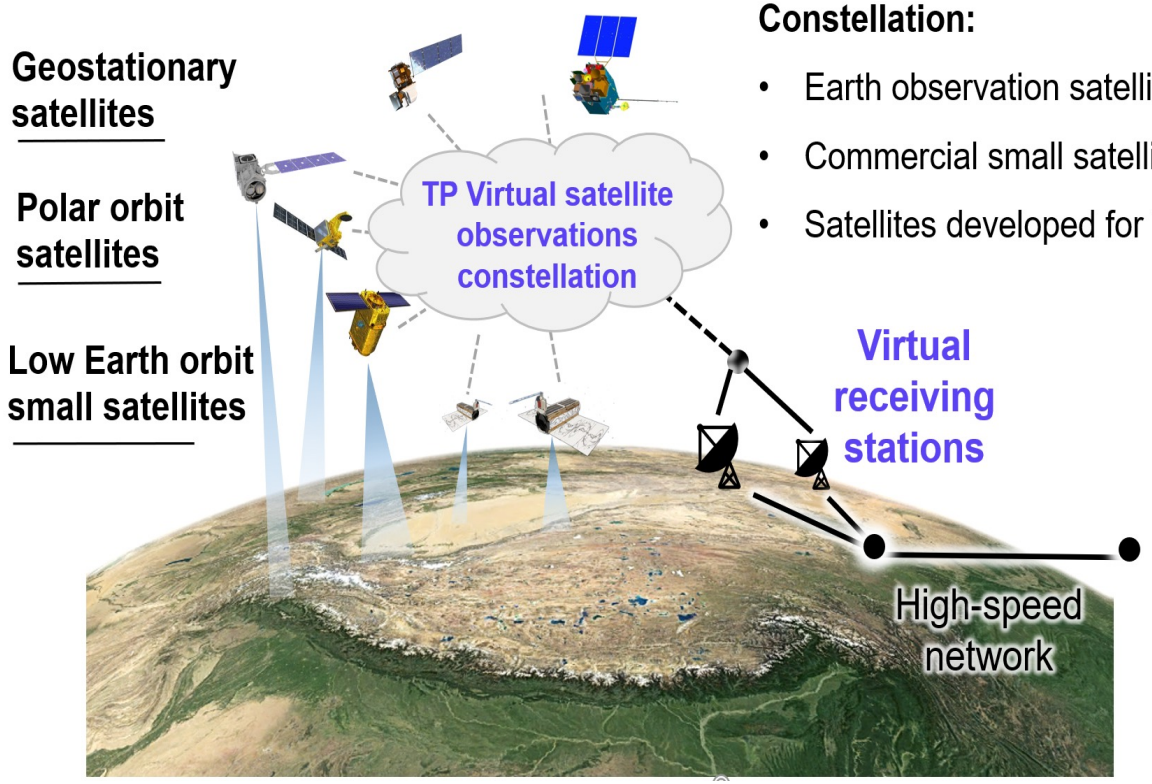

- Observation system in the Qilian Mountains
- Precipitation observation over the Tibetan Plateau
- P-band SAR flight campaign over the Bayi glacier
- International observation alliance of the Third Pole
- Observation system in Germany

2.5 Observation system in Germany

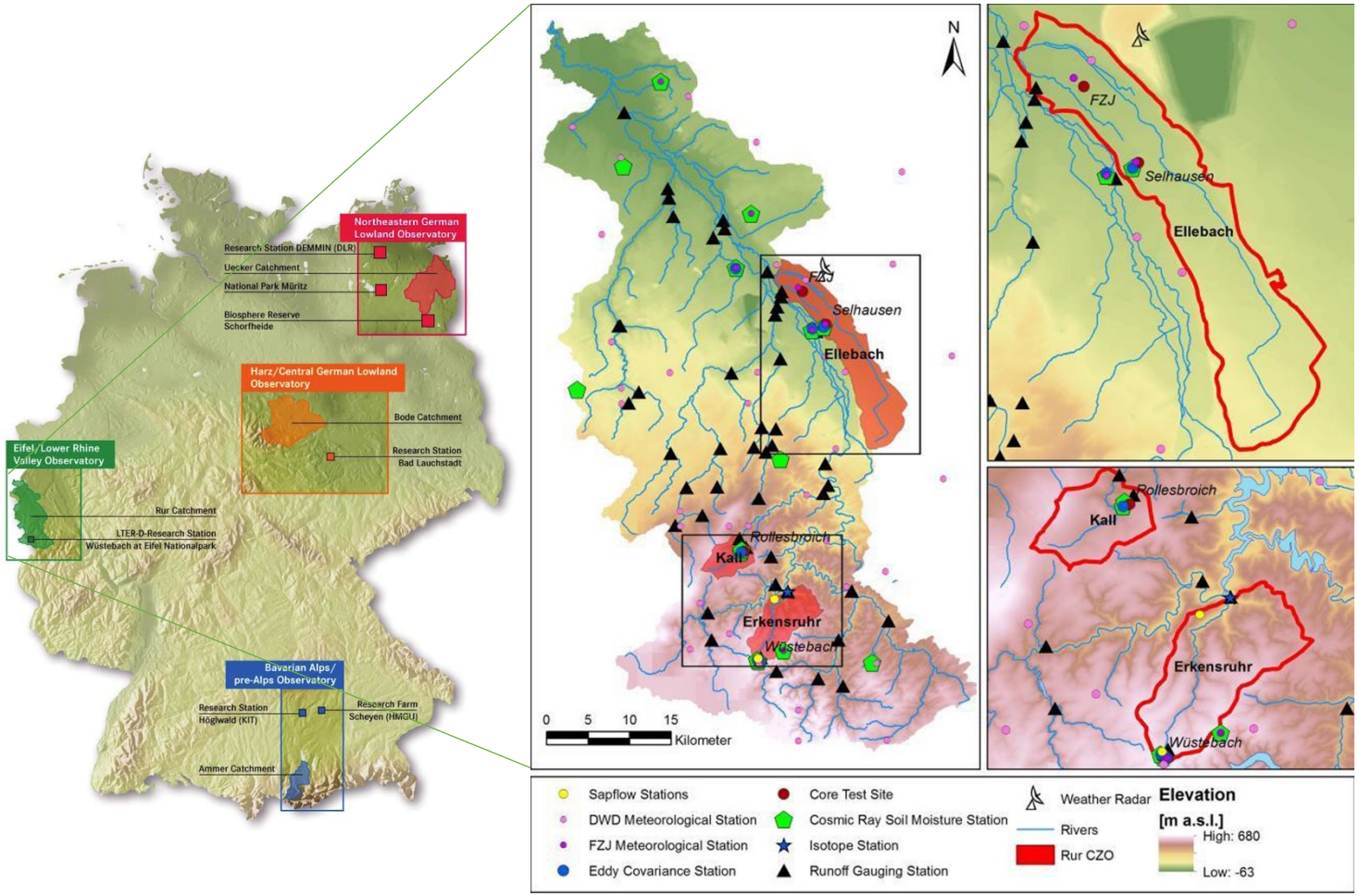

- TERENO Eifel/Lower Rhine Valley Observatory has 3 highly equipped sites

Meteorology (12 meteorological stations)

Land surface fluxes (sensible, latent and ground heat flux, carbon flux, four radiation components: 4 EC-stations)

Other water and energy related variables (runoff, water quality, groundwater levels, soil moisture content, soil temperature)

13 Cosmic-Ray Neutron Sensing stations

Source: Zacharias, S. et al, 2011; Bogena, H.R. et al, 2018.

3. Current progress of the project

- Retrieval of key ecohydrological variables from multi-source RS data
- Retrieval of key cryosphere variables from multi-source RS data
- Development of real time RS LDAS
- Closing water cycle at the watershed/regional scale based on the LDAS

3.1.1 soil moisture

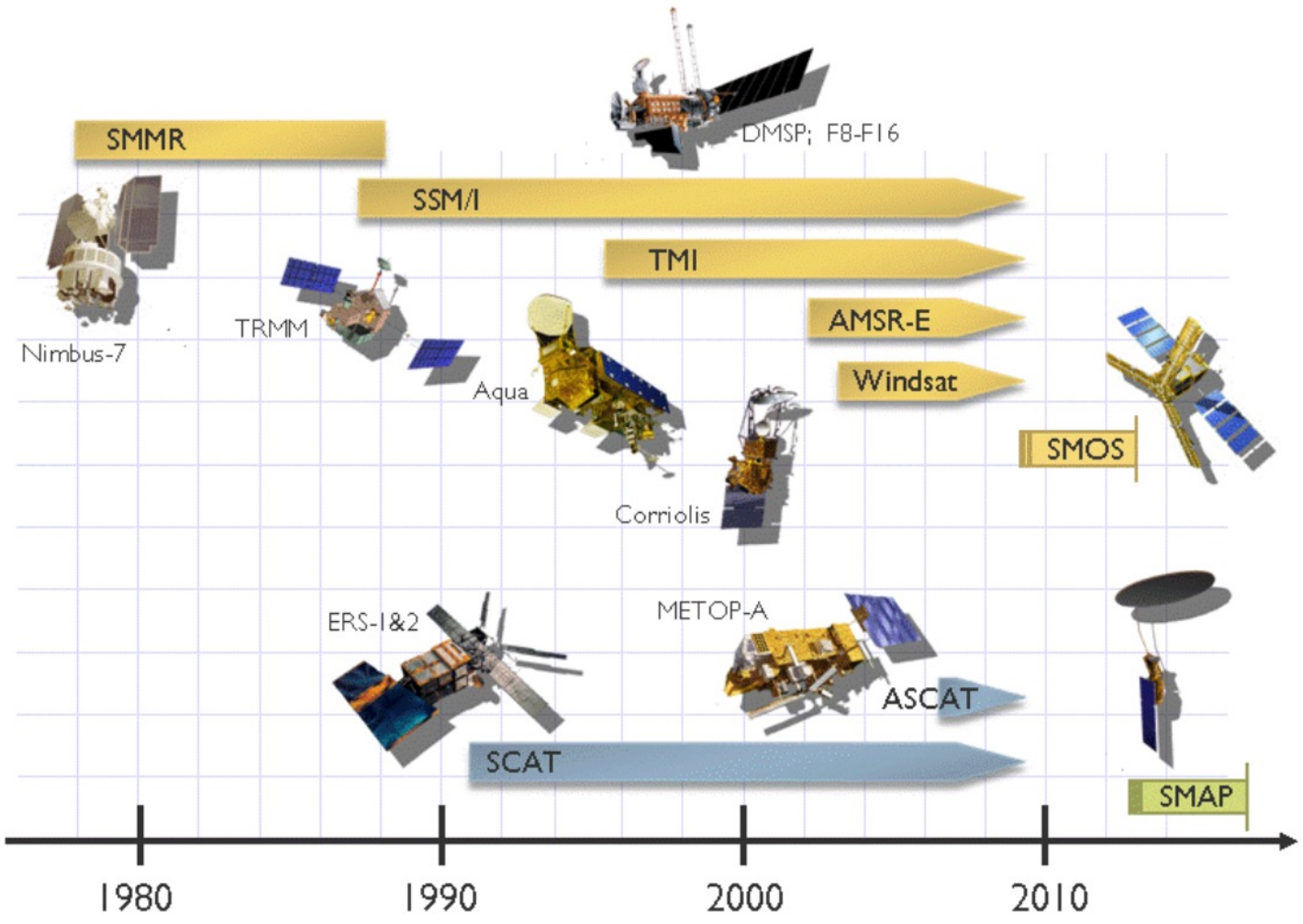

- RS soil moisture from space-missions and their timelines.

Source: European Space Agency and Technische Universität Wien.

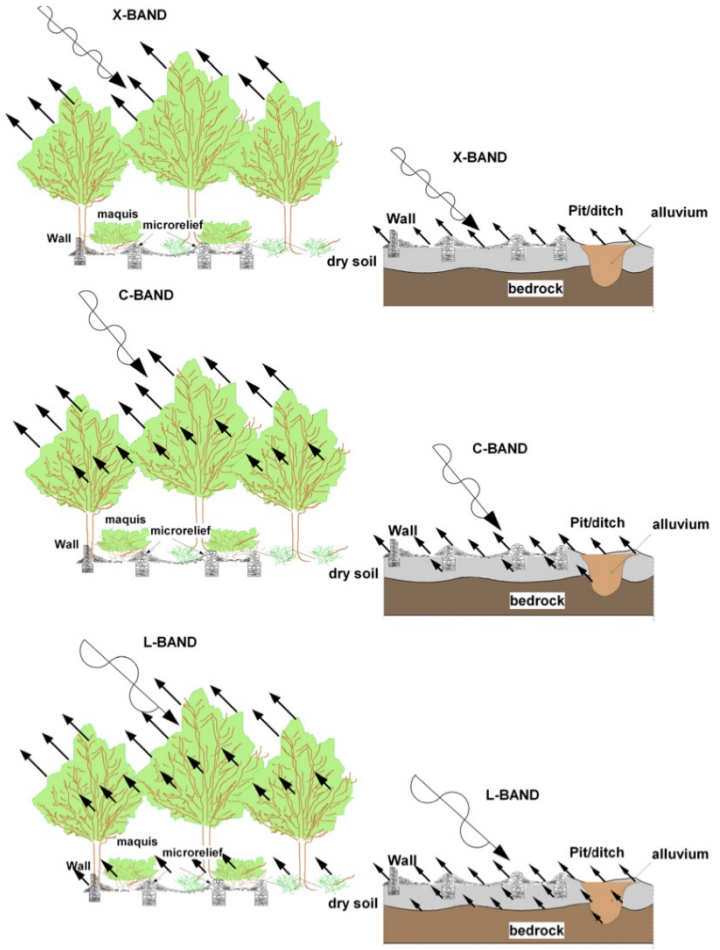

- Different penetration depths of SAR.

Source: Rosa, L & Masini, N., 2013.

3.1.1 soil moisture

- List of RS soil moisture used in this research.

Name of Satellite	Name of Product	Temporal Resolution	Band	Spatial Resolution	Projections	Period
Soil Moisture and Ocean Salinity - SMOS	SMOS CATDS L3 Daily Soil Moisture	Daily	L-band	25 km	Equal-Area Scalable Earth (EASE) Grid	2010.01-ongoing
Soil Moisture Active Passive Mission - SMAP	SMAP Enhanced L3 Radiometer Global and Polar Grid Daily Soil Moisture	Daily	L-band	9 km	Equal-Area Scalable Earth (EASE) Grid	2015.04-ongoing
Advanced Microwave Scanning Radiometer 2 - AMSR2	AMSR2/GCOM-W1 surface soil moisture (LPRM) L3 Daily Soil Moisture	Daily	X-band	25 km	Equal-Area Scalable Earth (EASE) Grid	2012.07-ongoing
Advanced SCATterometer - ASCAT	Metop ASCAT SSM DR2021 time series sampling (H119)	Daily	C-band	12.5 km	Discrete Global Grid (DGG)	2007.01-2020.12

3.1.1 soil moisture

- **Objective**: Tackle the issue of missing and inconsistent quality from soil moisture RS data of single sensor, and generate the seamless and accurate coarse-scale merged soil moisture RS product
- **Content**: On the Tibetan Plateau, the AMSR-2, SMOS, ASCAT-A and ASCAT-B soil moisture products in both ascending and descending were spatiotemporally fused to obtain 25 km merged soil moisture data based on the Bayesian Maximum Entropy (BME) method

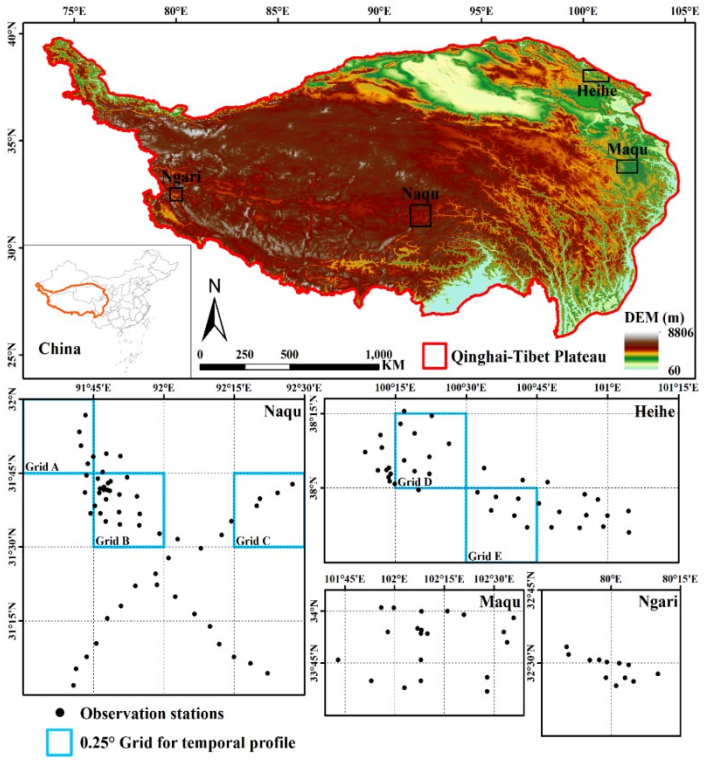

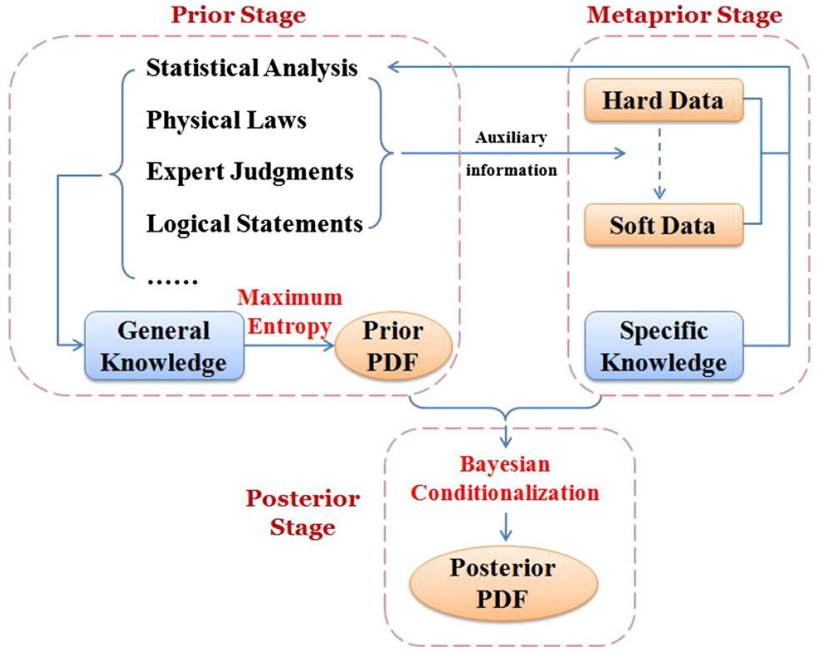

Workflow of the BME analysis

Source: Junyu H & Alexander K., 2017.

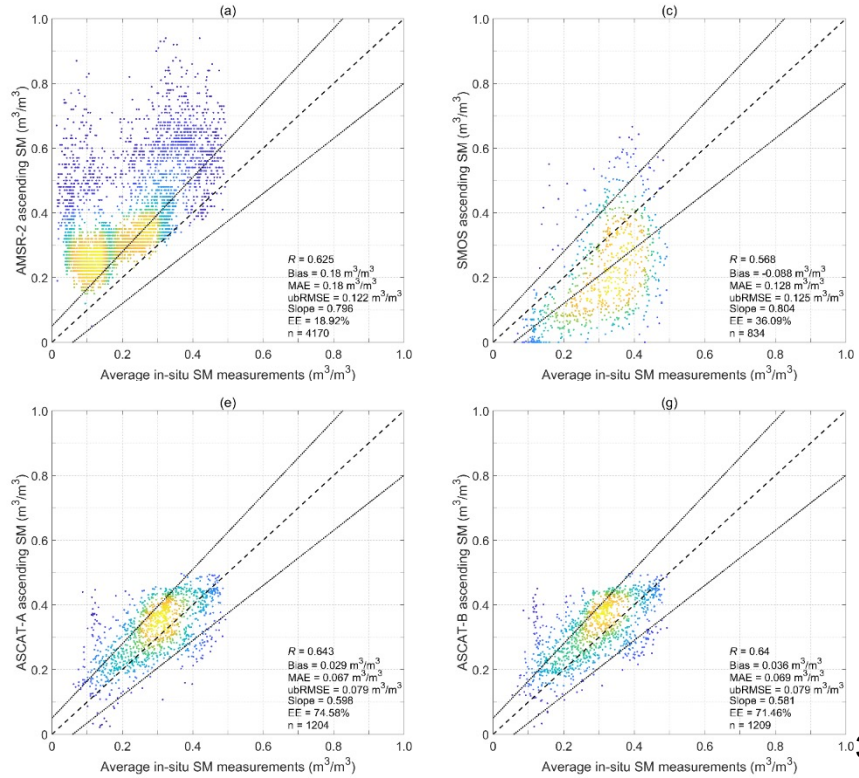

3.1.1 soil moisture

- Temporal variations of daily completeness of AMSR-2, SMOS, ASCAT-A\B, ESA CCI, merged SSM and pixels covered by snow and ice
- Spatial patterns of each pixel's completeness of (a-b) AMSR-2, (c-d) SMOS, (e-f) ASCAT-A, (g-h) ASCAT-B and (i) ESA CCI and (j) merged SSM
- Overall validation and spatial patterns of ESA CCI and merged SSM

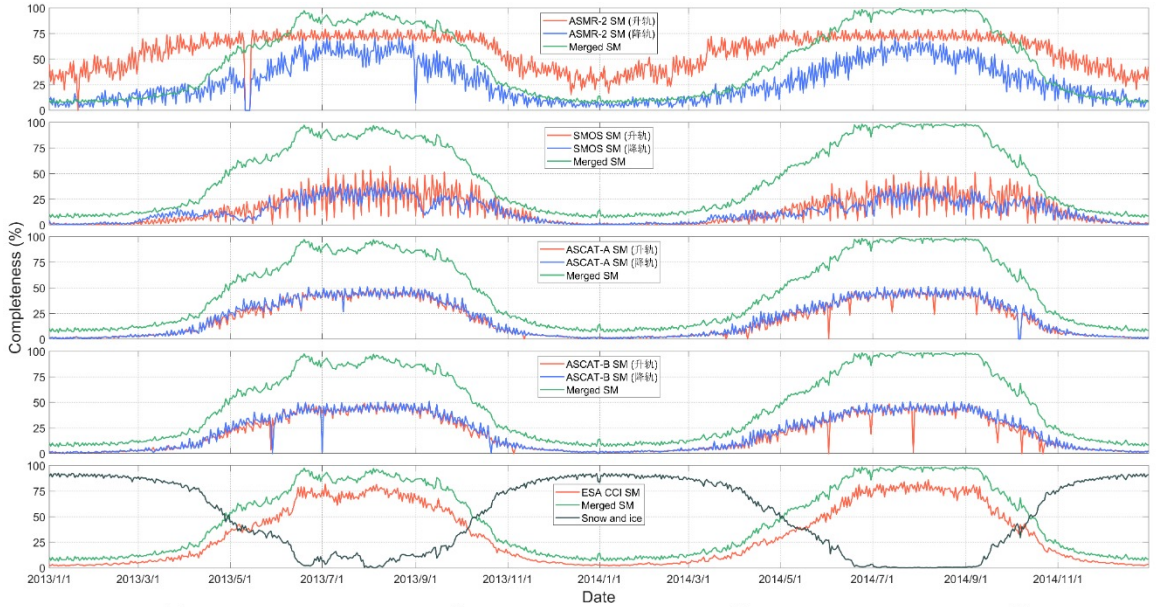

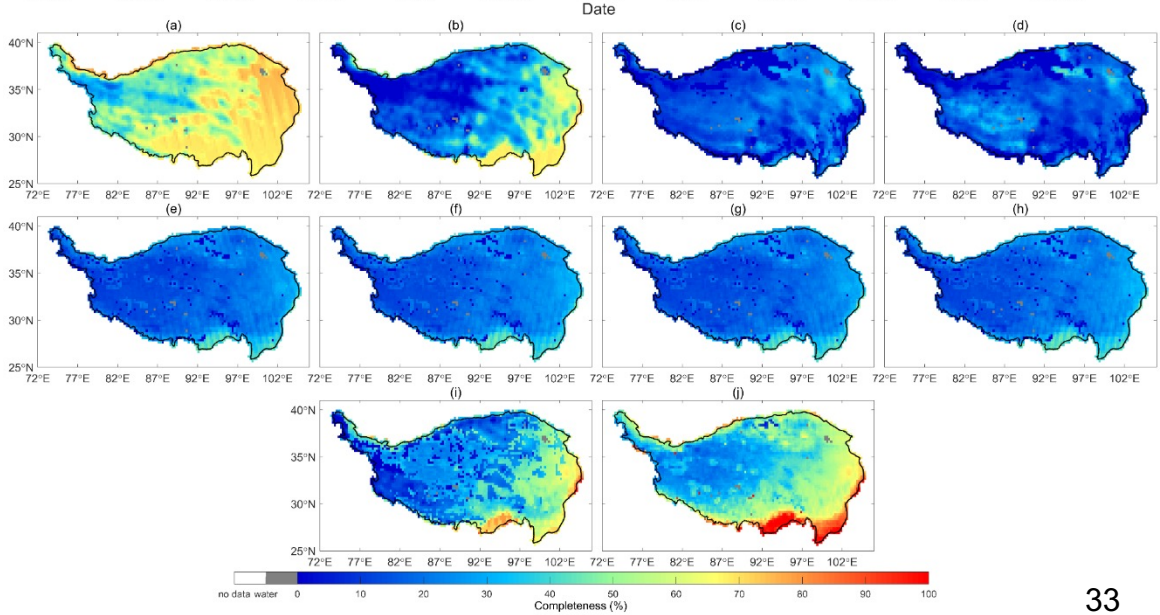

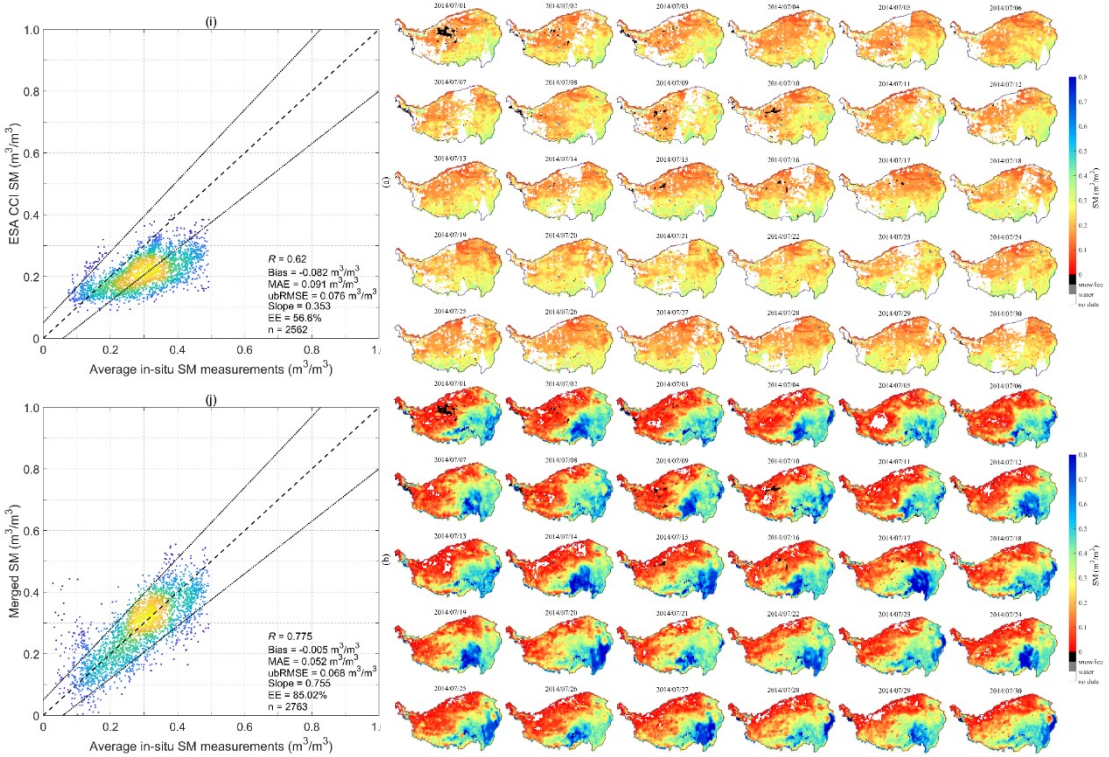

3.1.1 soil moisture

- Results for North-Rhine-Westphalia domain
- Time series of in situ observations against RS soil moisture for 13 CRNS stations.
- Time series of in situ observations against merged soil moisture for 13 CRNS stations.

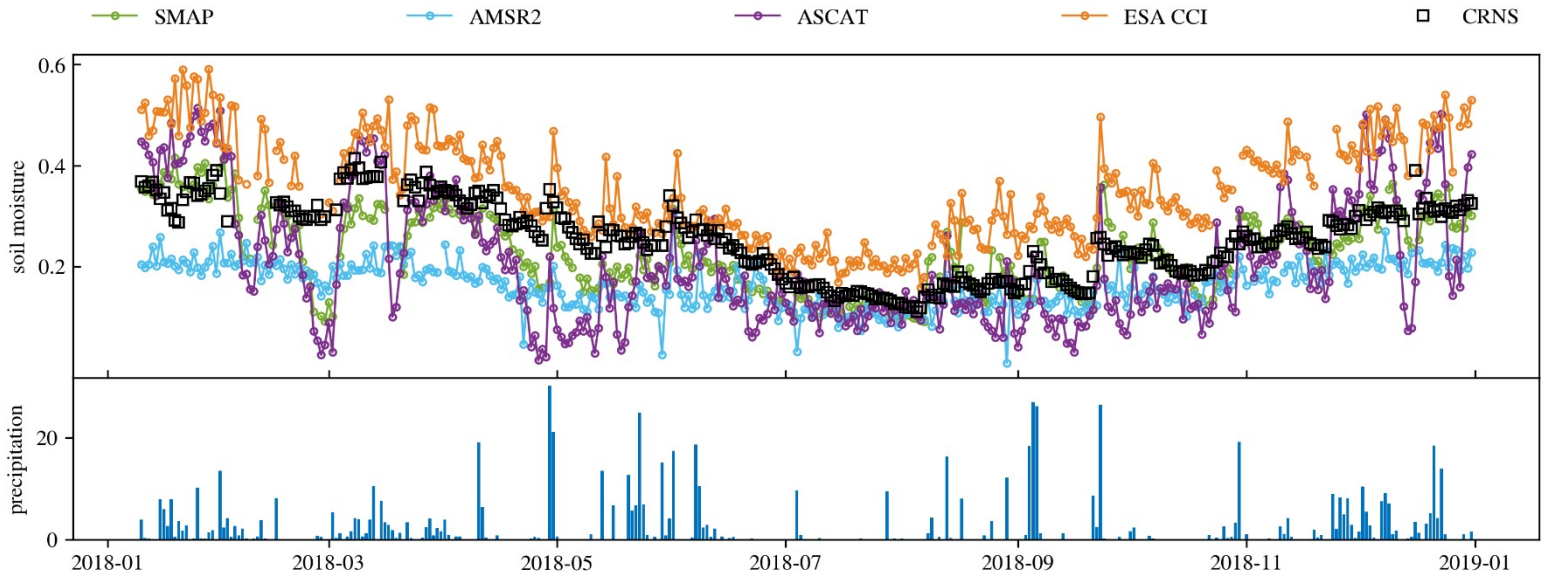

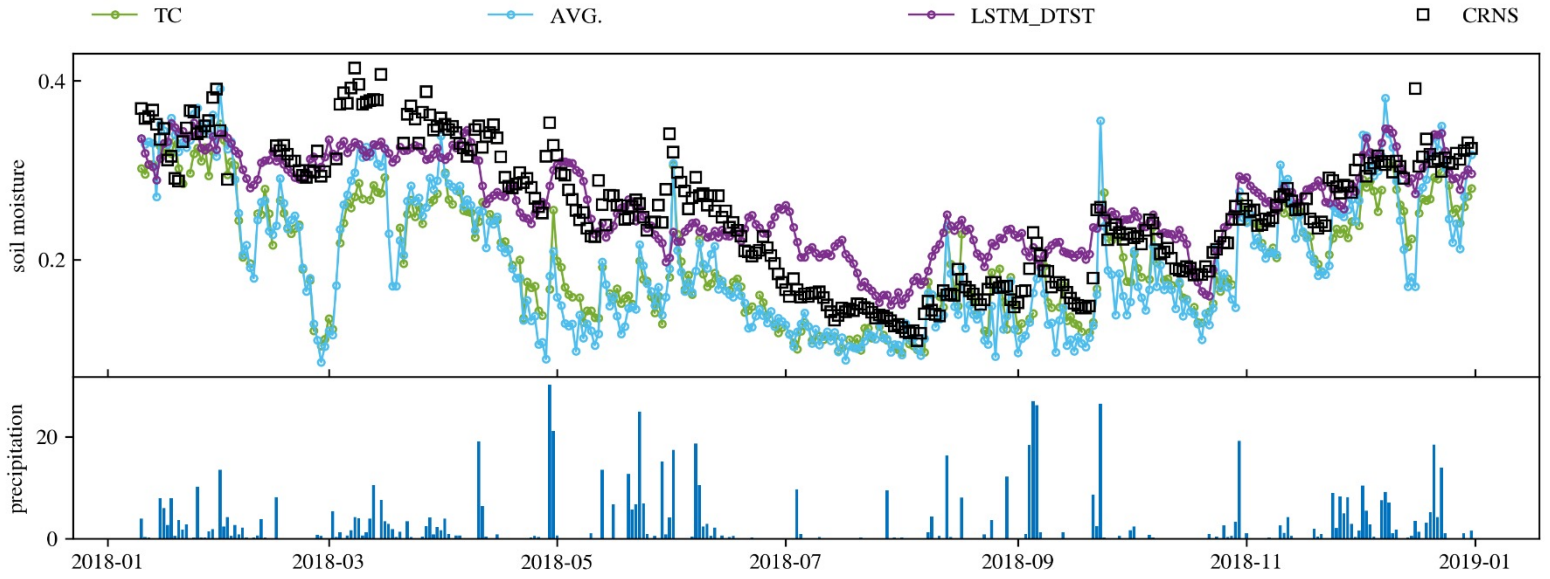

3.1.1 soil moisture

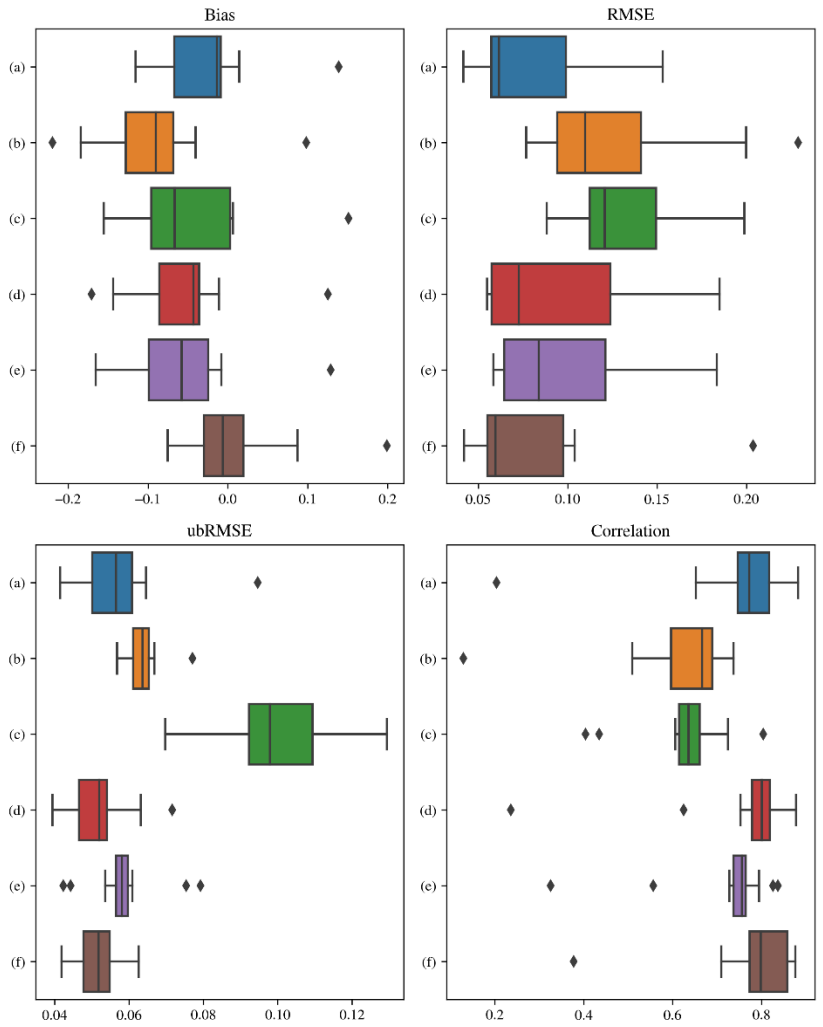

(a) SMAP; (b) AMSR2; (c) ASCAT; (d) Arithmetic average method; (e) TC based method and (f) LSTM method.

- The combined LSTM and TC soil moisture products demonstrate effective integration of the different remote sensing products.
- The LSTM method shows lower bias and better handling of spatial and temporal variations than the other merging methods.
- Data assimilation experiments with merged soil moisture products are currently ongoing.

3.1.2 evapotranspiration

An evapotranspiration (ET) model, named the Simple Terrestrial Hydrosphere Model, was developed for monitoring the global and regional ET pattern based on satellite observations.

Model Description

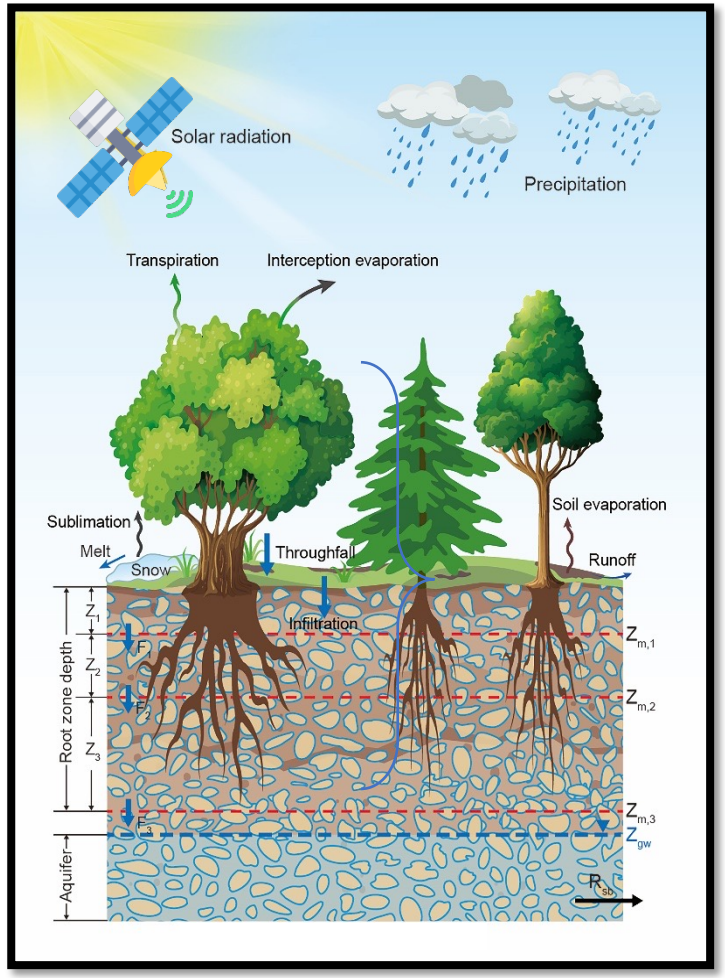

The key process in the model

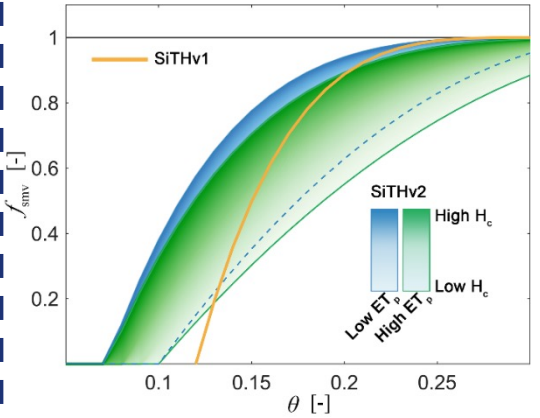

Critical threshold of SWC varied with PFTs and Environmental conditions

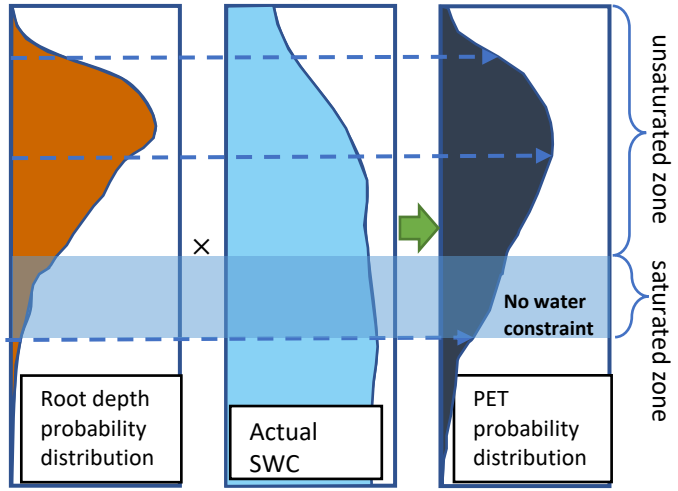

Input Data

- albedo
- vegetation greenness
- vegetation optical depth
- land cover
- emissivity
- radiation
- precipitation
- temperature

Satellite

Reanalysis

Zhang et al., JoH, (2022, 2023)

3.1.2 evapotranspiration

ET Validation at different scale

The newly developed ET model could capture the ET pattern and dynamics at different scales. As a result, the SiTH-derived ET estimates ranked well in similar products.

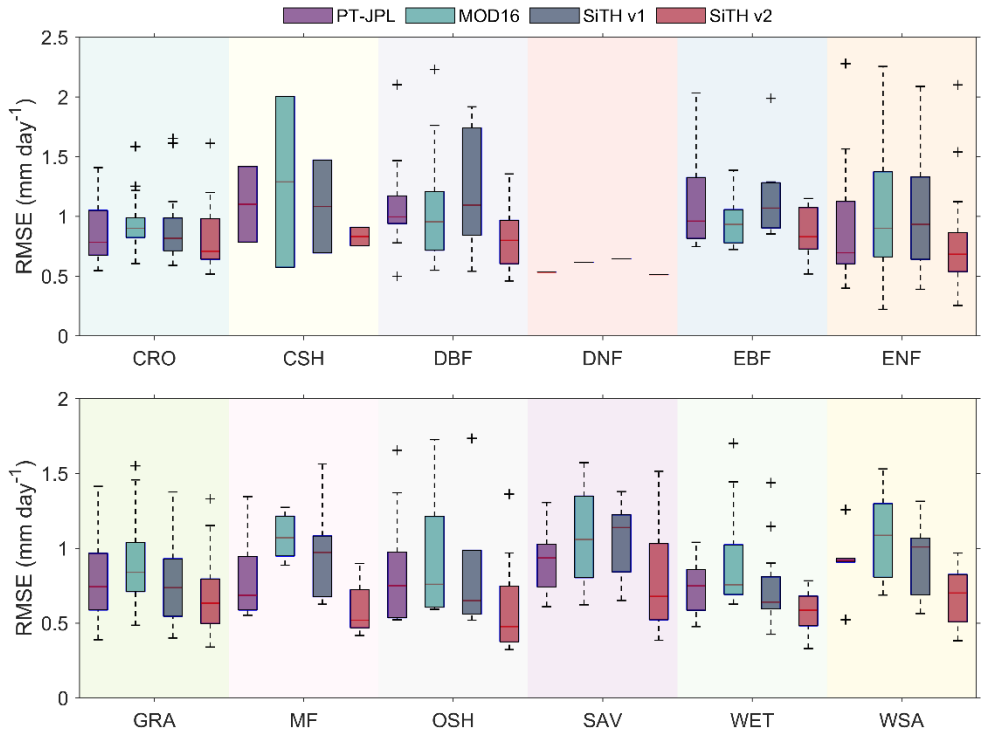

In-situ validation at PFTs level

Global pattern and zonally mean comparison

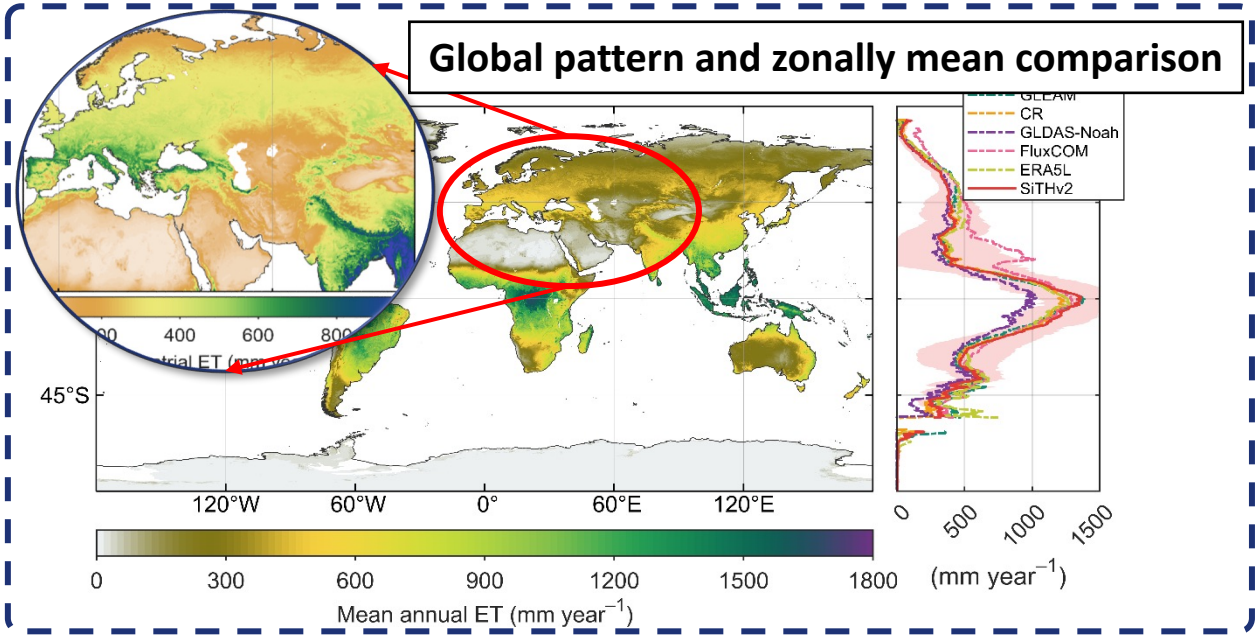

Global terrestrial ET variation and trend

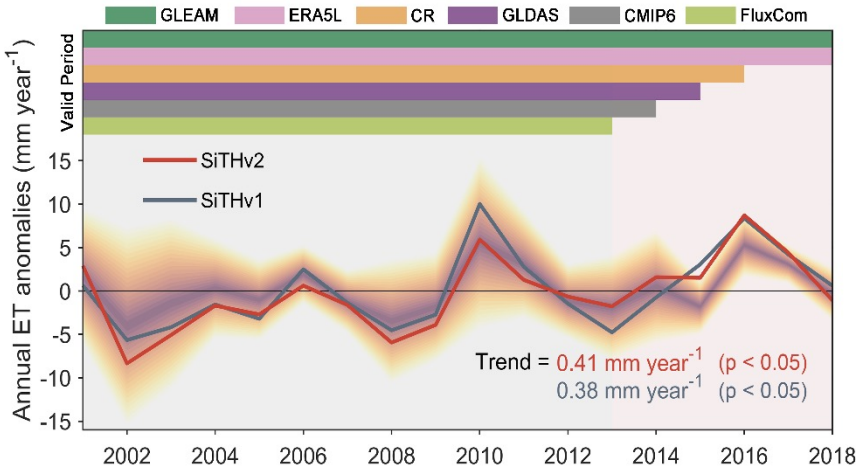

3.1.3 irrigation area mapping

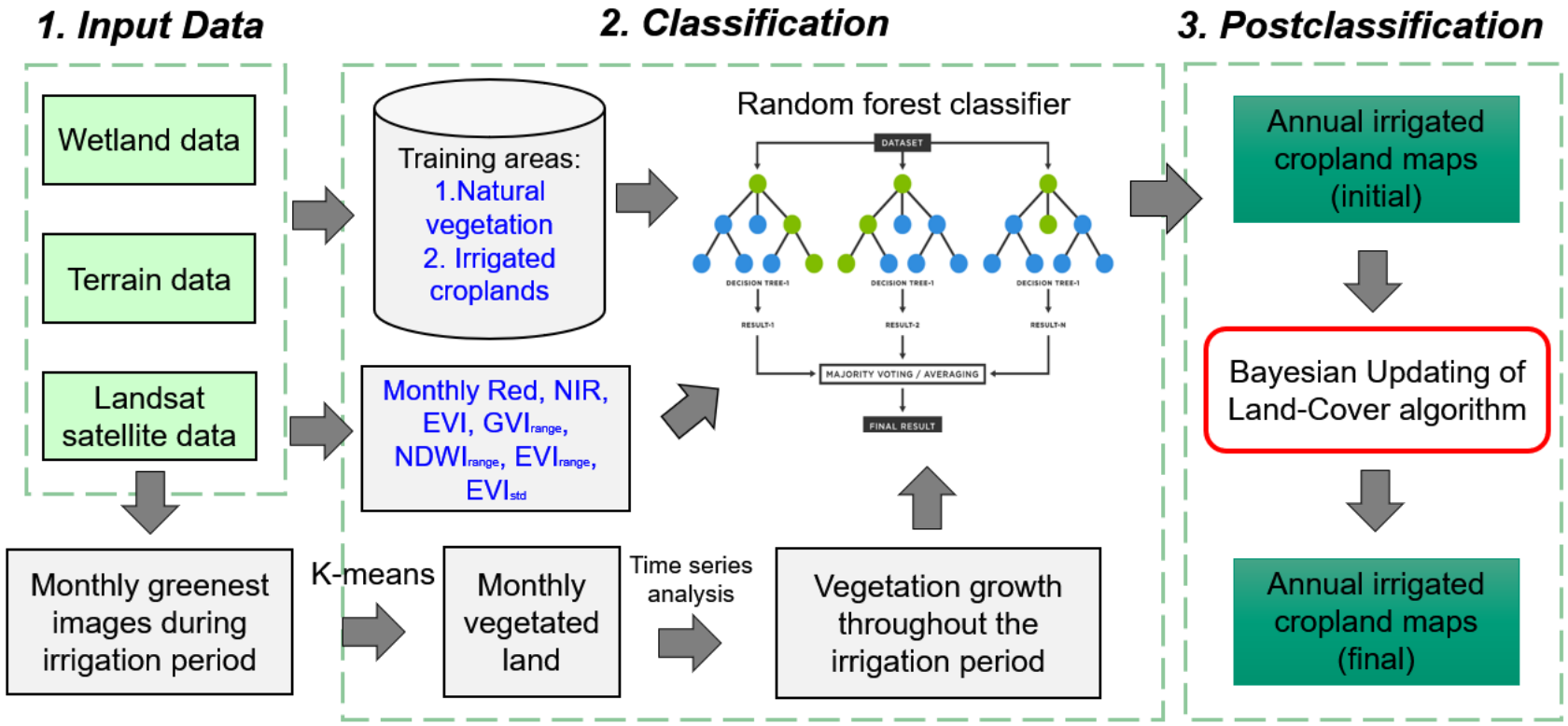

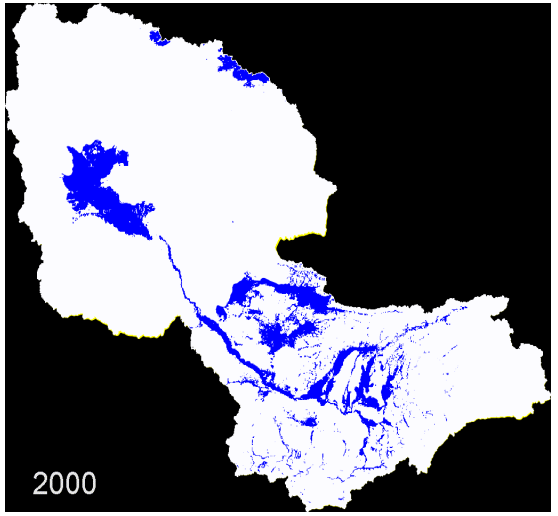

Amu River basin

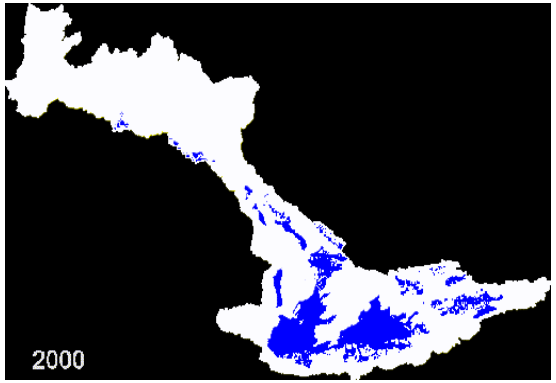

Syr River basin

- Annual irrigated cropland maps (1990-2020) in 10 basins in Central Asia were produced at a 30 m resolution.
- Validation indicated that the accuracy of these products is more reasonable than existing irrigation maps.

3.1.4 irrigation water use

Estimation of global irrigation water use based on microwave remotely sensed of soil moisture

Satellite-based datasets and process procedure

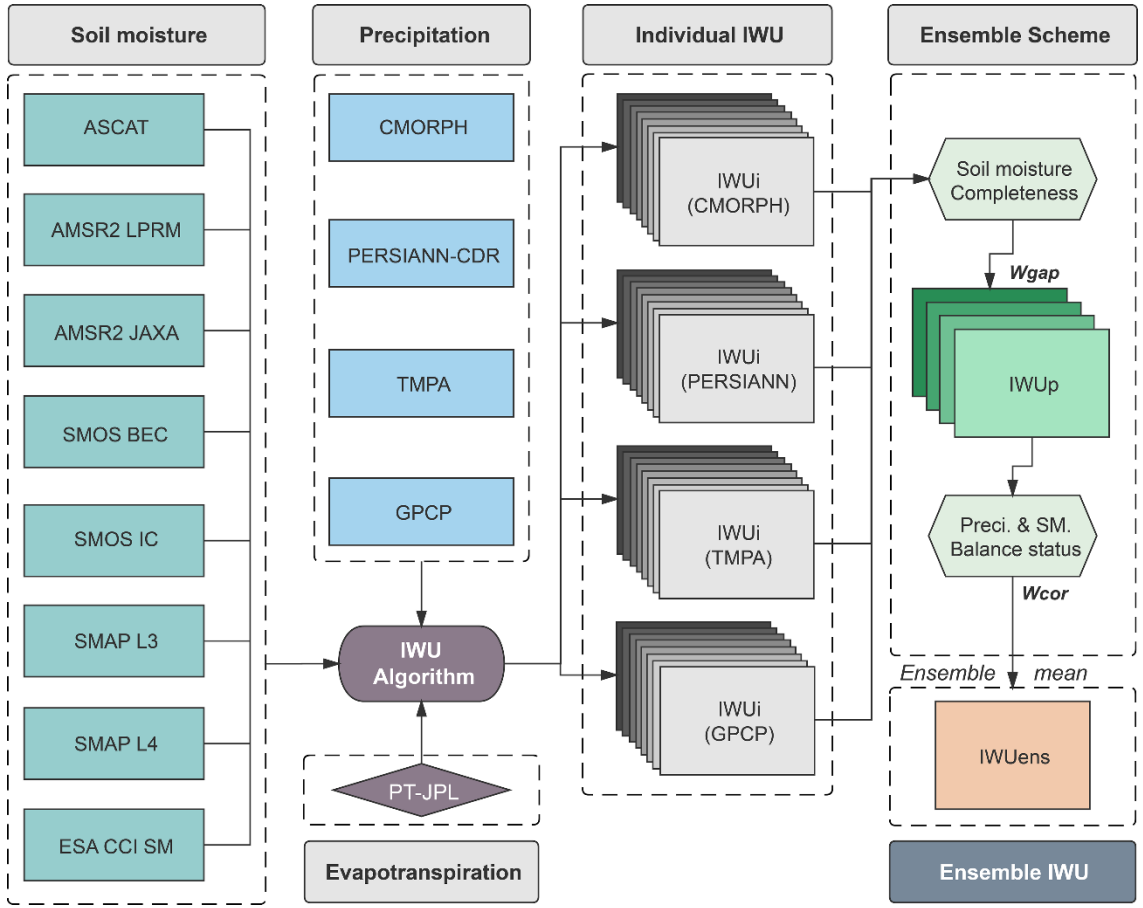

Soil water balance: $\frac{d\theta}{dt} = \mathrm{Ir} + \mathrm{P} - ET - Dg - R$

Irrigation Signal → **Irrigation water use**

Valid period and completeness of satellite-based soil moisture datasets

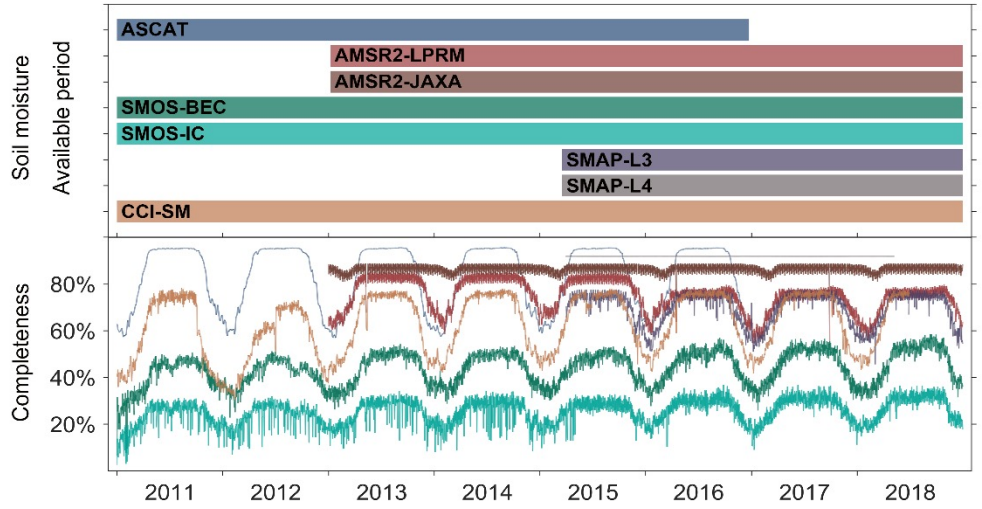

Zhang et al., WRR, (2022)

3.1.4 irrigation water use

Output dataset

Global pattern of mean annual IWU estimates

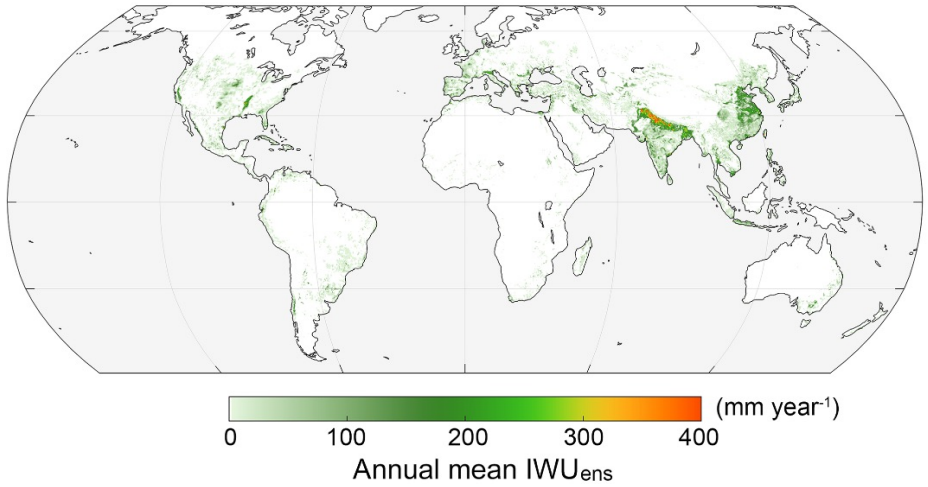

Country level comparison between IWU and Irrigated Area

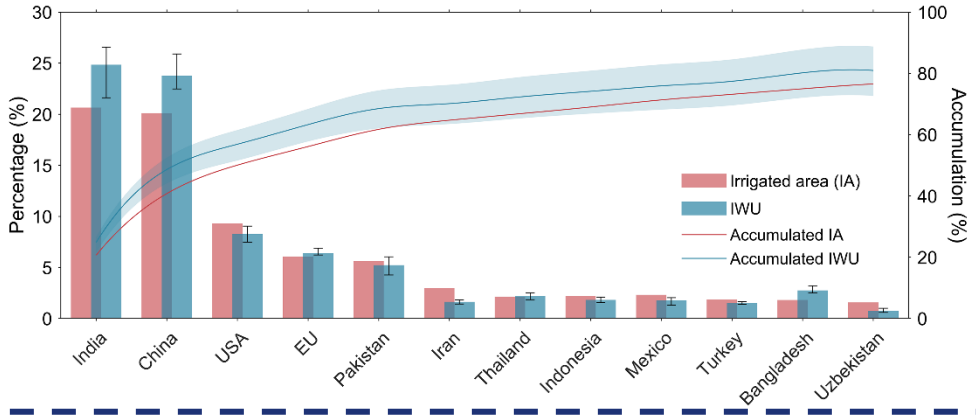

Validation and comparisons

Comparisons of the satellite-derived IWU with the reported irrigation water use data from US, China, and FAO statistics

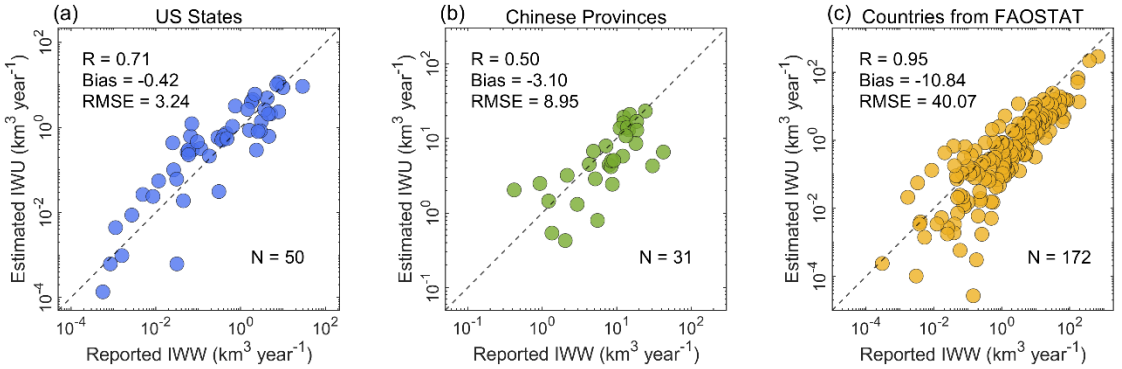

The ensemble scheme can reduce the uncertainties of IWU estimation

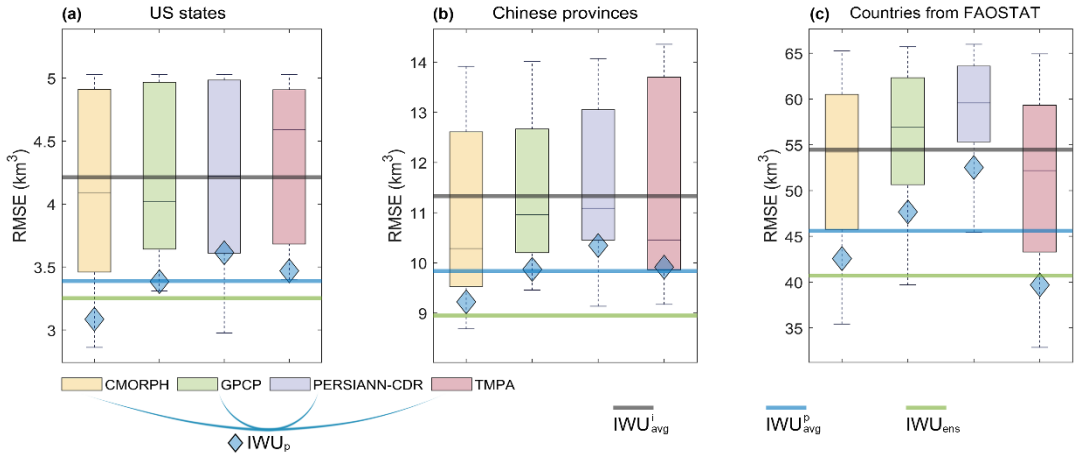

3.1.5 surface water bodies

A method for identifying small water bodies by fusing multisource satellite data

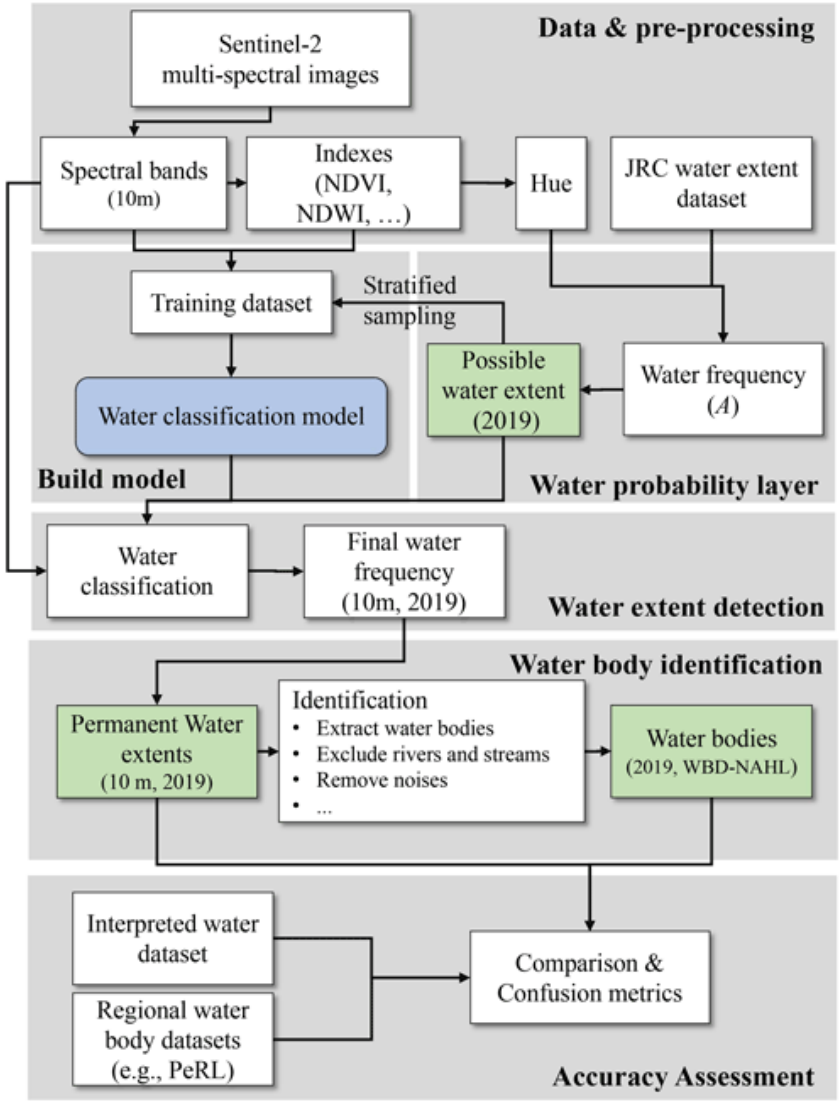

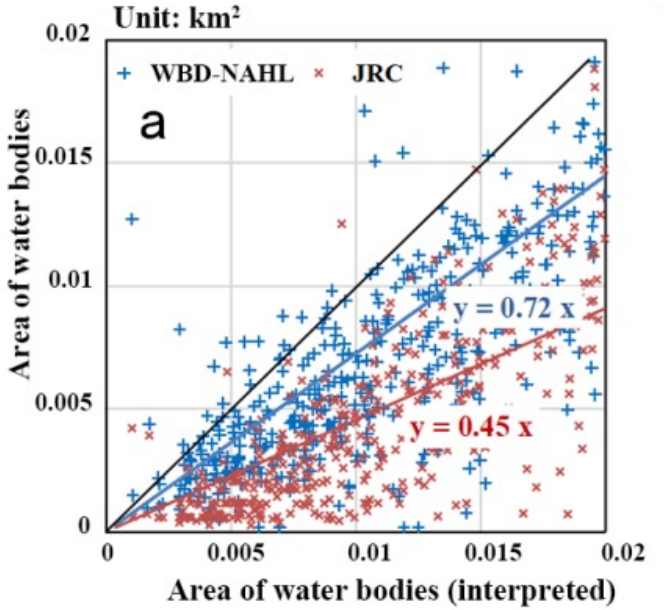

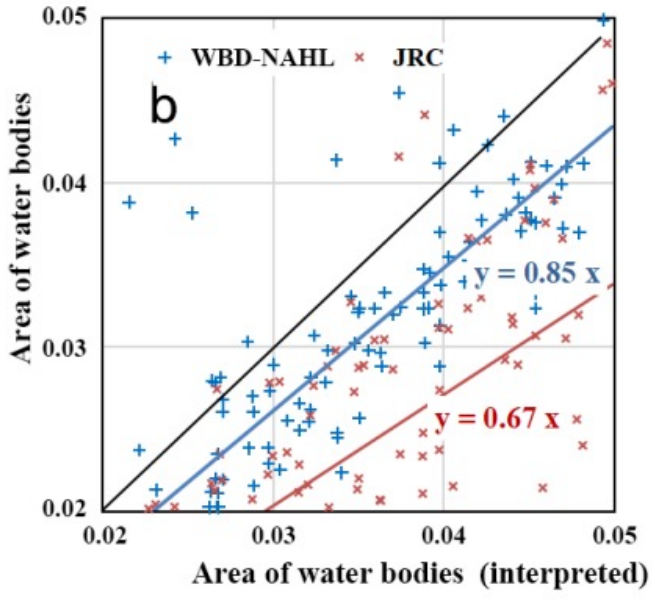

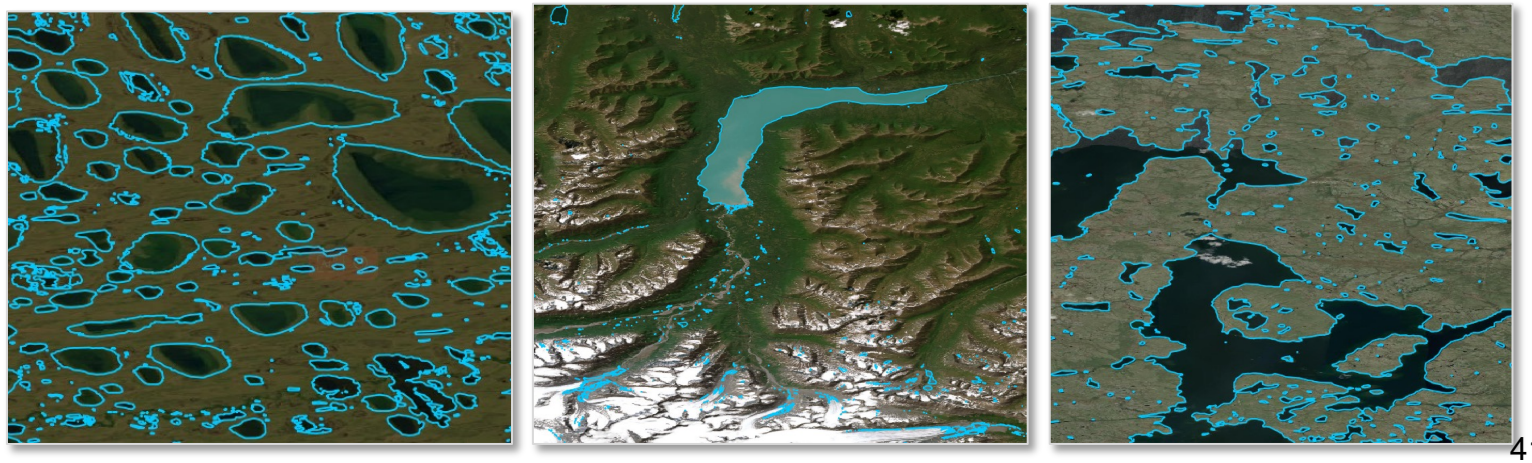

3.1.5 surface water bodies

Mapping water bodies as small as 0.5 ha and their changes over nearly 3 decades in central Asia

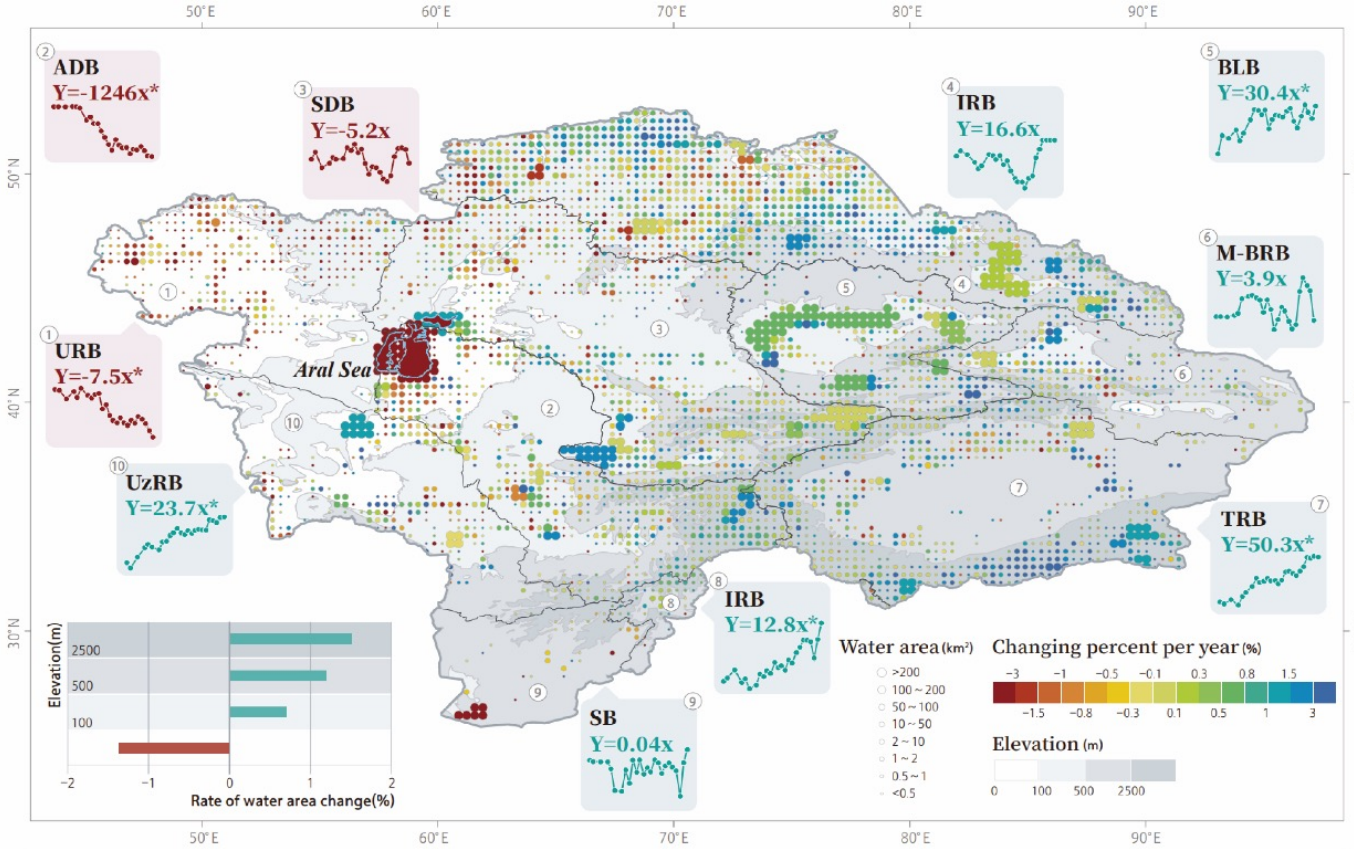

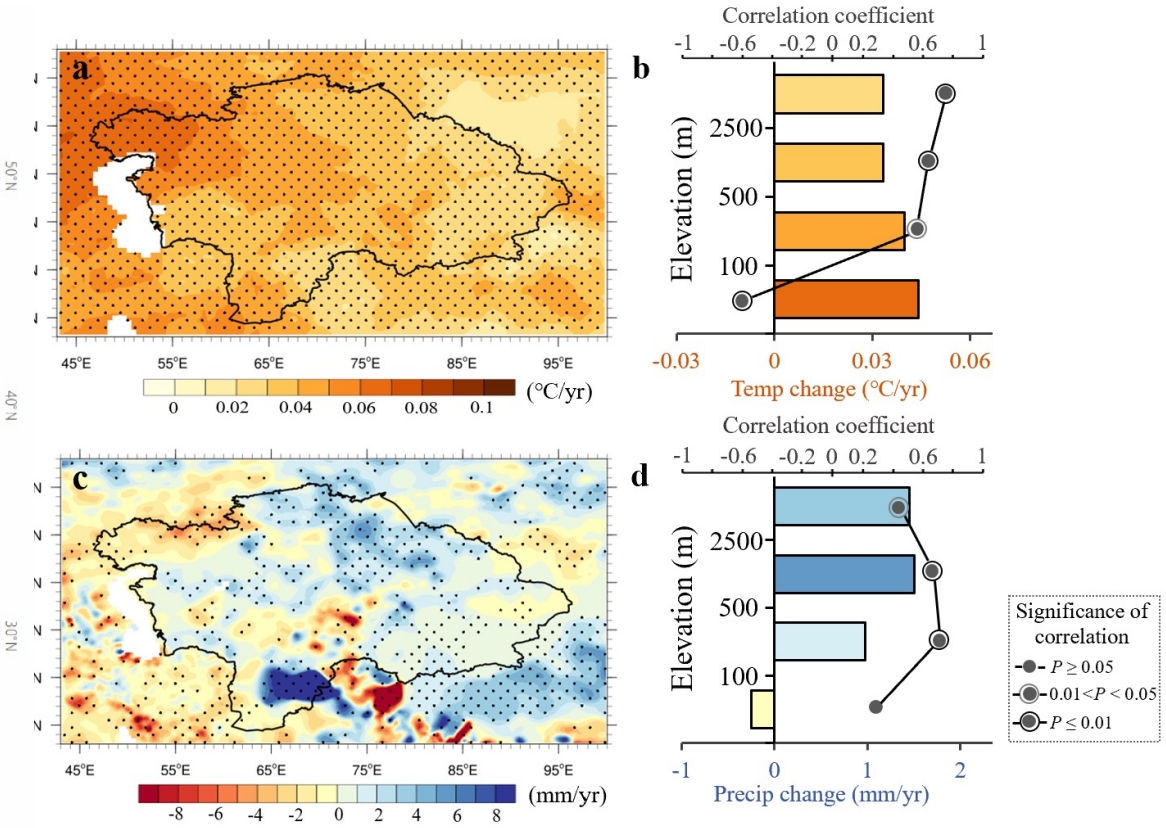

- The Aral Sea had been continuously shrinking between 1992 and 2020, but other lakes in arid central Asia has been expanding in numbers and areas over the same period, particularly the small and high-elevation water bodies, which has increased 15,507 new water bodies and gained 3,701.3 km².

(Su, Li, Feng, et al. 2021 *STE*; Li, Li, Feng, et al, 2021 *IJDE*; Su, … Feng*, et al., *NC*, In review)

3.1.6 tree cover

A machine learning method for deriving tree cover from time-series satellite data

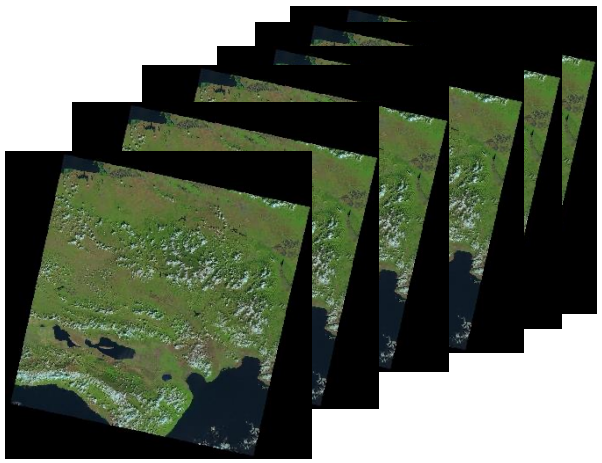

Time-series Landsat data

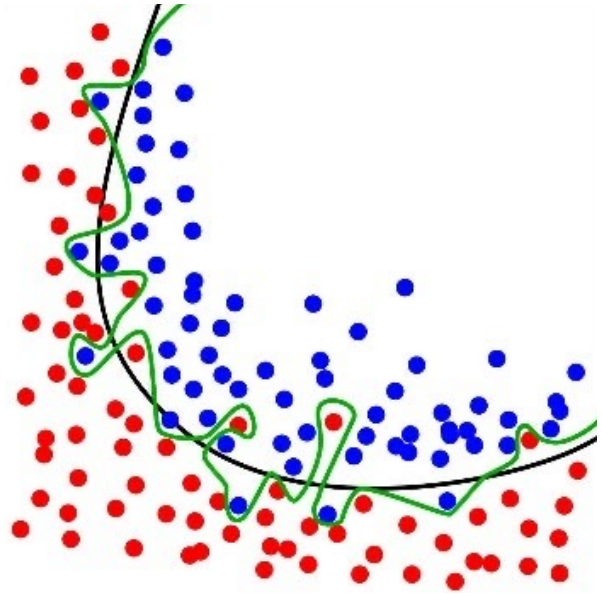

Boosting gradient algorithm

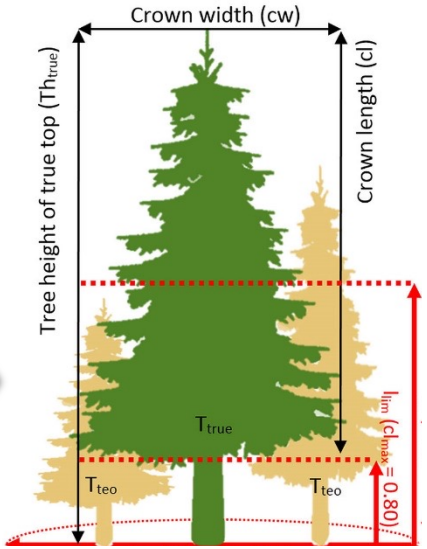

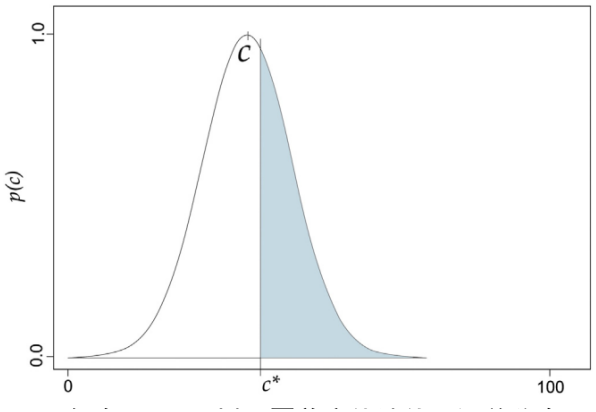

Model the distribution of tree cover

3.1.6 tree cover

Annual 30-m resolution tree cover (1990-2020) for the Himalayas

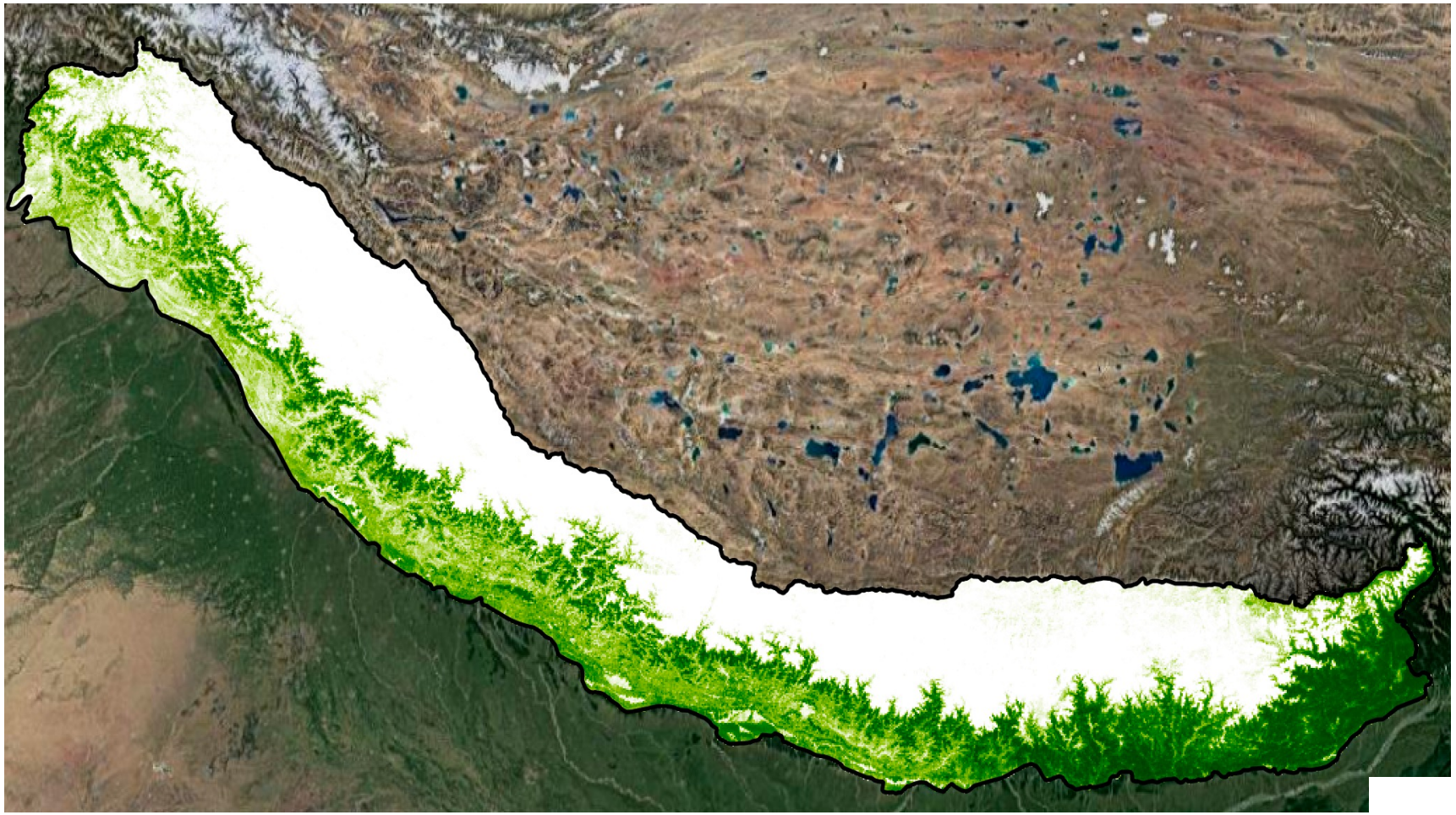

Tree cover (2020)

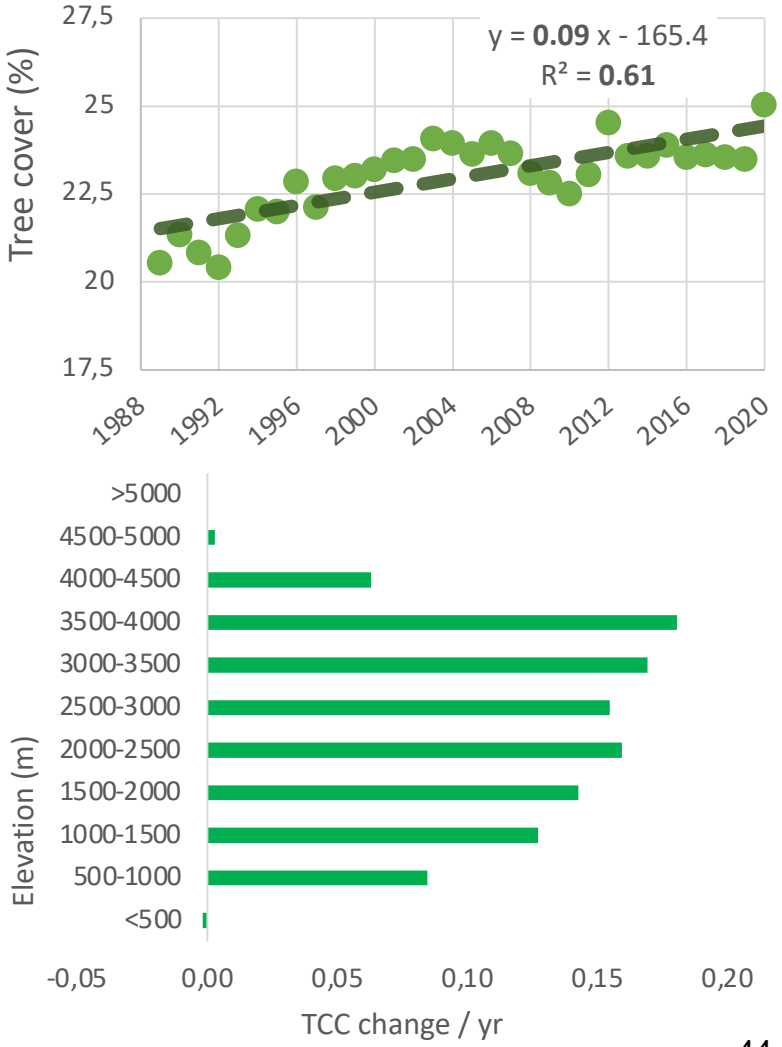

Wang, Feng*, et al. 2022, RS

- Retrieval of key ecohydrological variables from multi-source RS data
- Retrieval of key cryosphere variables from multi-source RS data
- Development of real time RS LDAS
- Closing water cycle at the watershed/regional scale based on the LDAS

3.2.1 permafrost

Input

In situ
1,002 sites for MAGT
452 sites for ALT

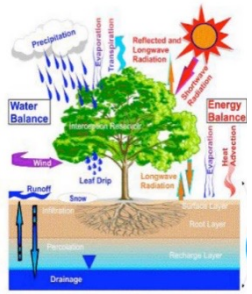

Climate data
Precipitation,
Solar radiation

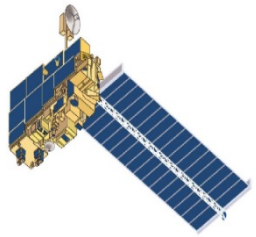

Remote sensed
FDD, TDD,
SCD, LAI,
SOC…

Machine learning

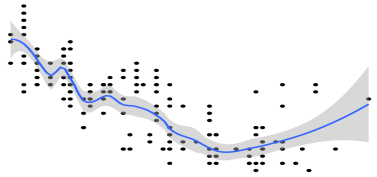

Generalized additive model

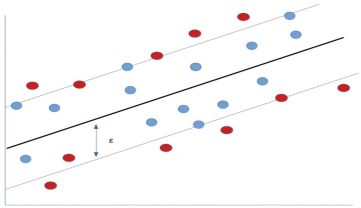

Support vector regression

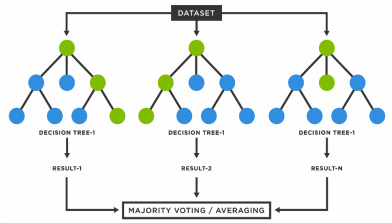

Random forest

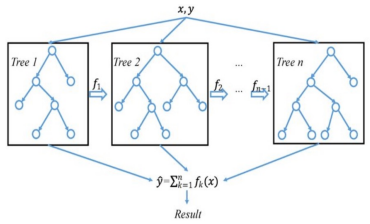

eXtreme gradient boosting

- Ensemble average
- 1,000 runs

Output

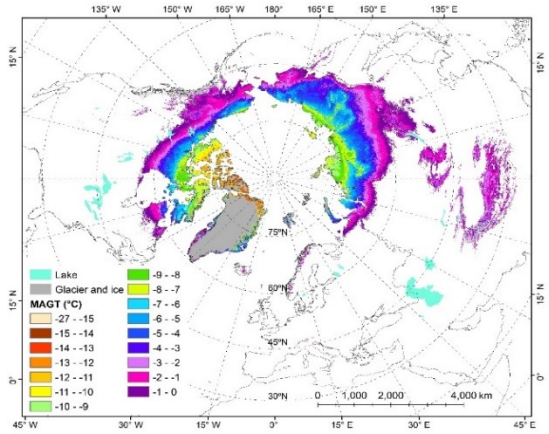

MAGT at ZAA

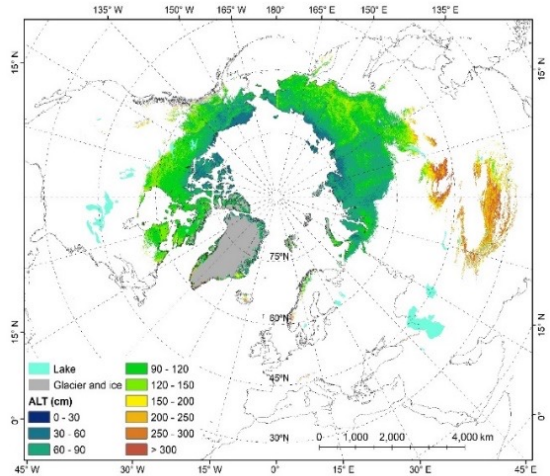

ALT

Ran, Li, et al., 2021 SCES; Ran, Li, et al., 2022 ESSD

3.2.1 permafrost

New permafrost zonation maps was produced on Tibetan Plateau and Northern Hemisphere. On Tibetan Plateau, the permafrost thermal stability type was divided according to the high altitude permafrost zonation system. A biophysical permafrost types were used to describe the complex interactions of climatic and ecological processes in the Northern Hemisphere.

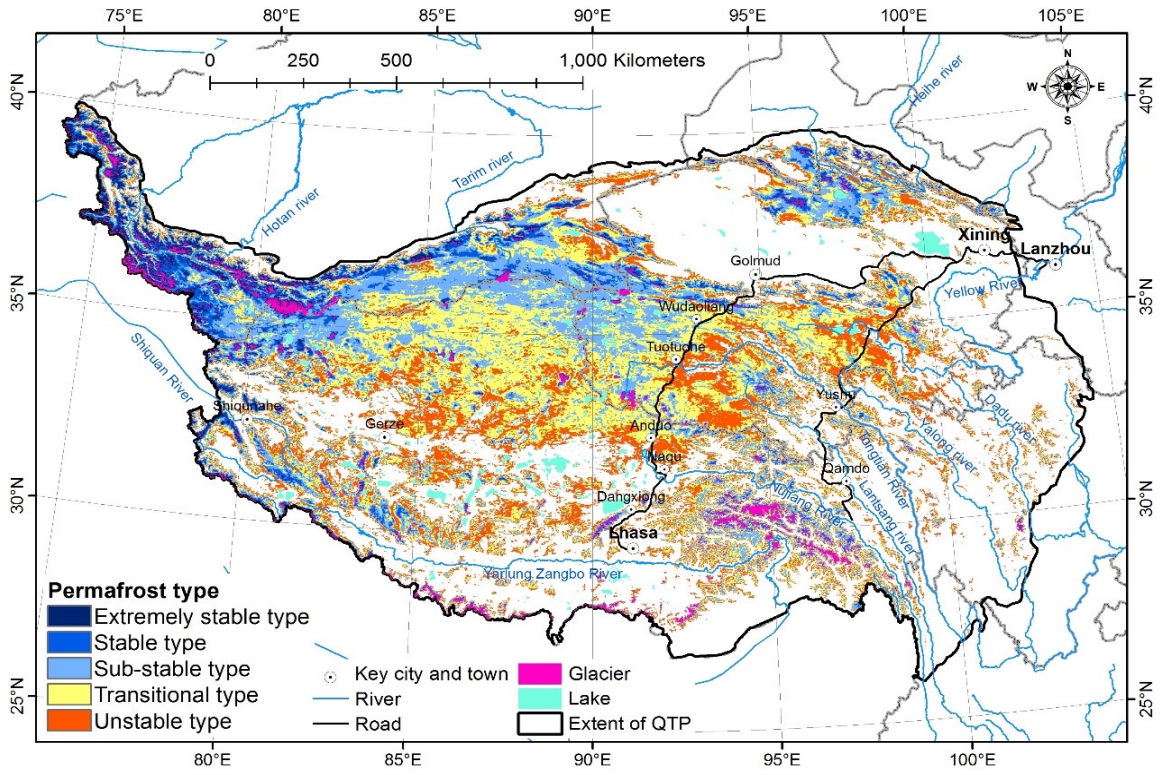

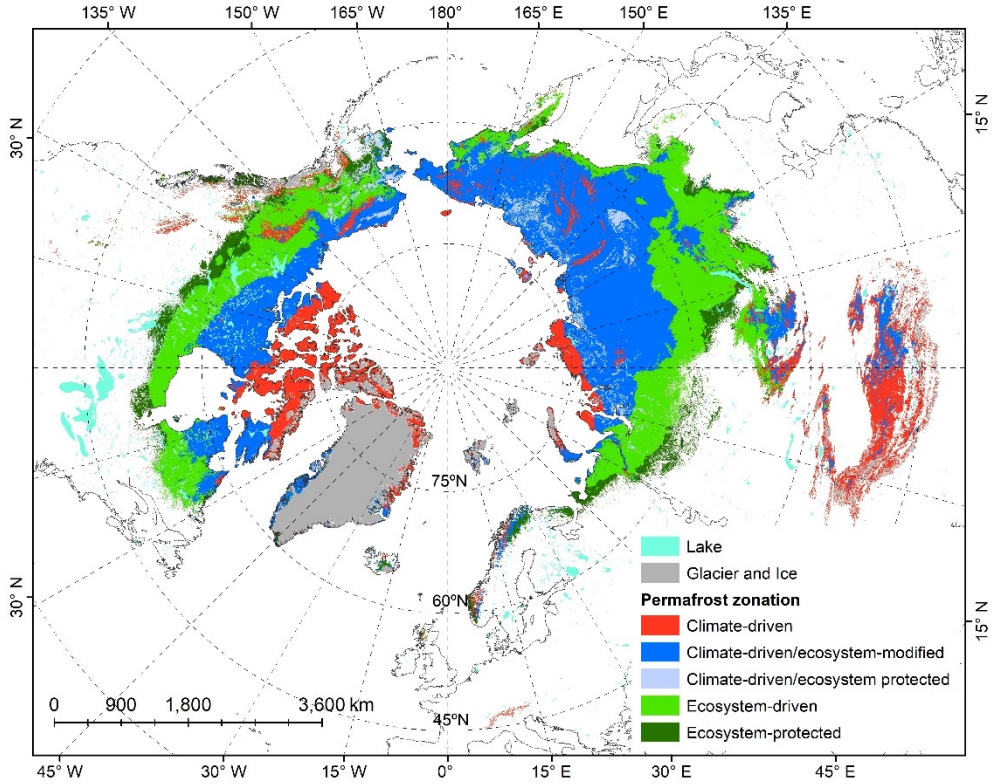

Ran, Jorgenson, Li, et al., 2021 ERL; Ran, Li, et al., 2021 SCES; Ran, Li, et al., 2022 ESSD

3.2.2 rock glacier

A deep-learning (DeepLab v3+) and MT-InSAR method for identifying rock glaciers

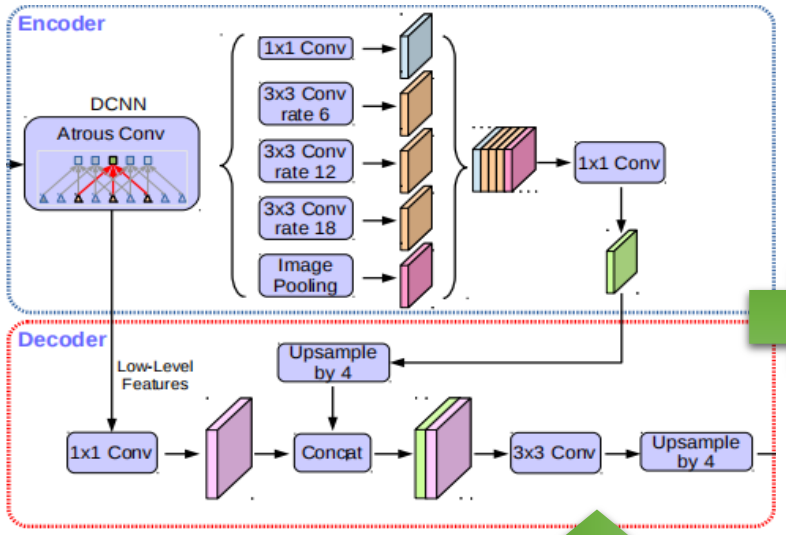

DeepLab v3+

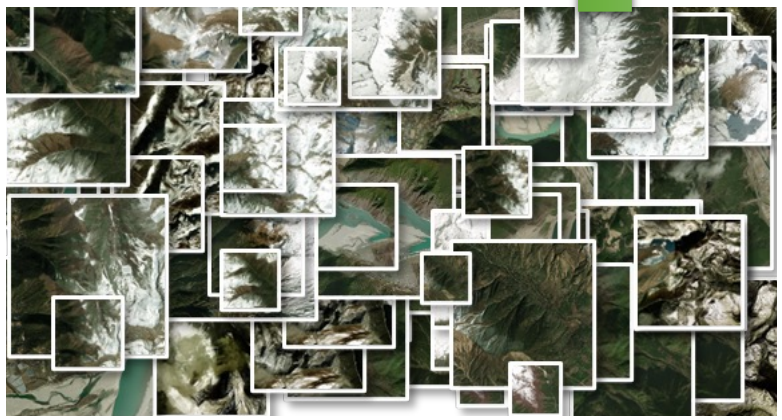

Millions of satellite images

Xu, Feng, et al., 2019

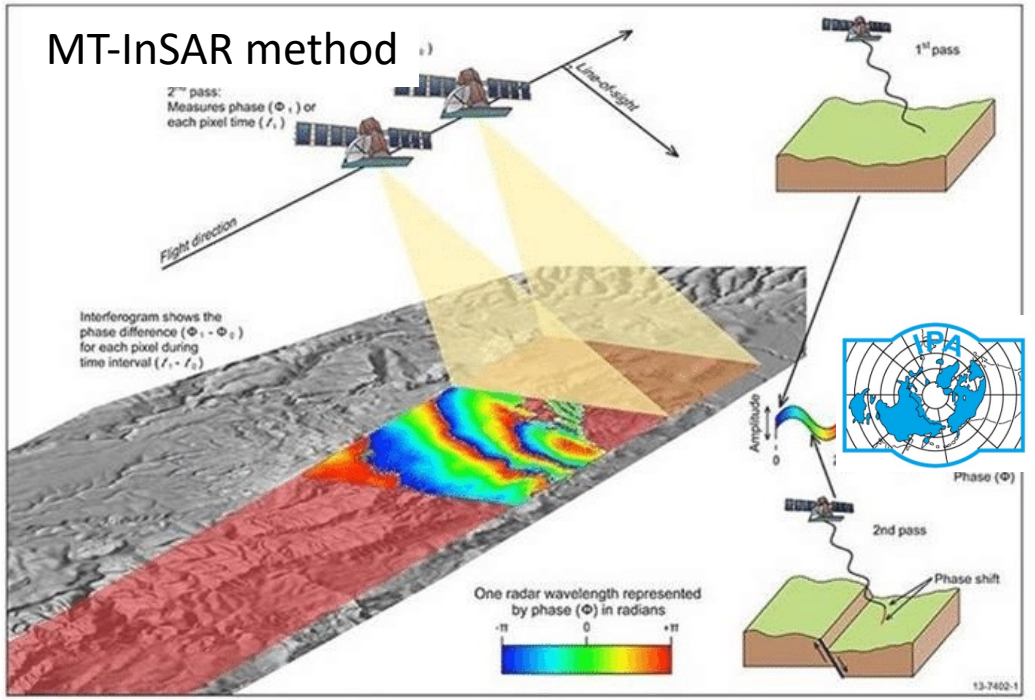

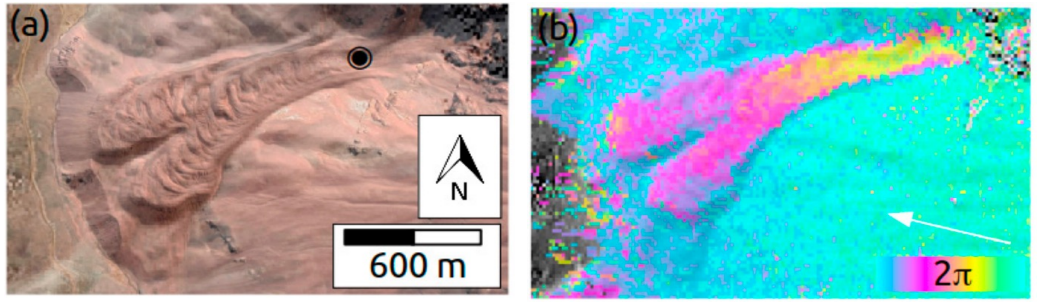

Zhang, Feng*, et al. 2021

Rock glacier kinematics

3.2.2 rock glacier

The first rock glacier inventory for Tibetan Plateau with >13,000 rock glaciers identified

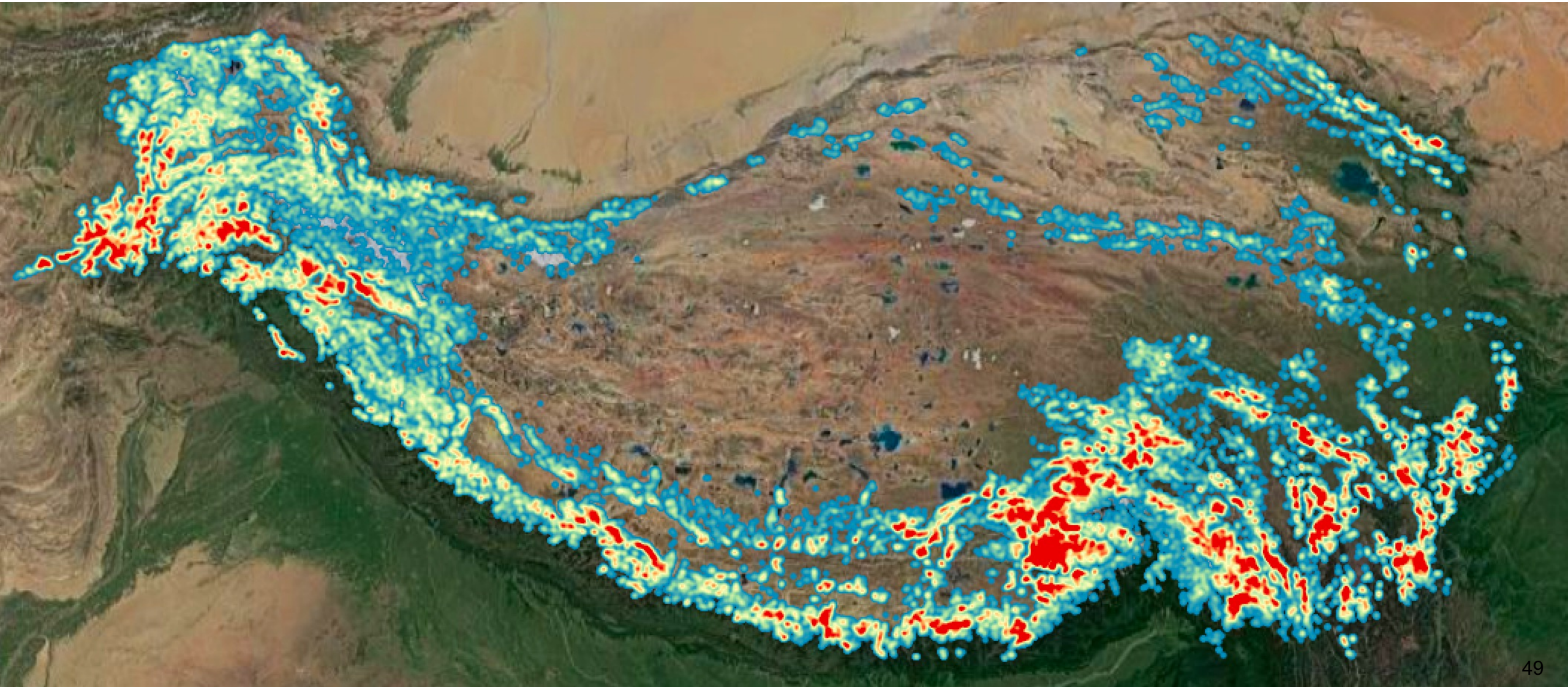

3.2.3 glacier mass balance

Case studies of glacier mass balance estimation using multi-source remote sensing data in the TP

Yanong Glacier(1974-2015)

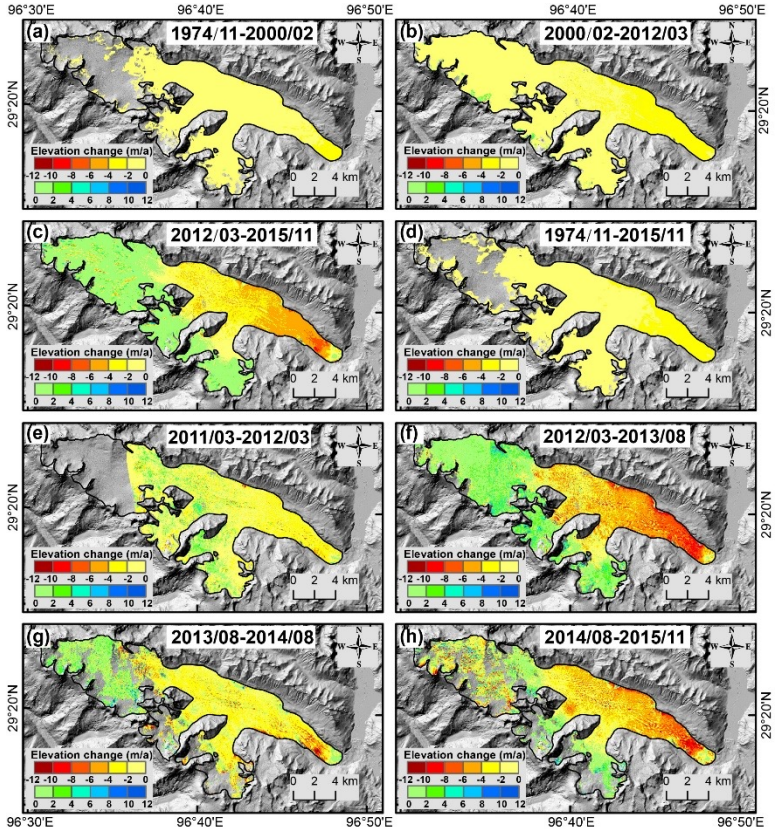

Zhou et al. (2022, RSE)

1974–2000: –0.48±0.20 m w.e./a

2000–2015: –0.95±0.07 m w.e./a

Eastern Tanggula mountain(2000-2020)

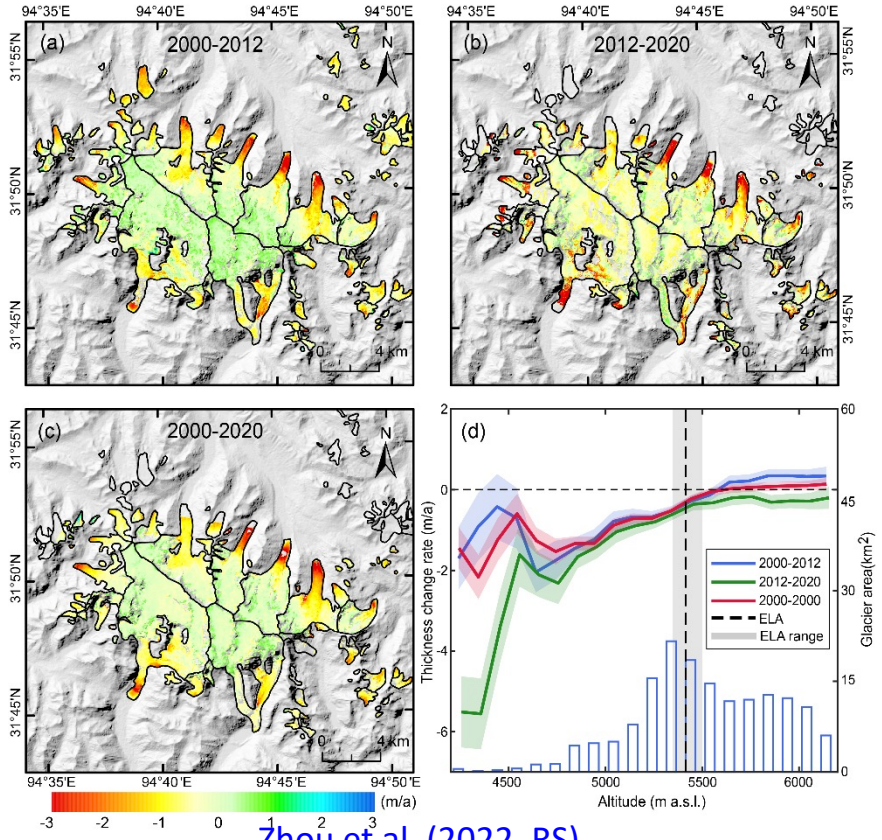

Zhou et al. (2022, RS)

2000–2012: –0.16±0.04 m w.e./a

2012–2020: –0.45±0.07 m w.e./a

Puruogangri Ice Cap(1975-2021)

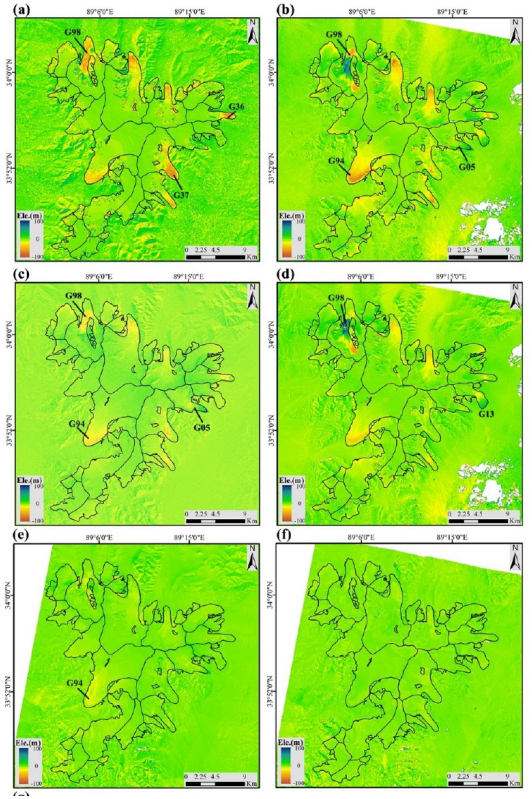

Ren et al. (2022, RS)

1975–2000: –0.23±0.02 m w.e./a

2000–2021: –0.29±0.02 m w.e./a

All of the above regions show varying degrees of accelerated glacier mass loss.

- Retrieval of key ecohydrological variables from multi-source RS data
- Retrieval of key cryosphere variables from multi-source RS data
- Development of real time RS LDAS
- Closing water cycle at the watershed/regional scale based on the LDAS

3.3.1 RS LDAS for Pan-TP

Overall Design

Land Data Assimilation

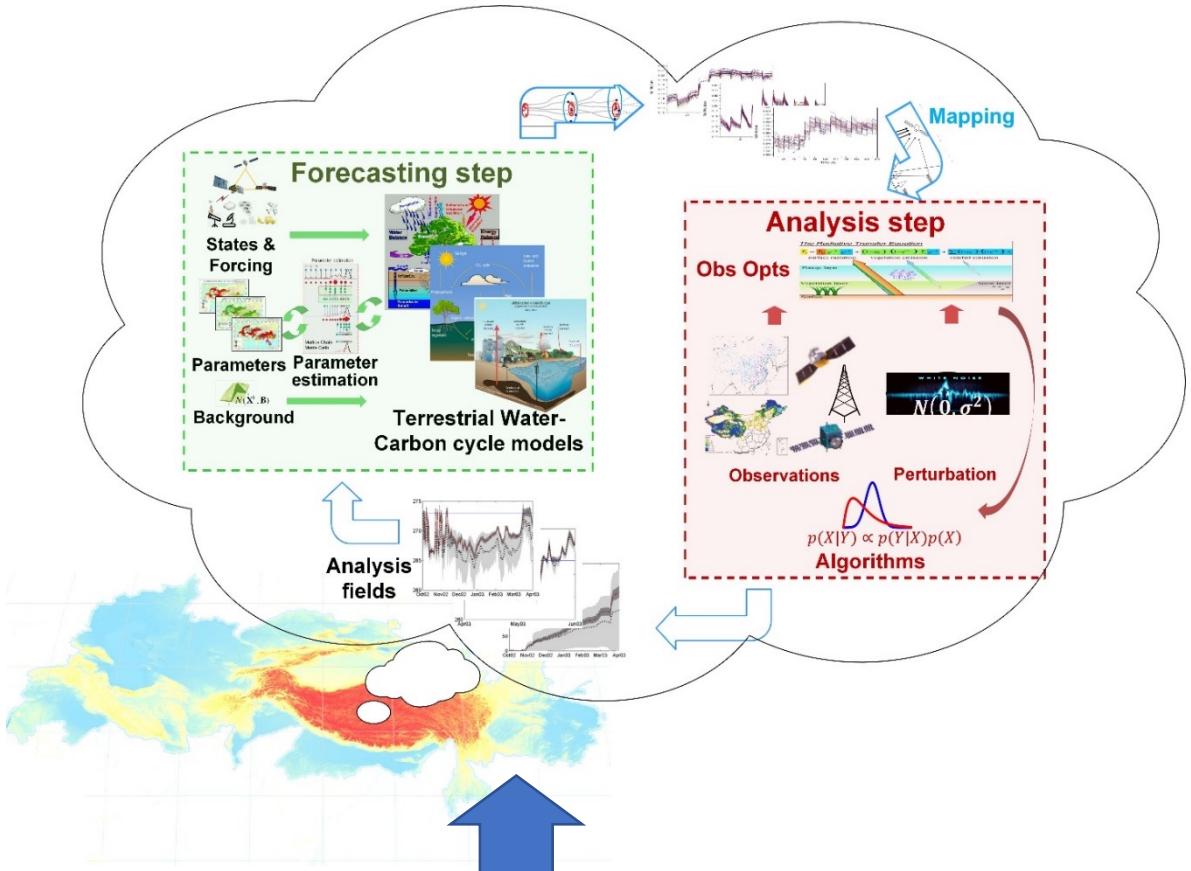

Remote Sensing Data

Soil Moisture
SMAP
NNsm
…

Soil Temperature
Aqua MODIS LST and GLDAS
AMSR-E/AMSR2
…

Snow
MODIS
VIRRS/NPP
…

LAI & Chlorophyll fluorescence
GLASS LAI
GOSIF
…

Cloud computing and storage (PIE-Engine)

3.3.1 RS LDAS for Pan-TP

Data Assimilation Software:

A Common Software for Nonlinear and Non-Gaussian Land Data Assimilation (ComDA)

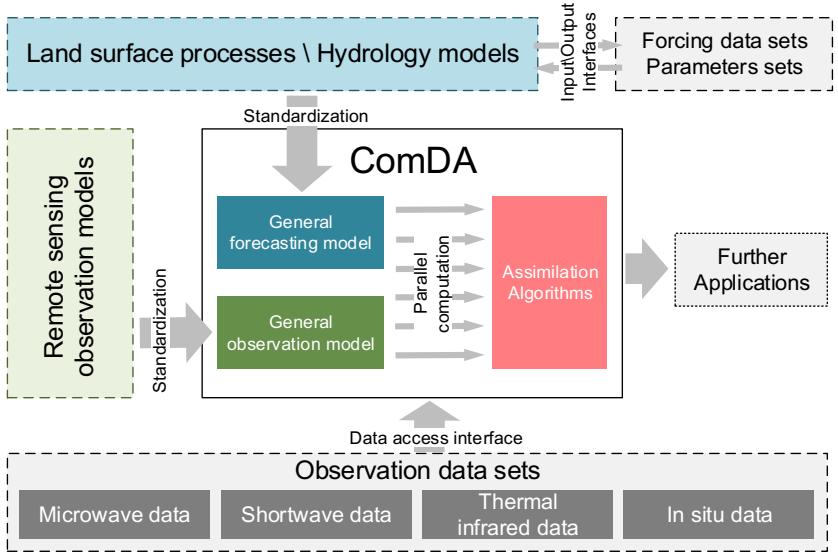

Materials

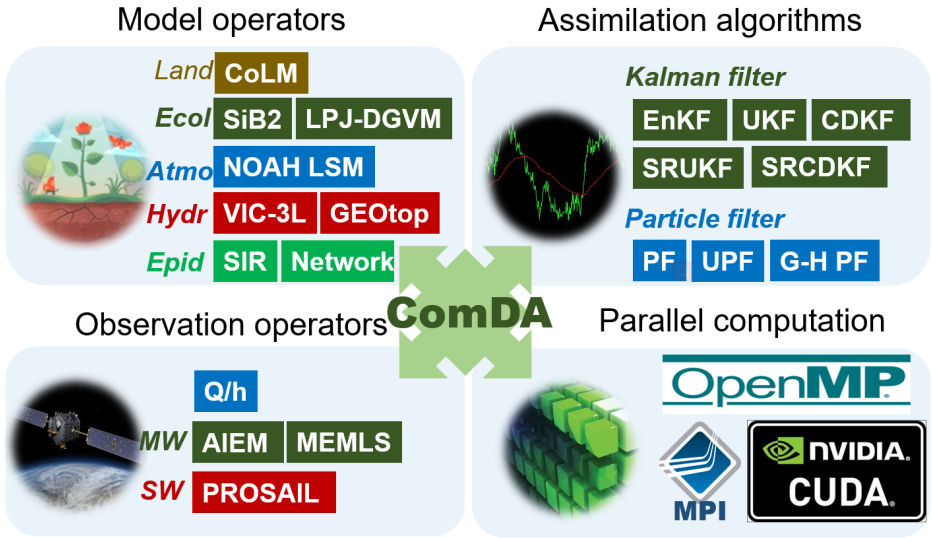

Online demo

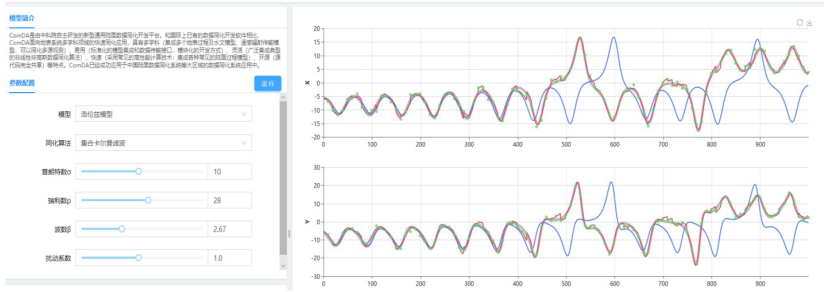

Practices

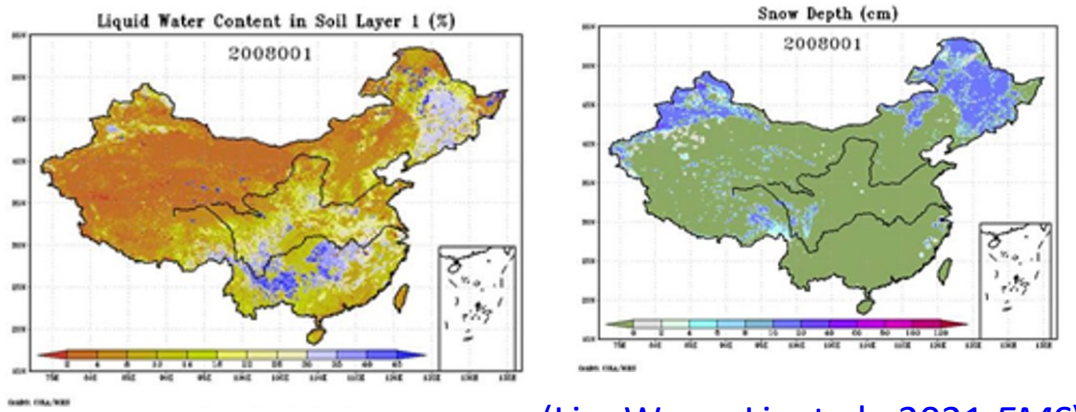

(Liu, Wang, Li, et al., 2021 *EMS*)

Forcing data: China Meteorological Forcing Data (CMFD)

Study region

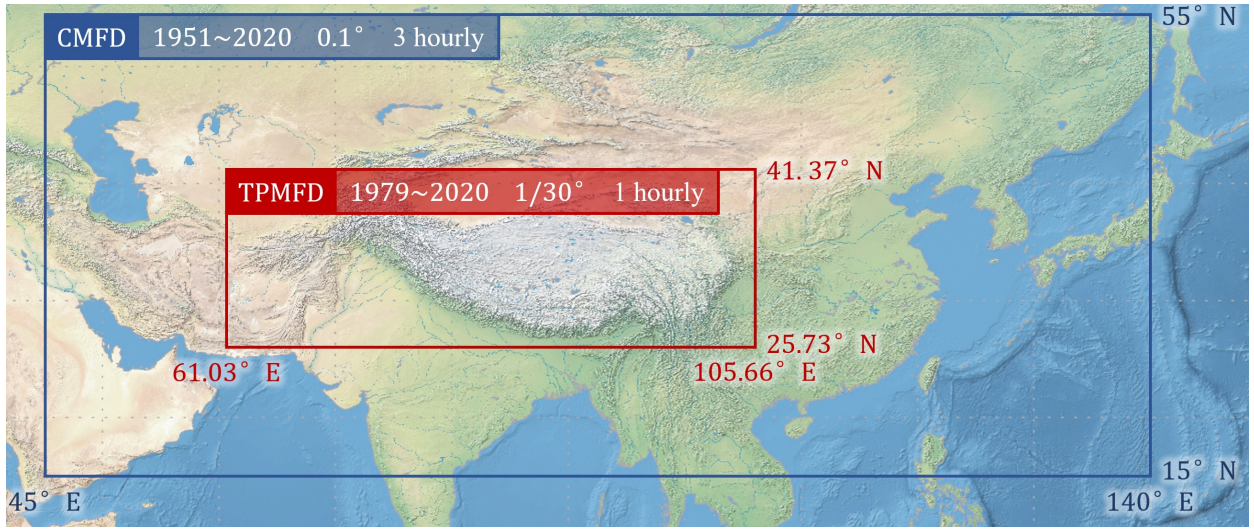

Core Algorithm

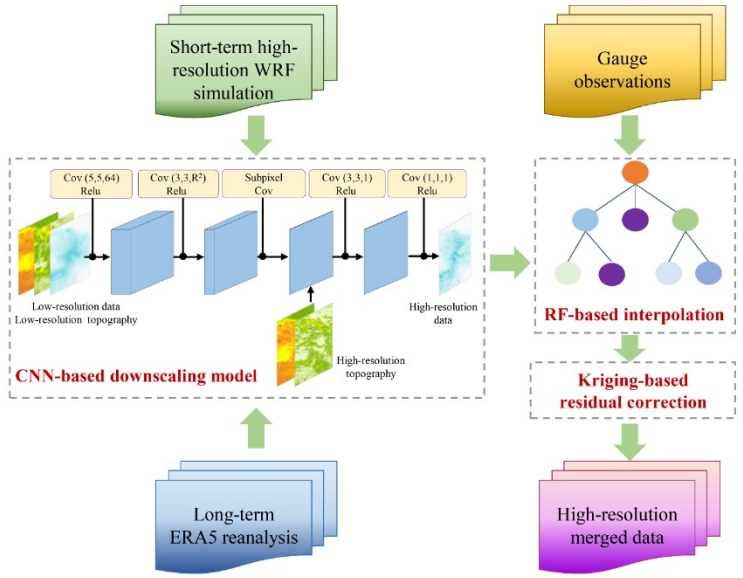

Air temperature

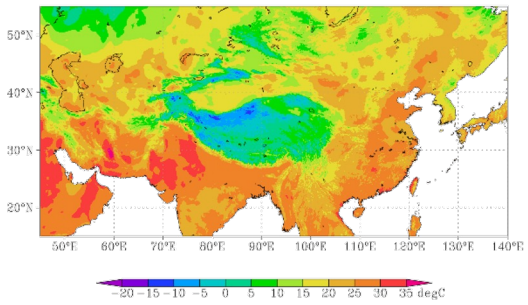

Surface air pressure

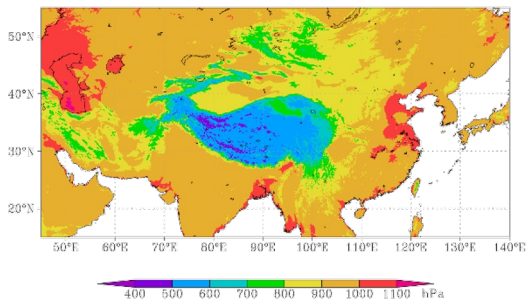

Specific humidity

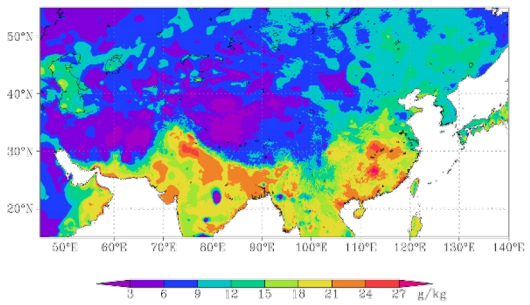

Wind speed

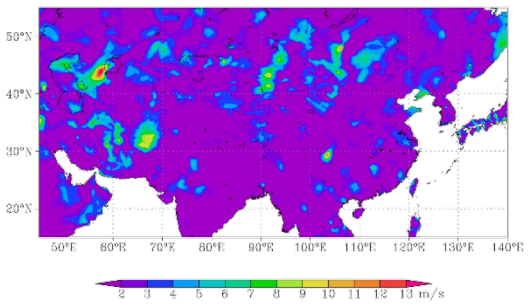

Data Assimilation Strategy

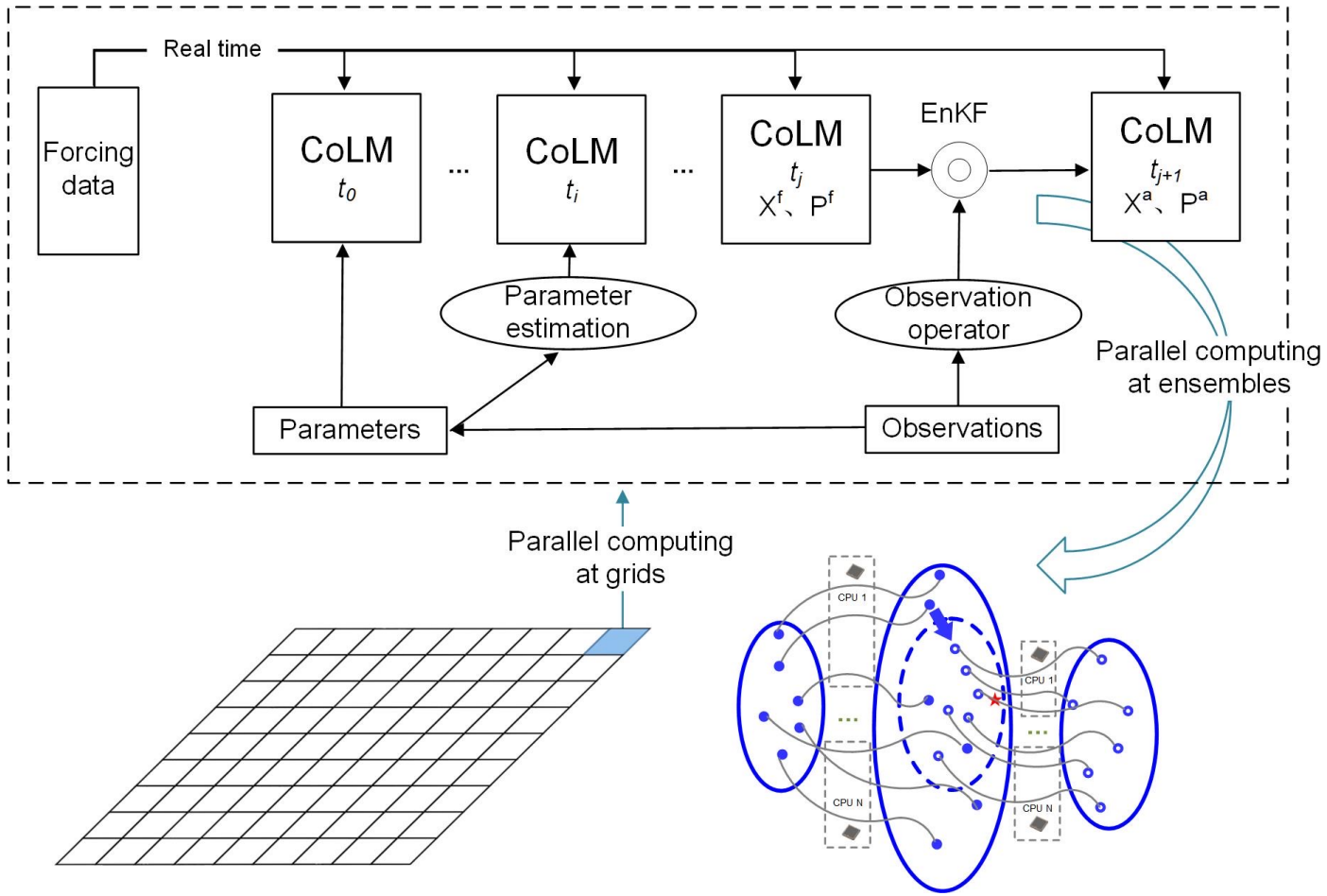

- Parameter estimation:

  MCMC

- Data assimilation algorithm:

  Ensemble Kalman filter

- Model operator:

  CoLM202X

- Parallel computing:

  OpenMP, MPI, CUDA

3.3.1 RS LDAS for Pan-TP

Users Interface for real time LDAS (in Chinese)

Products

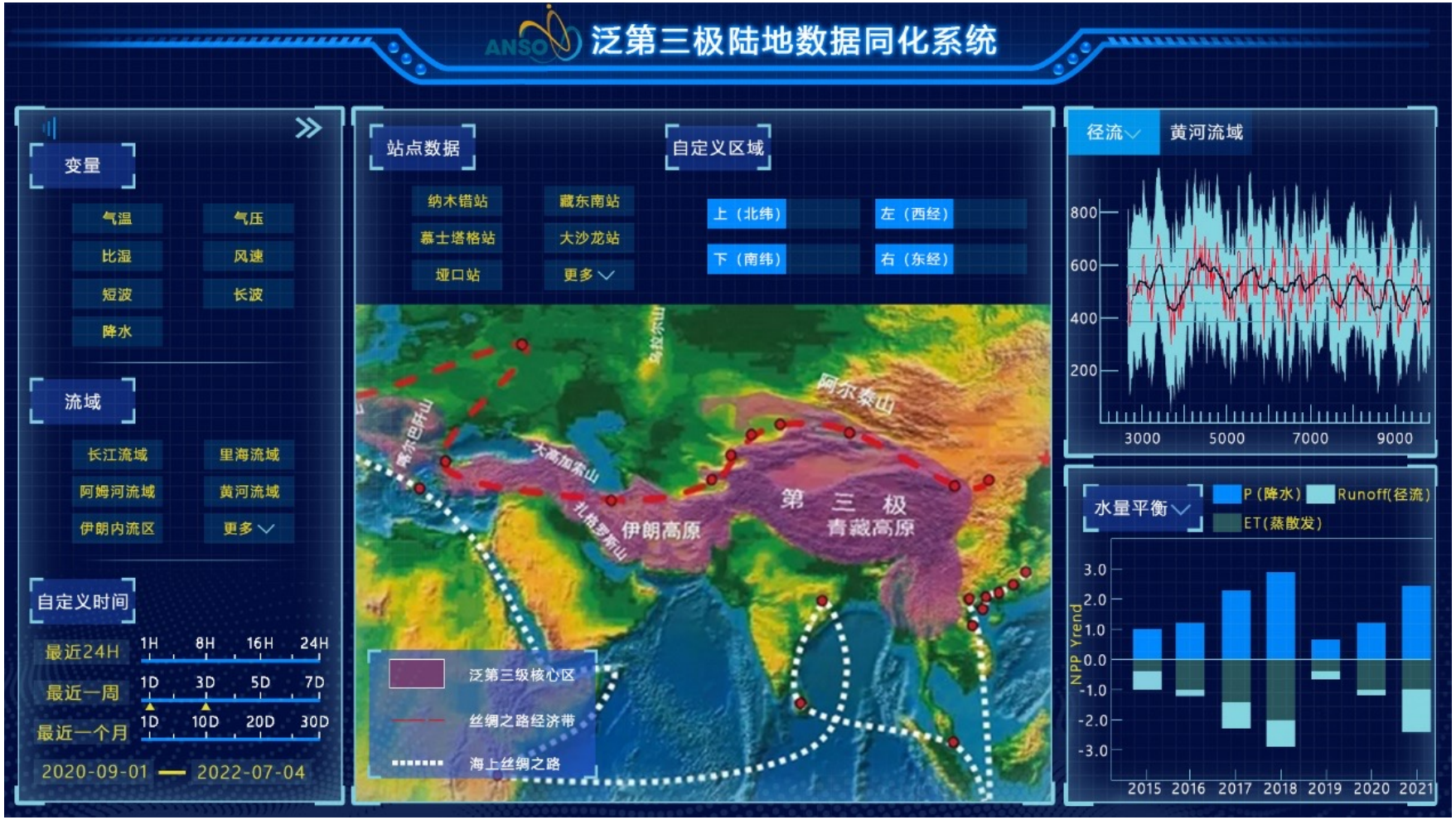

Ensembles forecasting

Water / Carbon / Energy balance

Data visualization with WebGIS

3.3.2 RS LDAS for EUROCORDEX-domain

- Development of a coupled land data assimilation system for the Terrestrial Systems Modelling Platform (TSMP)
- Land surface processes
  - Community Land Model (CLM)
- Surface runoff and subsurface hydrology
  - ParFlow
- Atmosphere
  - ERA5 (→ICON)

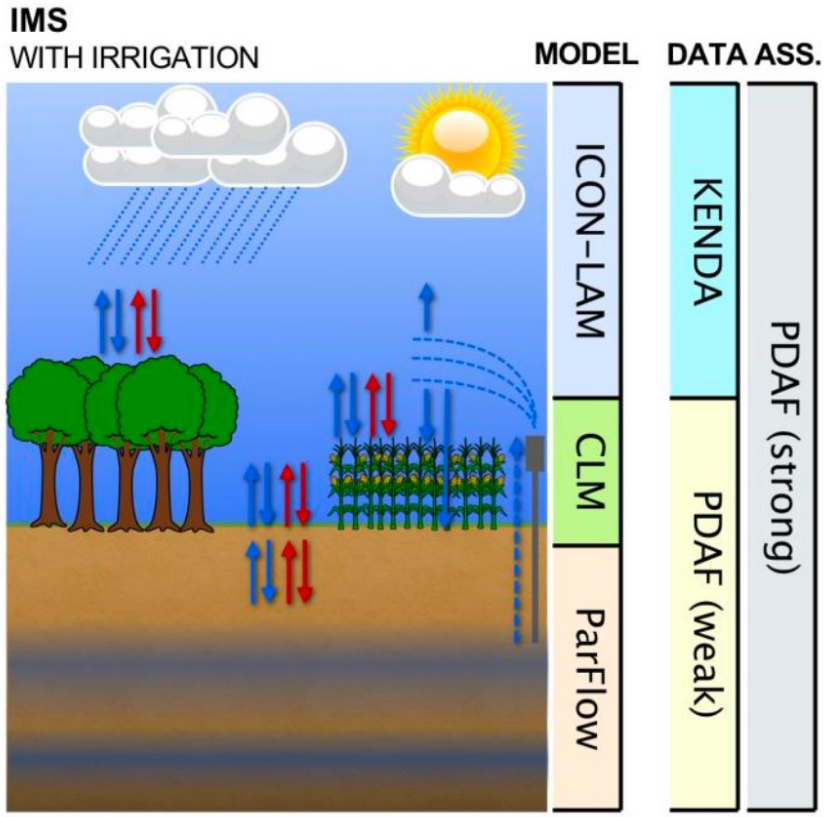

Illustration of the coupled data assimilation framework

3.3.2 RS LDAS for EUROCORDEX-domain

- Initial test for North-Rhine-Westphalia region, Germany: 300 km × 300 km
- Model: CLM3.5-PDAF or CLM3.5-ParFlow-PDAF
- DA: EnKF, period 2018.01.10 – 2018.12.31
- Atmospheric forcings: COSMO-REA6
- Soil texture: SoilGrids

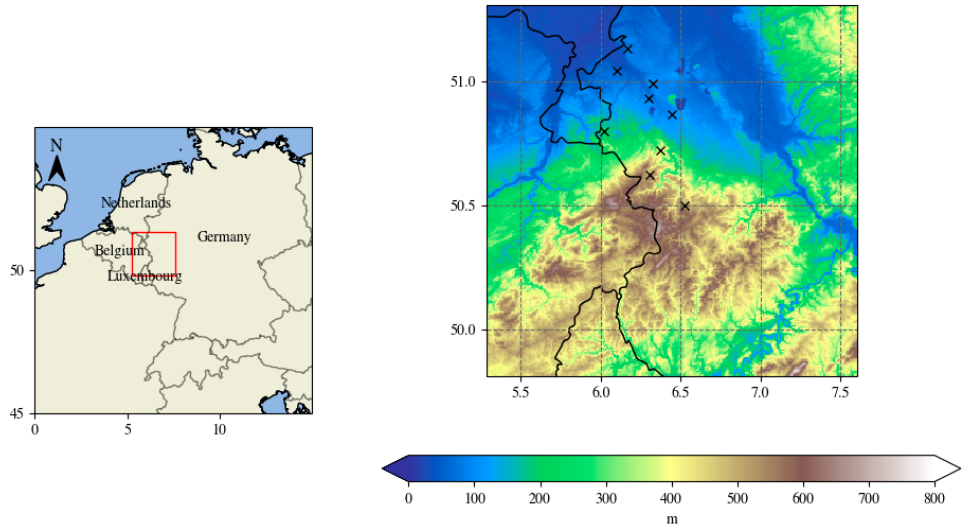

(a) Separate Retrieval Assimilation

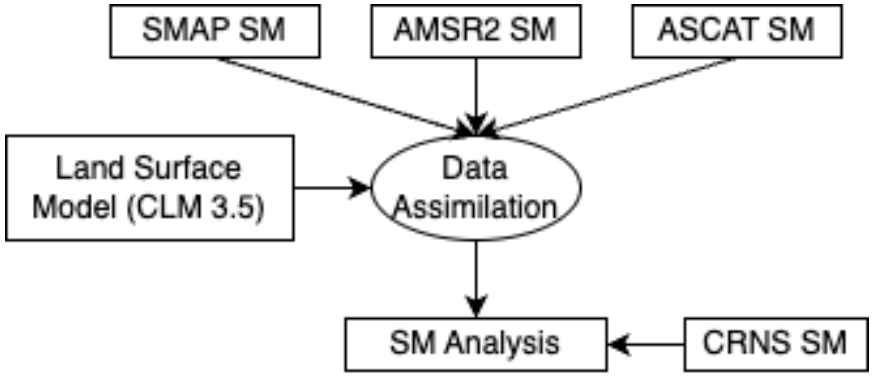

(b) Joint Retrieval Assimilation

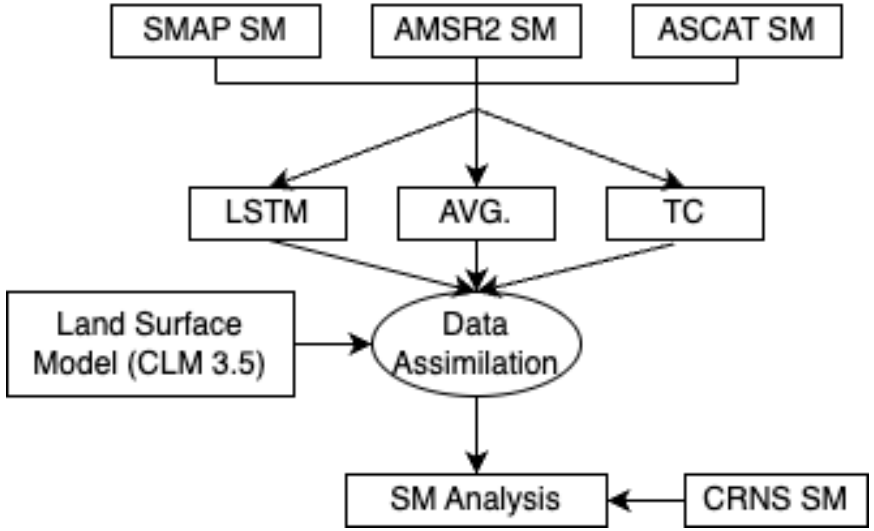

3.3.2 RS LDAS for EUROCORDEX-domain

- Development of a coupled land data assimilation system for the Terrestrial Systems Modelling Platform (TSMP)
- Land surface processes
  - Community Land Model (CLM)
- Surface runoff and subsurface hydrology
  - ParFlow
- Atmosphere
  - ERA5 (→ICON)
- Area of interest: EUROCORDEX
- Assimilate surface soil moisture RS retrievals into the model (SMAP)

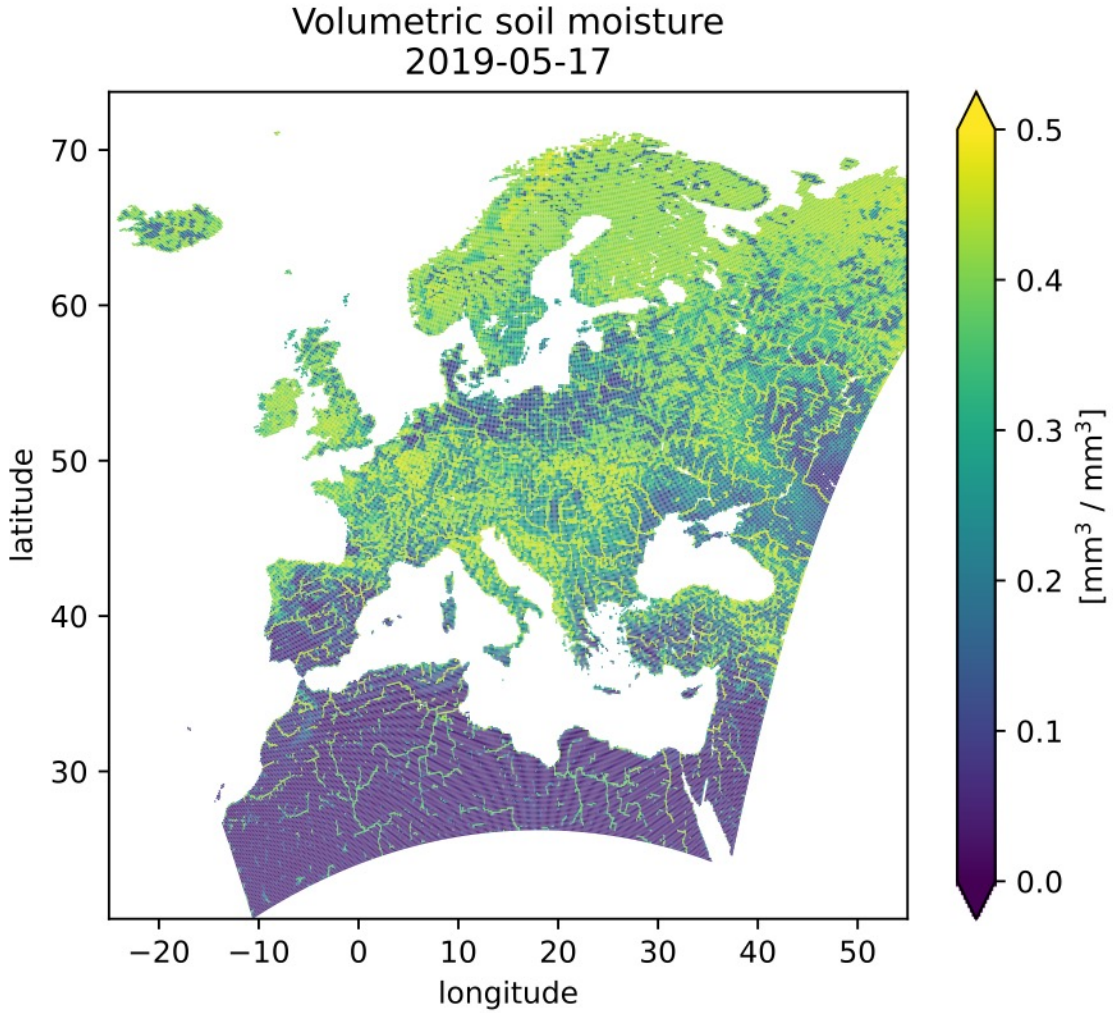

Open loop soil moisture prediction over EUROCORDEX (±11-km resolution)

3.3.2 RS LDAS for EUROCORDEX-domain

- LDAS should account for
  - 1. Model biases due to uncertain parameters (e.g. subsurface)
  - 2. Sensitivity to initial conditions

- Model **parameters** (e.g. hydraulic properties of the subsurface) can influence the model **state** (e.g. soil moisture) non-linearly
- Investigations into Ensemble Kalman Smoothers and iterative Ensemble Smoothers
- Initial results:
  - RMSE reduction 6% on average by parameter estimation only
  - Further investigations into high biases central Europe

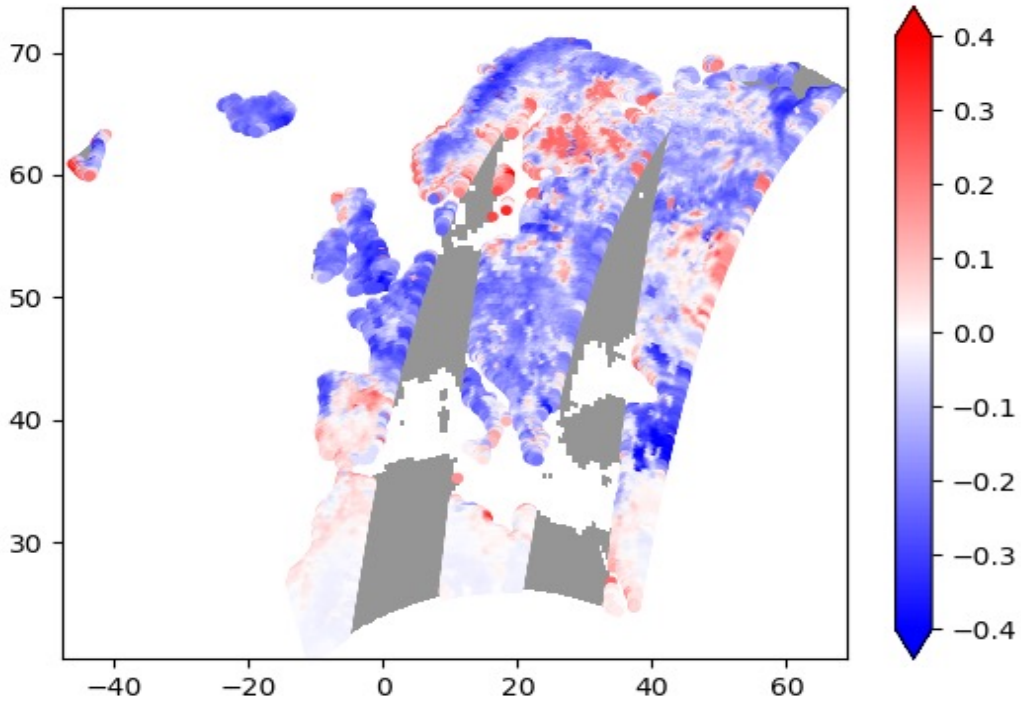

- Retrieval of key ecohydrological variables from multi-source RS data
- Retrieval of key cryosphere variables from multi-source RS data
- Development of real time RS LDAS
- Closing water cycle at the watershed/regional scale based on the LDAS

3.5.1 Hydrological cycle variation in the HRB

Upstream area

- In total, the upstream area received 8.66 × $10^9 m^3$ yr^{-1} of precipitation;
- Streamflow was 3.04 × $10^9 m^3$ yr^{-1}, or 207.1 $mmyr^{-1}$ as runoff depth, and rainfall, snowmelt, and glacier melt contributed approximately 71%, 25%, and 4%, respectively.
- The total ET was approximately 5.54 × 10^9 $m^3 yr^{-1}$, equivalent to an average of 376.5 mm yr^{-1}.

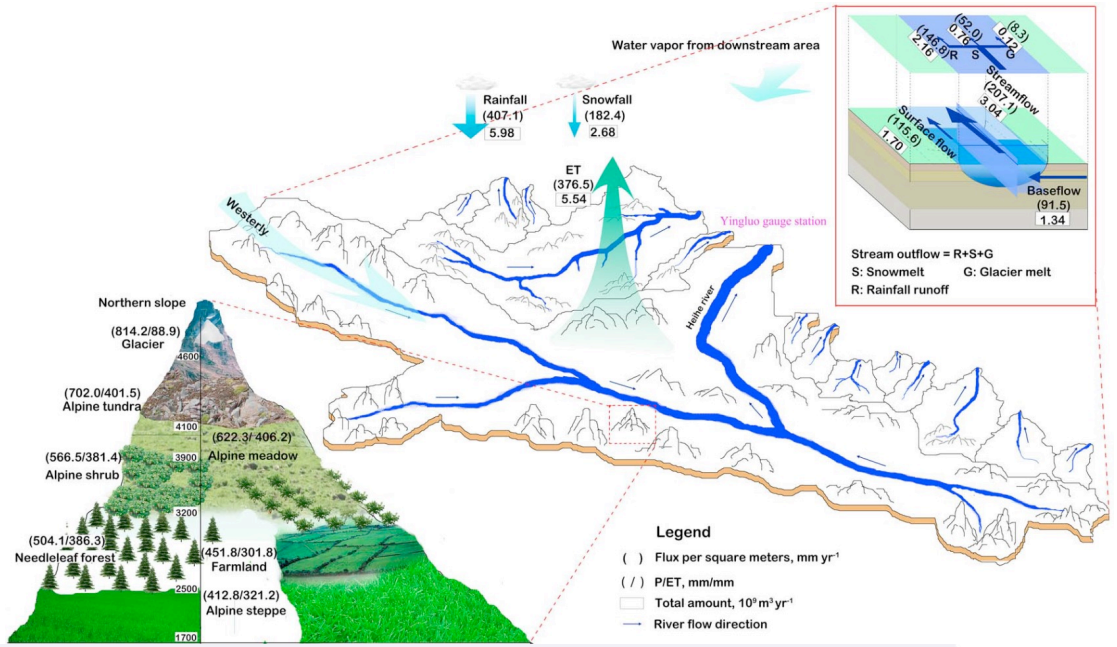

	Area (km^2)	Elevation zone (m)	Precipitation ($mm\ yr^{-1}$) Total	Rainfall	Snowfall	ET ($mm\ yr^{-1}$)	Runoff depth ($mm\ yr^{-1}$)	Runoff coefficient	Storage change of all storages ($mm\ yr^{-1}$)
Glacier	60.0	>4,600	814.2	423.6	390.6	88.9	976.9	1.20	−251.6
Alpine tundra	3,424.6	4,000–4,600	702.0	416.7	285.3	401.5	297.7	0.42	2.8
Alpine meadow	7,083.9	3,100–4,100	622.3	445.0	177.3	406.2	204.4	0.33	11.7
Alpine shrub	21.0	2,900–3,900	566.5	424.2	142.3	381.4	179.0	0.32	6.1
Needleleaf forest	786.8	2,500–3,200	504.1	390.7	113.4	386.3	117.8	0.23	0.0
Alpine steppe	1,612.5	1,800–3,100	412.8	331.3	81.5	321.2	88.2	0.21	3.3
Farmland	57.0	~2,700	451.8	369.9	81.9	301.8	122.6	0.27	27.4
Desert	1,637.5	1,680–4,000	425.4	306.5	118.9	257.6	164.6	0.39	3.2
City and town	3.0	2,280–2,940	426.5	393.1	33.4	417.0	7.4	0.02	2.1
Total (or average)	14,694.1	3,550	589.5	407.1	182.4	376.5	207.1	0.35	6.1

3.5.1 Hydrological cycle variation in the HRB

Midstream area

- The midstream area received approximately 2.483 × 10^9 m^3yr^{-1} (189.3 mm yr^{-1}) of precipitation.
- ET was the most dominant component and amounted to approximately 4.275 × 10^9 m^3yr^{-1} (mm yr^{-1}).
- Since the change in river channel water storage (Δch) was small compared to other changes.
- Irrigation is an absolute requirement for agriculture in the midstream area of the HRB.

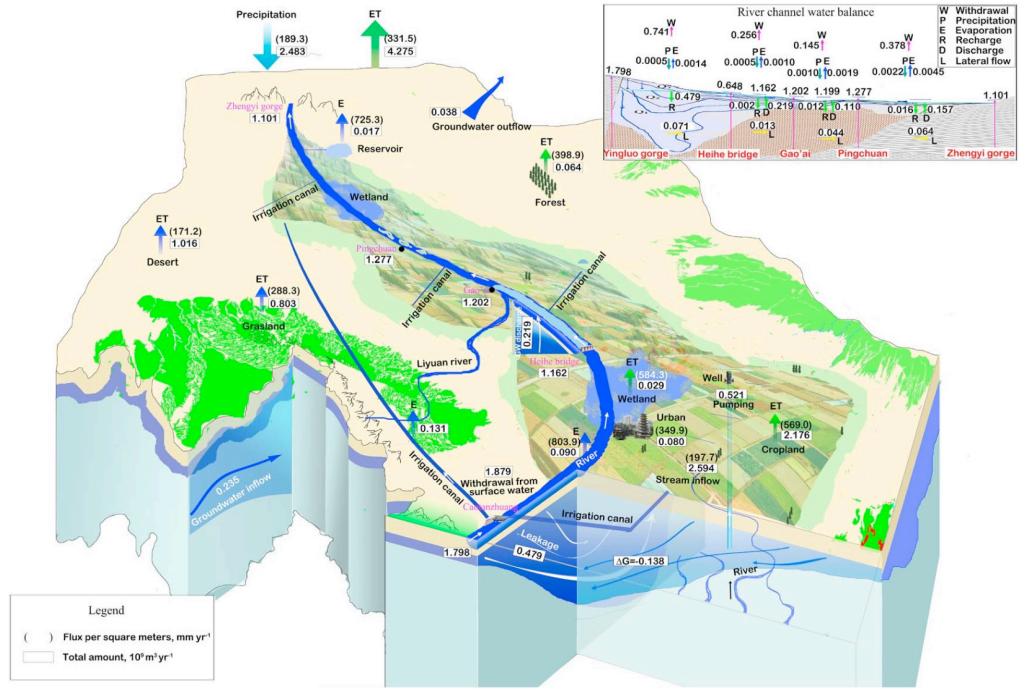

	Area (km^2)	Precipitation		ET		Transpiration proportion
		Total amount (10^9 m^3 yr^{-1})	Flux (mm yr^{-1})	Total amount (10^9 m^3 yr^{-1})	Flux (mm yr^{-1})	
Cropland	3,823.69	0.781	204.3	2.176	569.0	0.73
Grassland	2,783.36	0.748	268.6	0.803	288.3	0.51
Wetland	48.89	0.005	102.6	0.029	584.3	0.58
Forest	161.59	0.026	158.8	0.064	398.9	0.54
Urban and other built-up	227.68	0.039	171.7	0.080	349.9	0.41
Desert	5,939.12	0.857	144.4	1.016	171.2	0.34
Reservoir	23.70	0.003	127.7	0.017	725.3	
River	112.47	0.024	216.4	0.090	803.9	
Total (or average)	13,120.50	2.483	189.3	4.275	325.8	

3.5.1 Hydrological cycle variation in the HRB

Downstream area

- Natural vegetation areas (forest, shrub, steppe, and wetland), cropland, and the terminal lake (Sogo Nuur) used approximately **39%, 13%, and 4%** of the streamflow, respectively.
- The streamflow lost by ET in the desert was approximately 34%.
- The change in soil water and groundwater storage had a negative value before the implementation of the EWDP but gradually achieved a positive value after the implementation of the EWDP

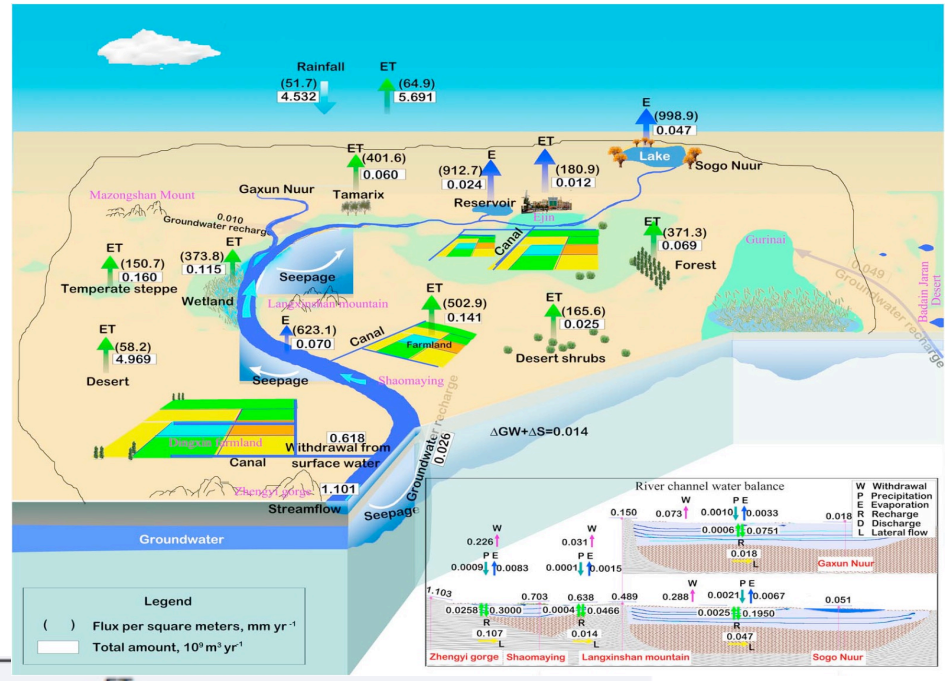

	Area (km^2)	Precipitation		ET		Ratio of ET to streamflow
		Total amount (10^9 m^3 yr^{-1})	Flux (mm yr^{-1})	Total amount (10^9 m^3 yr^{-1})	Flux (mm yr^{-1})	
Forest	184.95	0.008	43.5	0.069	371.3	0.063
Tamarix	149.53	0.007	43.8	0.060	401.6	0.054
Other desert shrubs	150.86	0.007	46.8	0.025	165.6	0.023
Temperate steppe	1,058.75	0.054	50.8	0.160	150.7	0.145
Wetland	308.15	0.016	52.4	0.115	373.8	0.104
Cropland	280.56	0.015	52.7	0.141	502.9	0.128
Urban and other built up	64.76	0.003	50.5	0.012	180.9	0.011
Lake	46.69	0.002	42.3	0.047	998.9	0.043
Reservoir	26.31	0.001	54.0	0.024	912.7	0.022
River	112.42	0.006	50.9	0.070	623.1	0.064
Desert	85,348.79	4.413	51.7	4.969	58.2	
Total	87,731.77	4.532	51.7	5.691	64.9	

3.5.1 Hydrological cycle variation in the HRB

water balance closure

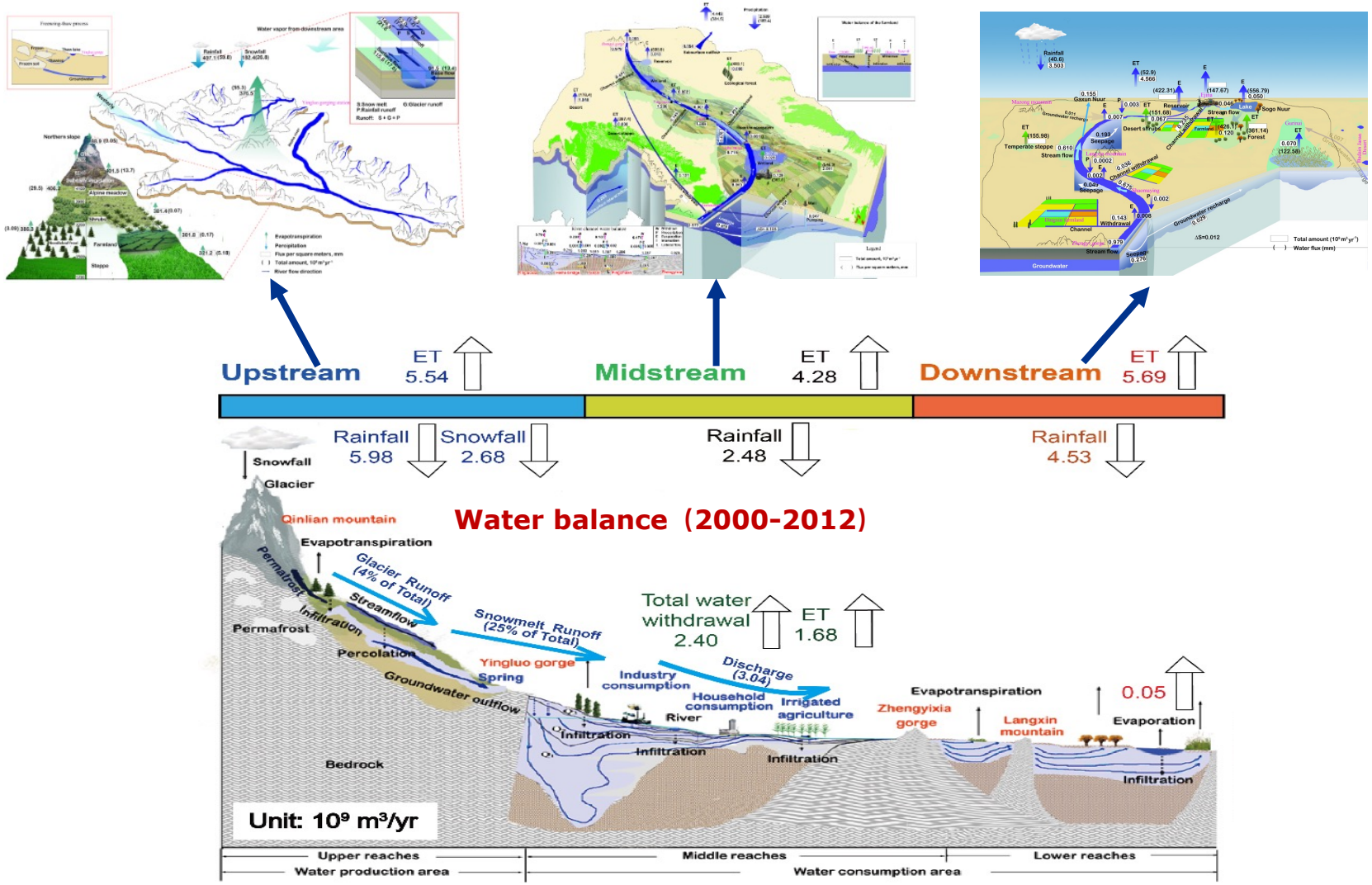

- Climate warming is a favorable factor in alleviating water scarcity
- Human activities have both positive and negative effects
- Water conflicts should be handled from a broad socioeconomic perspective

4. Plan of the project for the following year

Schedule

	2020				2021				2022				2023				2024			
WP0: Proposal preparation and project coordination																				
WP1: Retrievals of key ecohydrological variables																				
WP2: Development of LDAS_silk and LDAS_EU																				
WP3: Cal/val of LDAS_silk and LDAS_EU																				
WP4: Quantification of water cycle in silk road endorheic river basins and EURO-CORDEX																				

Thank you !

Xin Li

xinli@itpcas.ac.cn